Investigation of the Human Brain Neurochemistry in Pain Related Cortical Areas and Brainstem

Thesis (cumulative thesis)
presented to the Faculty of Arts Social Sciences
of the University of Zurich
for the degree of Doctor of Philosophy

by
Nuno Miguel Prates de Matos

Accepted in the spring semester 2017
on the recommendation of the doctoral committee:

Prof. Dr. rer. nat. Martin Meyer (main supervisor)
PD Dr. med. Dr. med. dent. Dominik Ettlin

Zurich, 2019

Summary

This doctorate thesis focuses on shortcomings in neurochemical investigations in human pain research by means of proton magnetic resonance spectroscopy (^{1}H-MRS). The first study (reproducibility study) explored the frequent issue of insufficient anatomical/functional specificity in ^{1}H-MRS investigations. We investigated the measurability of small substructures of the cingulate and insular cortex with adequate specificity by means of anatomically adapted measuring voxels and found that good data quality and high reproducibility are achievable despite strongly reduced voxel sizes. In the second study, we strived to make structures of the human brainstem accessible to functional ^{1}H-MRS investigations for the first time. We sought to enable the characterization of neurochemical dynamics in brainstem nuclei involved in pain processing by means of optimized ^{1}H-MRS-techniques. The results revealed reduced concentrations in the total N-acetylaspartate and GABA signal during orofacial stimulation in the trigeminal nuclear complex.

The third study deviates from the focus on ^{1}H-MRS, but it adds a valuable dimension to this doctoral thesis. In this work, the pain-specificity of pain-associated areas was investigated by means of fMRI using a nerve block to clearly differentiate painful from non-pain perceptions without changing physical stimulus. The main results indicate towards a pain-specificity of the posterior component of the insula and the parietal operculum.

Zusammenfassung

Diese Dissertation befasst sich mit Limitierungen der Magnetresonanzspektroskopie in der humanen Schmerzforschung. Die erste Studie untersuchte das verbreitete Problem der unzureichenden anatomisch-funktionellen Spezifität in ^{1}H-MRS Studien. Wir untersuchten die Messbarkeit kleiner Substrukturen des Cingulums und insulären Kortex mit adäquater Spezifität mittels an die Anatomie angepasster Messvoxel und fanden heraus, dass gute Datenqualität und hohe Reproduzierbarkeit erreichbar sind trotz stark reduzierter Voxelgrössen. In der zweiten Studie machten wir Strukturen des menschlichen Hirnstamms erstmals für funktionelle ^{1}H-MRS-Untersuchungen zugänglich. Wir ermöglichten die Charakterisierung neurochemischer Dynamiken in schmerzverarbeitenden Hirnstammkernen mittels optimierter ^{1}H-MRS-Techniken. Die Ergebnisse zeigten reduzierte Konzentrationen im gesamten N-Acetylaspartat- und GABA-Signal während orofazialer Stimulation im trigeminalen Kernkomplex.

Die dritte Studie weicht vom Fokus auf ^{1}H-MRS ab, fügt aber dieser Dissertation eine wertvolle Dimension hinzu. In dieser Arbeit wurde die Schmerzspezifität von schmerzassoziierten Hirnregionen mittels fMRI mit Hilfe einer Nervenblockade untersucht, um schmerzhafte von nicht-schmerzhaften Wahrnehmungen ohne Veränderung des Schmerzstimulus klar zu unterscheiden. Die Hauptergebnisse deuten auf eine Schmerzspezifität des posterioren Anteils der Insula und des parietalen Operculums hin.

Content

Preface

During a journey we often deviate from a planned route, sometimes because of encountered obstacles or because we decide to listen to our gut feeling, guiding us to new places, which were unimaginable beforehand. The original plan for my PhD-thesis was the continuation of the proton magnetic resonance spectroscopy (^{1}H-MRS) studies conducted by our group (Gutzeit et al., 2011; Gutzeit et al., 2013). These two studies were part of an emerging field in pain research, which sought out to uncover the neurochemical underpinnings of acute pain processing. In these studies, significant multiple neurochemical pain-related alterations in the insular cortices were identified.

At the start of my work, I aimed at providing a valuable contribution to this new field of neuroscientific research by applying the same experimental paradigm to other brain structures in order to start an extensive mapping of pain-related neurochemical processes across regions of the pain-processing network.

However, while my technical understanding about ^{1}H-MRS deepened, I became increasingly aware of significant shortcomings in commonly used functional ^{1}H-MRS-paradigms in the field of human pain research. As a consequence, I saw myself at a crossroad with two possible directions: On the one hand, I could follow the direction intended by my original plan; a probably more comfortable and quicker road although with the bad aftertaste of being subject to the same methodical shortcomings common in the field. On the other hand, I could decide for an unknown, possibly longer and bumpier road, although with the prospect of a more satisfactory destination.

So we decided to follow the bumpy path by changing the emphasis of my PhD more towards the methodical aspects of ^{1}H-MRS and addressed frequent methodical issues of ^{1}H-MRS in the field of pain research (and research in general). This project became a highly interdisciplinary endeavor, demanding a

close relationship between the Center of Dental Medicine, University of Zurich and ^{1}H-MRS-specialists from the Institute of Biomedical Engineering of the Swiss Federal Institute of Technology in order to successfully tackle the aforementioned issues.

Needless to say, this new path took us much longer to walk than expected. The financial resources we received for the original plan were enough to cover my employment as a PhD student at the Center for Dental Medicine for two years, which was not nearly sufficient. Solving the technical challenges was highly time-consuming. After the two years, we were unsuccessful in acquiring new funding. Fortunately I had the chance to take a part-time research position at the Institute for Complementary and Integrative Medicine of the University Hospital Zurich. This position allowed me to obtain new valuable scientific skills, but it also strongly limited my available time to work on the PhD-projects which further delayed their completion.

Four and a half years after the inception of my doctorate program, the journey was at the end. This thesis is not only the result of sustained and sizable efforts from my mentor Dr. Mike Brügger and the highly committed multidisciplinary group of scientists who accompanied me along this path. Equally important were the test participants who agreed to let themselves suffer pain for the sake of science. I had the first contact with this kind of research in the year 2006 as a participant in Dr. Mike Brügger's first study. I started as a test subject attracted by the payment but continued to participate again and again due to my growing scientific interest in and fascination for the topic. I believe that my extensive experience as a volunteer in a multitude of pain studies (and studies in general) helped me in bringing a level of sensitivity and empathy towards the subjects participating in our experiments. Besides of all the technical and methodical aspects of a well-conducted ^{1}H-MRS pain research I had learned during my studies, I realized that the development of an empathic and comforting approach

to the test subjects is of equal importance. Keeping the volunteers calm and giving them the sense of “control” over the situation is at least as important as the cleanliness of the scientific/methodical approach.

This journey — despite (and maybe because of) the sometimes rough sections, its long distance and sharp turns — led me to a place of contentment and pride for the accomplished work. The awareness of the methodical pitfalls and the knowledge how to prevent/ameliorate them gives me confidence in the potential of ^{1}H-MRS-method in providing essential insights into the processing of acute pain and the formation of chronic pain in particular.

1 Introduction

Our relationship to the conscious experience called pain is a complex one. It has been our friend for millions of years, fostering our survival as a species by teaching us how to avoid things that endanger us. It tells us if and what part of the body needs rest in order to promote its healing. And: Pain is highly subjective. Each person perceives pain in their unique way, depending on their (epi-)genetic constitution but also on brain-based processes such as mood, perceived stress level, episodic memories, psychological traits, interpretation of environmental situations, just to name a few (Tracey and Mantyh, 2007; Denk et al., 2014).

Thus, the experience of pain is not a simple unidirectional propagation of nociceptive signals from the body through the peripheral (PNS) to the central nervous system (CNS) as suggested by René Descartes in the 16th century and still adopted by many. Modern views tell a different story, one of highly dynamic processes in complex brain networks which produce the qualia called pain.

The question how the multifaceted pain experience emerges in the nervous system from simple nociceptive signals has been the subject of a plethora of neuroscientific studies. Since the advent of neuroimaging techniques, our understanding has grown tremendously about the brain networks involved in the processing of acute pain. We also gained new insights about how the communication patterns between pain processing areas could explain dynamic aspects of pain perception. And, we are also starting to understand which brain processes contribute to chronic pain. Chapter 2 provides an overview and describes these findings in more detail.

The catalyst of this neuroimaging revolution in the field of human pain research is probably the functional magnetic resonance imaging technique (fMRI).

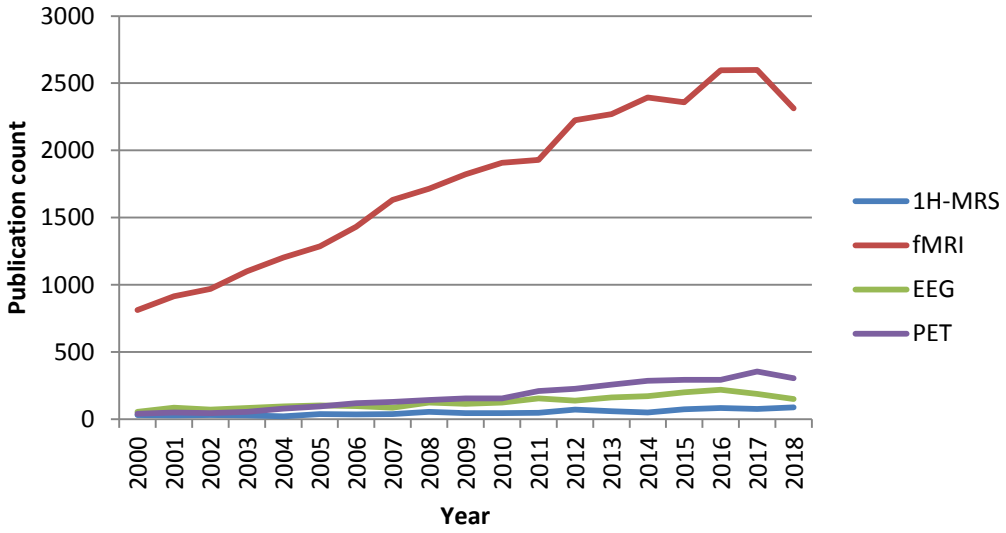

Figure 1: Illustration of the yearly publication frequency of pain studies using one of four different neuroimaging techniques: EEG, PET, ^{1}H-MRS and fMRI. Data is based on Pubmed searches (February 2019) using the designation of the methods as keyword in combination with the keyword "pain".

Since its inception in the early 90's by Seiji Ogawa (Ogawa et al., 1990), this method has granted noninvasive access to the brain activity of living human beings, allowing researchers to observe how brain activity patterns correlate with pain perception. Although other methods, such as electroencephalography (EEG), magnetoencephalography (MEG) and positron emission tomography (PET) have also contributed significantly to our current understanding, the fMRI-technique may have played the biggest role due to the availability of MR-scanners and its relatively high spatial and temporal resolution (Figure 1).

However, despite the important contribution provided by fMRI, it lacks a certain "depth". This technique is based on the indirect observation of relative changes in blood perfusion through quantification of the blood-oxygen-level dependent (BOLD) contrast (Logothetis et al., 2001). This contrast works by the quantification of changes in the T2* decay in a given voxel as a consequence of alterations in the ratio of oxyhemoglobin (oxyHb) to deoxyhemoglobin (deoxyHb)

due to a process called hemodynamic response (D'Esposito et al., 2003). In this process, increases in neuronal and glial activity, such as neurotransmission, modulate the level of vasodilatation and vasoconstriction, resulting in a local overcompensation of oxygenated blood thus increasing the ratio of oxyHb to deoxyHb (Lauritzen et al., 2012). Due to the diamagnetic nature of oxyHb, the overcompensation with fresh blood leads to longer T2* relaxation times, finally causing an increase in the fMRI-signal (D'Esposito et al., 2003).

Yet, until this day, the link between neurotransmittory systems and BOLD-dynamics are still not fully understood (Logothetis, 2008; Lauritzen et al., 2012). Research suggests that the activation of both excitatory and inhibitory neurons increase the cerebral blood flow and hence the BOLD signal (Logothetis, 2008). In contrast, decreases in BOLD-signals have mainly been linked to the activity of inhibitory interneurons, although exceptions exist (Lauritzen et al., 2012). To sum up, based on the BOLD signals alone, it is not possible to deduce the excitatory and inhibitory processes (Lauritzen et al., 2012).

A less common MR-based technique is the proton magnetic resonance spectroscopy (^{1}H-MRS). In contrast to fMRI, ^{1}H-MRS is capable of providing direct concentration estimates of multiple neurochemicals in a pre-defined part of the brain in a non-invasive fashion. In that sense, this method can be regarded as a kind of virtual tissue biopsy, granting simultaneous information about the underlying energy metabolism, myelination and membrane metabolism, neurotransmitter status, antioxidant and osmolyte concentration levels, just using a standard MR scanner (Graaf, 2007; Stagg, 2013).

The application of ^{1}H-MRS to pain research has promising potential by providing novel insights, also through its combination with other neuroimaging techniques such as fMRI. However, ^{1}H-MRS is still mainly a clinical tool for the identification of tumors and other pathological tissue conditions. Many applied ^{1}H-MRS-sequences are not optimized for specific neuroscientific investigations like pain

research due to the large measurement volumes used and static nature of the examinations.

In this doctorate thesis I have started at this point. During the examination of available literature on the dynamic neurochemical processes of pain processing in distinct brain regions using ^{1}H-MRS, we realized that the applied ^{1}H-MRS procedures were often suboptimal hence limiting its vast potential in pain research.

We addressed frequent methodical limitations common in experimental ^{1}H-MRS investigations. Therefore, the **first study** of my thesis tackled the issue of the lack of anatomical/functional specificity. In the context of a reproducibility study, neurochemical profiles were measured using common ^{1}H-MRS sequences and MR-equipment in order to enable a generalization to most clinical and scientific settings. For this purpose, four cortical regions prominent in pain processing were measured with optimized structural and functional specificity. The measurements were repeated at four different days in order to evaluate the impact of the reduced voxel dimensions on spectral quality and associated reproducibility metrics. In addition, the systematic effects of participant movement, tissue composition in the measurement volume and time of day on neurochemical quantification were explored in order to obtain valuable knowledge for the planning of future (pain) studies using ^{1}H-MRS.

In the **second study**, we strived to open a new door for the field of pain research: To make structures of the human brainstem accessible to functional ^{1}H-MRS investigations for the first time. We sought to enable the characterization of neurochemical dynamics in brainstem nuclei involved in the processing of nociceptive signals. In order to achieve this goal, ^{1}H-MRS-techniques from spinal cord research were optimized for neurochemical quantifications in the brainstem (Hock et al., 2016; Wyss et al., 2017). In addition, we also addressed issues of systematic quantification errors common in functional ^{1}H-MRS studies which

may mimic real neurochemical effects. The presented approaches add to the validity of ^{1}H-MRS in experimental settings.

In the **third study** I had a contributing role as a co-author. Although this study deviates from the focus on ^{1}H-MRS, it adds a valuable dimension to this doctoral thesis. In this work, an innovative experimental approach was used to clearly differentiate painful from non-pain perceptions without changing physical stimulus strengths as perceptions were modulated by means of lidocaine injections.

Before the presentation of these three studies, several chapters are presented in order to provide a foundation to readers unfamiliar with this field in order to foster a basic understanding for some of the rationales of the study 1-3 and the proposed ideas for future research.

2 ^{1}H-MRS: A Methodical Overview

Its uniqueness compared to other MR-based methods is that ^{1}H-MRS focuses on specific resonance frequencies attributable to single substances (Stagg, 2013). As all magnetic resonance-based techniques, its signals are governed by the larmor equation.

$$\omega = -\gamma B_0$$

The larmor frequency ω defines the frequency of signals obtained by MR techniques and describes the precession frequency of proton nuclei when they become polarized, either parallel or antiparallel to an external magnetic field B_0 (B_0 corresponds to a static magnetic field of a scanner, typically 1.5, 3 or 7 Tesla) (Graaf, 2007). In addition to B_0, ω depends on the gyromagnetic ratio γ which is a nucleus-specific constant. Now, if B_0 is the only factor influencing ω, how are different substances identifiable simply based on the larmor frequency?

2.1.1 Differentiation of Neurochemical Compounds Based on Chemical Shift and Scalar Coupling

The answer is that the larmor frequency of proton nuclei is also affected by their chemical environment. This phenomenon is caused by shielding (or screening) of proton nuclei from the B_0 field by the magnetic fields generated by surrounding electrons (Figure 2) (Graaf, 2007; Stagg, 2013). This effect is called chemical shift and constitutes the basic concept of ^{1}H-MRS. As a consequence of this mechanism, neurochemicals in a ^{1}H-MRS-spectrum are typically represented over a frequency range. This frequency range is usually not reported in Hertz, but rather in parts per million, or PPM. The advantage of the use of PPM is the independence of the chemical shift from the underlying magnetic field strength,

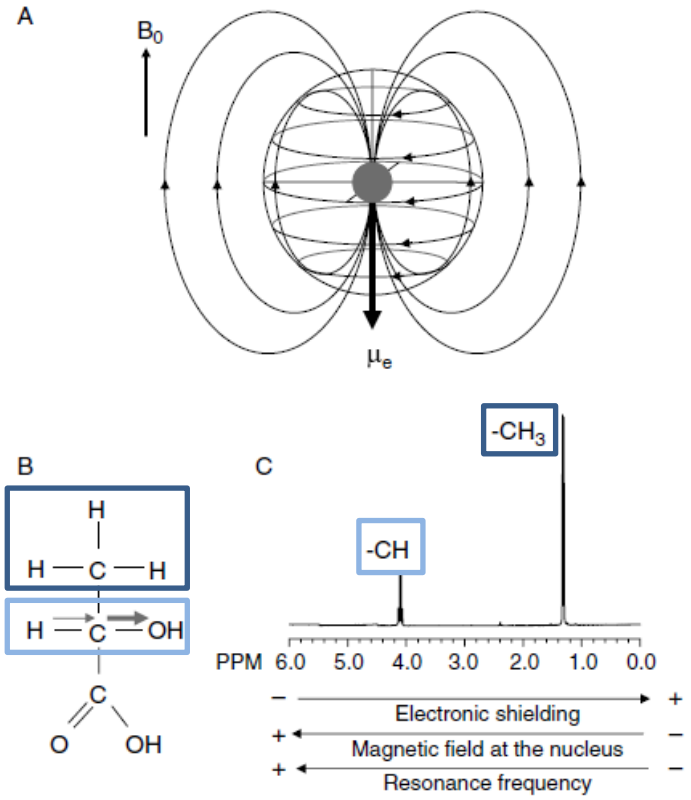

Figure 2: Chemical shift phenomenon. A) The electrons surrounding a proton nucleus can be imagined as currents due to their charge, creating a magnetic moment μ_e. As μ_e is oppositely oriented to the magnetic moment of the nucleus polarized to B_0, the effective magnetic field affecting the nucleus is reduced, resulting in an altered larmor frequency. B) The strength of the electronic shielding also depends on the characteristics of the electron bonds. In this example, the electronegative oxygen exerts a pull on the electron, leading to a reduced electronic shielding at the methine (-CH) protons. As a consequence, the resulting reduction in the larmor frequency is less pronounced compared to other protons C) The different larmor frequencies of the methine (-CH) and methyl (-CH_3) protons due to the electronegative oxygen is sufficient to explain the basic configuration of the MR spectrum of the substance lactate (From De Graaf (2007, modified by the author).

allowing the comparison of spectra from different MR scanners working at 1.5, 3, 7 Tesla etc. Therefore, chemical shifts are usually defined as follows:

$$\delta = \frac{v - v_{ref}}{v_{ref}} x\ 10^6$$

where v refers to the frequencies of the neurochemical-of-interest and v_{ref} refers to the reference molecule, usually tetramethylsilane (TMS), to which $\delta = 0$ has been assigned (Graaf, 2007). Neurochemicals measured using ^{1}H-MRS are usually represented over a ppm-range of 0-4.

As illustrated, the chemical shift phenomenon provides direct information about the chemical environment of nuclei, thereby enabling the detection of neurochemicals. Furthermore, as the signal originates directly from the nuclei in a specific neurochemical, the area of the spectrum is proportional its concentration, thus making ^{1}H-MRS a quantitative method (Stagg, 2013).

Spectral resonances are usually not just represented by a single frequency peak, but are present as characteristic multiplet structures with various peaks. The mechanism causing the splitting of frequencies into multiplet structures is called scalar coupling or J coupling, or spin-spin coupling (Graaf, 2007). This additional feature is caused by interactions between nuclei with magnetic moments, either directly through space (dipole coupling) or through electrons in the bonds (scalar coupling) (Graaf, 2007). Here I shall provide a strongly simplified example in order to illustrate this process. For a system with two nuclei with a spin, four different spin configurations are possible depending on the parallel and antiparallel spin orientation of nuclei and electrons. The possible energy level transitions give rise to additional resonance frequencies for each nucleus, thus creating additional peaks for each nucleus. Depending on the energetic levels of each configuration, some may occur more often than others, resulting in possible different peak heights in the multiplet structure. Scalar couplings are constants as they are solely based on the fundamental principle of spin-spin pairing and are thus independent of the external magnetic field (Graaf, 2007).

Hence, the phenomena of chemical shift together with scalar coupling contribute to the individual and distinguishable spectral pattern of a given neurochemical.

However, depending on the external magnetic field, chemical shift and scalar coupling differ in their contribution to the discriminability of distinct neurochemicals. For example, increases in B_0 may be beneficial for the neurochemical discrimination due to higher chemical shift dispersions (leading to bigger distances between the substances represented on the ppm-axis), but the multiplet structures become less apparent as the multiplet peaks are shifted toward each other from a relativistic point of view. At 3T, multiplet structures are more prominent, allowing their utilization for the identification of substances with strongly overlapping chemical shifts.

2.1.2 Water vs. Neurochemicals

Water is by far the most abundant substance in the brain, with water spectra amplitudes more than three orders of magnitude larger compared to the spectra of neurochemicals (Figure 3)(Stagg, 2013). As a consequence, the removal of water peaks either by suppression or spectral subtracting methods is essential in order to reveal the neurochemical signals.

The sizeable difference between water and neurochemical signals is the reason for the modest spatial and temporal resolution of ^{1}H-MRS compared to other imaging techniques. fMRI utilizes mostly the large signal generated by water, providing it the necessary signal-to-noise ratio (SNR) for whole-head acquisitions with millimeter voxel dimensions in seconds. Due to the comparably small signal obtained by ^{1}H-MRS, large voxel sizes are needed (typically 8 cm^3 in single voxel protocols) to compensate for the small signals and many acquisitions (typically

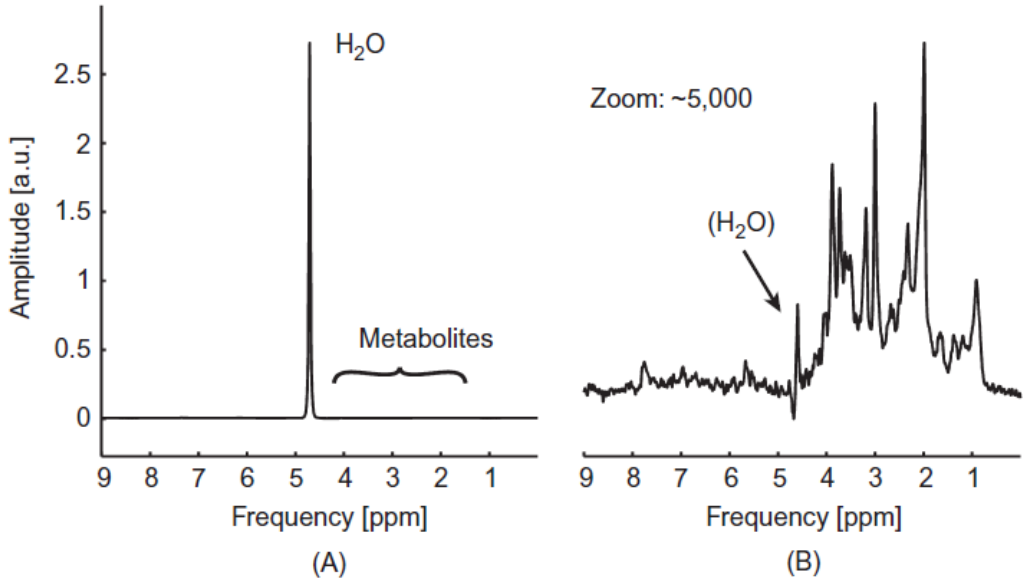

Figure 3: Illustration of the minute proportion of neurochemical signal compared to the water signal usually acquired with ^{1}H-MRS. A) The water signal is approximately 5000 times higher than the signal from the neurochemicals. In order to process neurochemical spectra, the water peak is usually suppressed, B) revealing the spectrum containing neurochemical information. (From Stagg & Rothmann, 2013)

128) must be averaged in order to remove substantial noise from the data. As a result, the measurement of a neurochemical spectrum typically requires minutes in order to provide single concentration estimates. The acquisition time strongly depends on other parameters such as the strength of the static magnetic field, voxel size, applied localization techniques and MR-hardware used .

2.1.3 Localization of ^{1}H-MRS-Signals

For neuroscientific investigations, single-voxel techniques are frequently used for the derivation of neurochemical information from a specific region, including the empirical ^{1}H-MRS studies conducted in this thesis. The usage of a single voxel ^{1}H-MRS (SV-MRS) compared to ^{1}H-MRS-imaging (MRSI) brings some advantages, like improved data quality due to better shimming and thus improved B_0

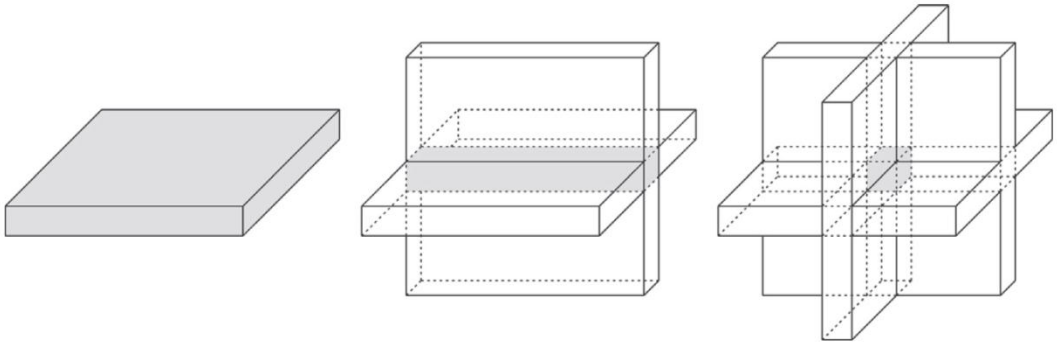

Figure 4: Depiction of gradient-based localization technique for SV-MRS such as PRESS and MC-PRESS. This method combines three slice-selective RF-pulses. With each pulse, an additional selective dimension is added, in the end resulting in a voxel providing the spectral information. (From Stagg & Rothmann, 2013, modified by the author)

homogeneity. And theoretically, the capability of adapting voxel sizes and orientation to the structural shape of a region-of-interest (ROI) is an advantage for measurements aiming for optimal anatomical and functional homogeneity.

The main localization method at 3 Tesla is the gradient-based Point Resolved Spectroscopy (PRESS). Both ^{1}H-MRS studies conducted in this thesis used PRESS, whereas the study focusing on the brainstem applied a novel variant of the PRESS sequence called Metabolite Cycling PRESS (MC-PRESS). The localization procedure is the same; the MC-PRESS variant differs due its preservation of the water peak.

PRESS sequences usually apply three slice-selective RF-pulses: A 90° and two 180° RF-pulses with a specific echo time (TE) defining the time between RF-pulses. The first RF pulse flips protons from the longitudinal axis to the transverse plane in the first slice. The following 180° pulses consecutively refocus the magnetization, resulting in spin echoes originating from a voxel defined by the intersection of all three RF-pulses (Stagg, 2013) (Figure 4). The PRESS

sequences are usually combined with water suppressing pulses such as VAPOR (Variable Pulse power and Optimized Relaxation delays), or in the case of MC-PRESS, up- and downfield pulses result in upward and downward oriented water peaks, which cancel themselves out during averaging, enabling the neurochemical quantification (Dreher and Leibfritz, 2005). The advantage of MC-PRESS is, the water peak of each acquisition is preserved and can be used for frequency alignment, phase and eddy current correction before averaging of neurochemical spectra. Hence, MC-PRESS enables the reduction of frequency shifts caused by pulsatile effects of blood vessels/CSF and B_0 drifts, making it suitable for regions subject to high levels of pulsation such as brainstem structures.

The TE strongly influences the obtainable neurochemical information. As complex multiplet structures such as neurotransmitters decay quicker, short TE are needed in order to obtain the most signal possible from substances such as glutamate (Glu), Glutamine (Gln) or GABA. Therefore, neuroscientific investigations usually apply TEs of 30-40 ms. In contrast, clinical investigations usually use TEs > 100 ms in order to reduce the baseline distortions due to macromolecules and lipids, but at the cost of a loss of the signal of neurotransmitter systems.

One of the drawbacks of all localization methods, including PRESS, is the chemical shift displacement artifact (CSD) (Stagg, 2013). Although the physical effects of chemical shift and scalar coupling are the basis for all MRS techniques, they also have associated issues that need to be recognized in order to provide meaningful results. As described above, magnetic field gradients are applied to define the spatial characteristics of the RF-pulses. But as described in 1.2.1, different compounds have different larmor frequencies and are therefore excited at slightly shifted voxel locations (Kreis, 2004; Stagg, 2013). The direction of the shift depends on the excitation orientation of the first 90° RF-pulse from

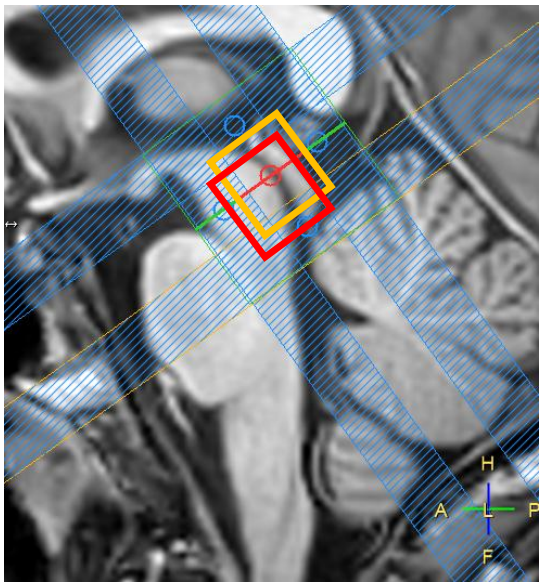

Figure 5: Depiction of a measurement voxel planning of a MC-PRESS sequence in the human periaqueductal gray superimposed on a sagittal T1-weghted MPRAGE image. Chemical shift displacement artifact is illustrated by the red and orange box. The orange box represents the voxel providing the signal of creatine, the red box represents the relatively displaced voxel of lactate (unpublished data from own ongoing research).

the PRESS sequence. In essence, this means that each neurochemical has its own voxel, each shifted to each other depending on their chemical shift properties. In order to minimize CSD, the voxel sizes can be reduced (as the chemical shift displacement is proportional to the voxel dimensions) or outer-volume suppression bands can be applied in order to create a voxel containing signals from all neurochemicals-of-interest (Figure 5).

2.1.4 Spectral Quality: Spectral Resolution and Signal-to-Noise Ratio

The signal used in ^{1}H-MRS provided by PRESS sequences is usually the free induction decay (FID) of the second spin-echo. The T2-decay of the spin-echo contains the different larmor frequency contributions originating from the underlying compounds. The decay-signal is transformed from the time to the

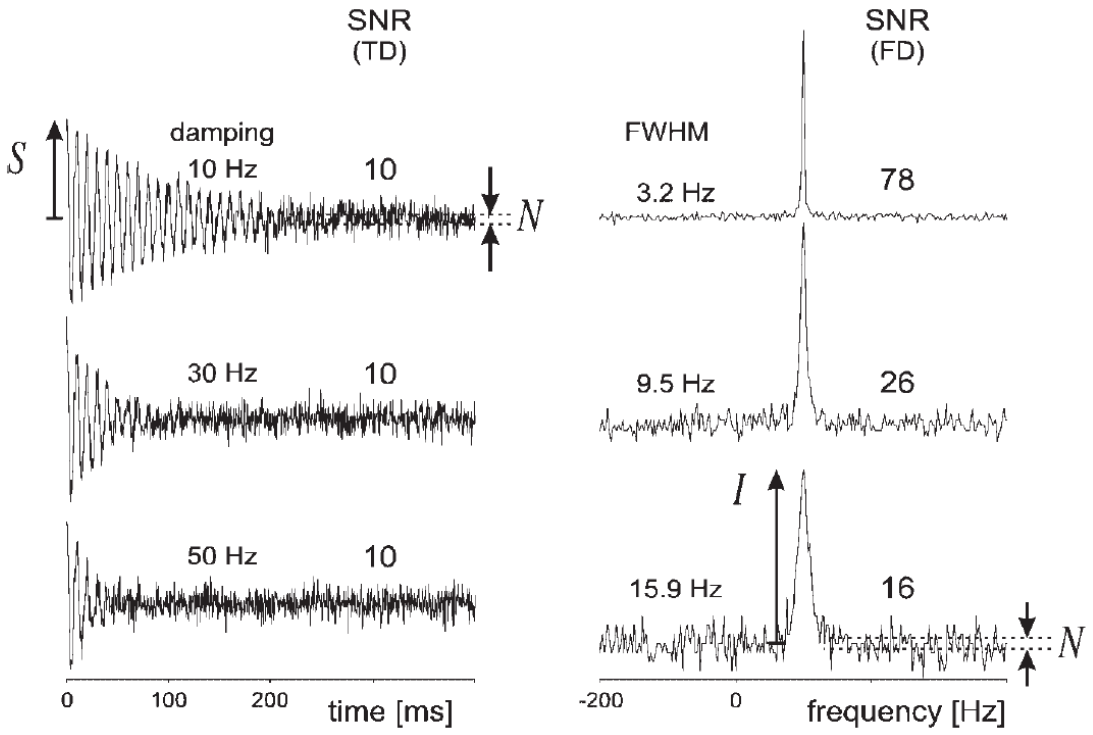

Figure 6: Link between spectral characteristics in the frequency domain (right) compared to the characteristics of the FID. In the left panel, three FIDs are depicted with different levels of signal damping, imitating different signal decay rates. In all three FIDs, the noise (N) is kept constant at a signal-to-noise (SNR) rate of 10. In the right panel, the corresponding data in the frequency domain is presented. Firstly, it is evident that the slower the decay, the better the spectral resolution (indicated by the linewidth using full width at half maximum (FWHM) estimates). Secondly, although the SNR in the time domain remains the same, it differs significantly in the frequency domain due to a reduction in signal intensity (I) with shorter decays. (From Kreis, 2004)

frequency domain by means of a fast fourier transformation (FFT), revealing the different frequency components in the signal. Spectral quality is directly connected to the T2-decay pattern (Figure 6): The longer the decay, the better the linewidth (LW) of the peaks in the frequency domain. LW is usually reported as full-width-at-half-maximum (FWHM) and represents the width of the peak at its half height. LW is reported in Hertz.

The spectral noise level is reported as signal-to-noise ratio (SNR) and is usually calculated as ratio of the peak amplitude to the standard deviation of the noise (Kreis, 2004). From figure 6 it is evident, that with narrower LW the SNR also

improves. LW and SNR are the most important determinants of spectral quality. Narrow LWs are crucial for the resolution of small multiplet structures such as neurotransmitters. SNR is also important as it needs to be low in order to unveil the small multiplet structures of interest.

As mentioned in section 2.1.2, in comparison to other imaging methods, ^{1}H-MRS suffers inherently from low signal levels. In order to compensate for small levels of signals, usually large voxel dimensions are applied, typically 8 cm^3. The problem is that with large voxels, the shimming of the B_0 in the voxel becomes less efficient, leading to larger field heterogeneity. As a consequence, the FID-decay shortens, resulting in worse spectral resolution. The aim of the reproducibility study conducted in the frame of this thesis questions this approach: As small voxels are easier to shim, the spectral resolution should improve. And as improved peak linewidths result in improved signal-to-noise ratios, SNR reductions should be compensated by the increased peak amplitudes up to a certain degree. Thus, a reduction in voxel sizes might be acceptable in order to improve anatomical and functional homogeneity.

2.1.5 Quantification of MR Spectra and Related Quality Measures

The most common software applied for the quantification of in-vivo MR spectra is LCModel (Provencher, 1993; Provencher, 2001). This software uses a linear combination of basis spectra (also named model spectra, hence the name LCModel) of all neurochemicals included in the analysis and fits them together on the raw spectrum in order to identify the contribution of each included neurochemical to the fitted spectrum.

A good fit between the fitted and raw data is indicated by the residual as evenly distributed noise around 0 (see Figure 7). LCModel provides LW and SNR estimates for the largest peak in the spectrum, usually *N*-acetylaspartate (NAA, large peak at 2.0 ppm) for spectral quality control.

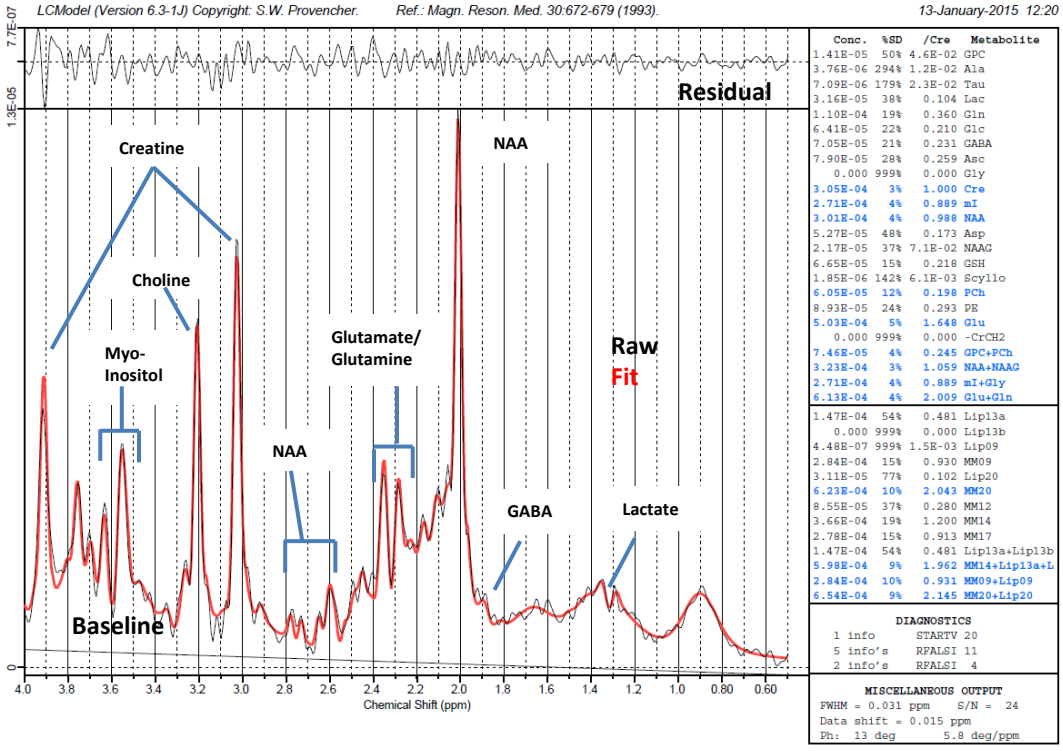

Figure 7: Exemplary LCModel output from a 2.4 cm^3 voxel recorded in the posterior insular cortex (TE = 32ms, TR = 2500ms, 384 acquisitions) at 3T from a healthy male volunteer (data from own unpublished research). The main area of the output shows the fitted spectrum consisting of the linear combination of basis spectra (red line) over-imposed on the eddy current and phase-corrected raw data. The line under the fit represents the baseline. The residual (Raw-Fit) is displayed above the spectrum. On the right, absolute concentration estimates, concentration ratios (concentrations relative to Creatine) and fitting errors (Cramer-Rao lower bounds as %SD) are provided. In addition, peaks are labeled to provide a sense for the main contributing neurochemicals.

Another useful quality measure provided by LCModel are the fitting-error estimates calculated as Cramer-Rao lower bounds (CRLBs). CRLBs represent the stochastic uncertainty for a single measurement as lower bounds for the variance (Kreis, 2004). This metric considers inherent limits of fitting with a model, together with estimates of the interdependence of fitting parameters, effects of prior knowledge constraints and spectral quality measures such as LW and SNR for its variance estimates (Kreis, 2004).

There is a debate going on about which CRLB values are considered reliable for a quantification estimate. The common opinion shared by many researchers/experts is that a CRLB < 20% is regarded as reliable (Stagg, 2013). From my point of view, the focus on a simple value could be too conservative and should depend on other aspects like the expected effect sizes and study sample. As mentioned before, CRLBs represent a stochastic uncertainty assuming the model is correct. As such, the quantification error is normally distributed around the "true" concentration value. The higher the CRLBs, the broader the distribution of the concentration estimates, resulting in a reduced sensitivity of the method to detect signal changes. Following this rationale, the higher the CRLBs, the larger sample size is needed in order to reduce the variance.

As CRLBs consider both, LW and SNR, it is a more accurate measure to judge the quantified data compared to statements of SNR and LW alone (Kreis, 2004). However, for quality control it is beneficial to set quality thresholds. For example, in the TBSNC-study, we applied a threshold of 0.070 ppm for the LW of the NAA-peak as recommended by Kreis (2004). In addition, we chose a SNR-threshold of 10. Both thresholds were chosen in order to allow for sufficient data quality for an improved quantification of GABA.

3 Neural Correlates of Pain

3.1 From Pure Nociception to a Multifaceted Pain Experience

3.1.1 Formation and Propagation of Nociceptive Signals

Under normal circumstances, the sensation of pain starts with the detection of (potentially) noxious stimuli or inflammation by the PNS. The underlying mechanisms are summarized in figure 1. In this process called nociception, receptors and ion channels located at the endings of myelinated A-δ and

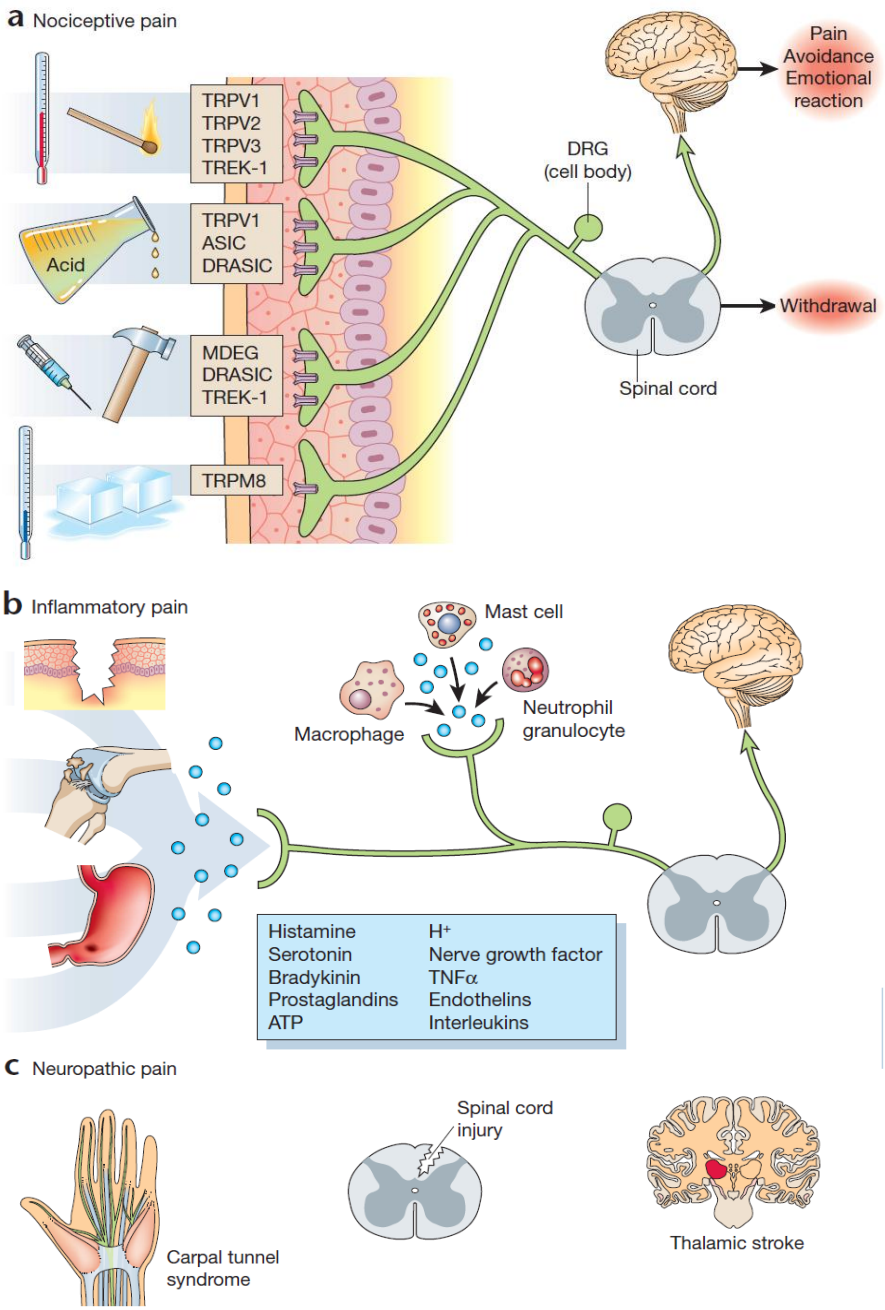

Figure 18: Illustration of nociceptive, inflammatory and neuropathic pain mechanisms. a) Nociceptive pain: Noxious stimuli affecting the body are detected via receptors located at the nerve endings, which are transduced to electrical signals and propagated to the dorsal horn of the spinal cord. There the nociceptive signal induce withdrawal reflexes via interneuron circuits or are relayed to pain-processing structures. b) Inflammatory pain is caused by chemical mediators released as a consequence of tissue damage, inflammation or released by cancer tissue. Chemical mediators act on the nerve endings, thus modulating nerve fiber responses. c) Neuropathic pain originates as a consequence of lesions or dysfunction of the nervous system. (Figure from Scholz and Woolf, 2002 modified by the author)

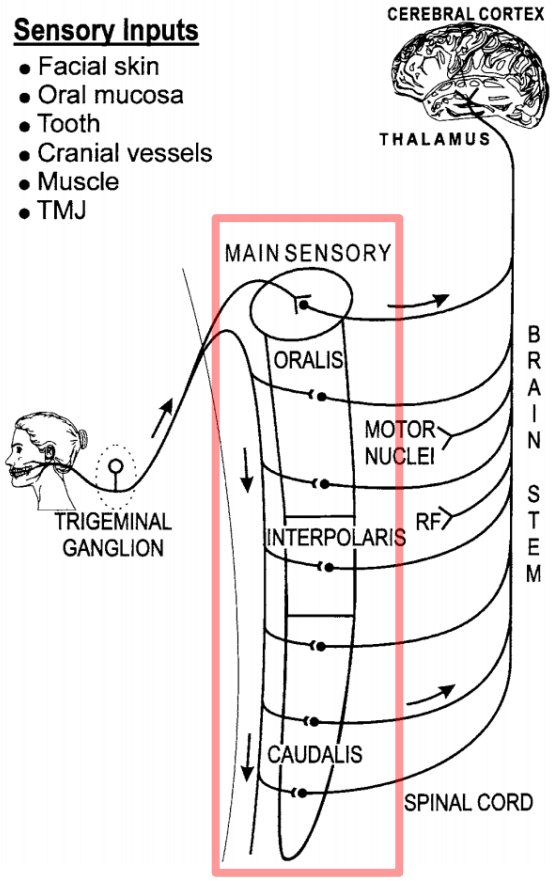

Figure 9: Schematic depiction of the craniofacial nociceptive signal cascade. Noxious and inflammatory signals from the facial skin, oral mucosa, teeth, cranial vessels, muscles and the temporomandibular joint are propagated via the trigeminal nerve. It enters the brain at the level of the pons and relays nociceptive information to 2nd-order neurons via synapses located in nuclei of the trigeminal brainstem sensory nuclear complex (TBSNC) indicated by the red box. On the one hand, most of the 2nd-order neurons relay nociceptive input to the ventroposterior thalamic nucleus (VPM) of the thalamus. On the other hand, some 2nd-order neurons project to brainstem structures, such as the cranial nerve motor nuclei or the reticular formation. (Figure from Sessle, 2000, modified by the author)

unmyelinated C nerve fibers translate various modalities of noxious stimuli (such as heat, cold, mechanical forces and acid) into electrical currents which are relayed to the CNS via 1st-order synapses (Scholz and Woolf, 2002). Inflammatory pain resulting from tissue damage and inflammation functions via the modulation of the same nerve endings through the release of an “inflammatory soup” consisting of a multitude of chemical mediators promoting peripheral sensitization (Scholz and Woolf, 2002). Noxious and inflammatory stimuli from the body synapse in the dorsal horn of the spinal cord (figure 8). In contrast, stimuli originating from the craniofacial areas are mainly propagated via the trigeminal nerve and enter the brain at the level of the pons and synapse in nuclei of the trigeminal brainstem sensory nuclear complex, (TBSNC) (Sessle, 2000; DaSilva and DosSantos, 2012)(see figure 9).

Already at the level of the dorsal horn and the TB , nociception is subject to modulation and regulation (Sessle, 2000; Scholz and Woolf, 2002). In physiological conditions, signals are modulated by local circuits and through top-down regulated efferents from pain-modulating networks in order to promote homeostasis (Tracey and Mantyh, 2007). Descending pain regulatory mechanisms are discussed in section 2.1.2.

After being subject to a first modulation, nociceptive signals are projected in a smaller extent to brainstem and cerebellar structures. Most of the ascending nociceptive signals are projected to thalamic nuclei, where they are further transmitted to (sub-) cortical structures for final integration and interpretation.

3.1.2 Brain networks involved in the creation and "coloring" of pain experience.

The term nociception refers to the *detection of tissue damage by specialized transducers attached to A-ð and C fibers including their modulation* due to inflammatory processes described in the last section (Loeser and Melzack, 1999).

In contrast, a pain experience is the outcome of the modulation and interpretation of nociceptive signals by the brain strongly influenced by various factors such as context, mood and cognitive characteristics (Figure 10).

Ronald Melzack (1999) proposed the existence of a "pain neuromatrix", often also termed pain matrix, a network of brain areas which represents the neural substrate of a pain experience. Since the advent of neuroimaging techniques, a multitude of studies have been conducted using fMRI and PET to identify such a network (Apkarian et al., 2005; Tracey and Mantyh, 2007). These studies managed to identify a multitude of regions that showed activity changes during acute pain experience. Various reviews summarize these findings (Peyron et al.,

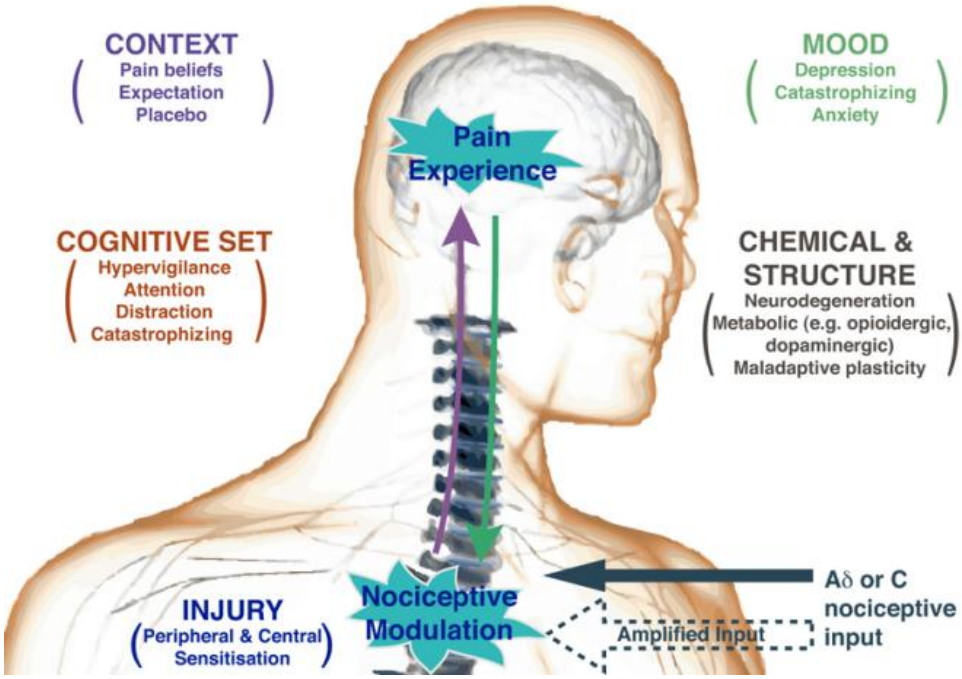

Figure 10: Illustration of the main processes involved in nociceptive modulation and the "coloring" of pain experience (Figure from Tracey and Mantyh, 2007; modified by the author).

2000; Apkarian et al., 2005; Farrell et al., 2005) . Figure 11 provides an overview of the identified brain structures commonly involved in pain perception.

Yet, although this regions are frequently (depending on the experimental procedures) activated during pain perception, it does not mean that they are pain-specific, but rather that they, besides many other things, also process pain (Tracey and Mantyh, 2007). Pain stimuli are highly salient. As such they activate brain mechanisms involved in orienting the attention and body towards a stimulus, perception of the stimulus, evaluation of its unpleasantness and possible danger, triggering of memories, avoidance movement patterns etc. The same applies to other salient stimuli such as loud noises and bright flashes of light. Based on these assumptions it was not surprising when researchers found

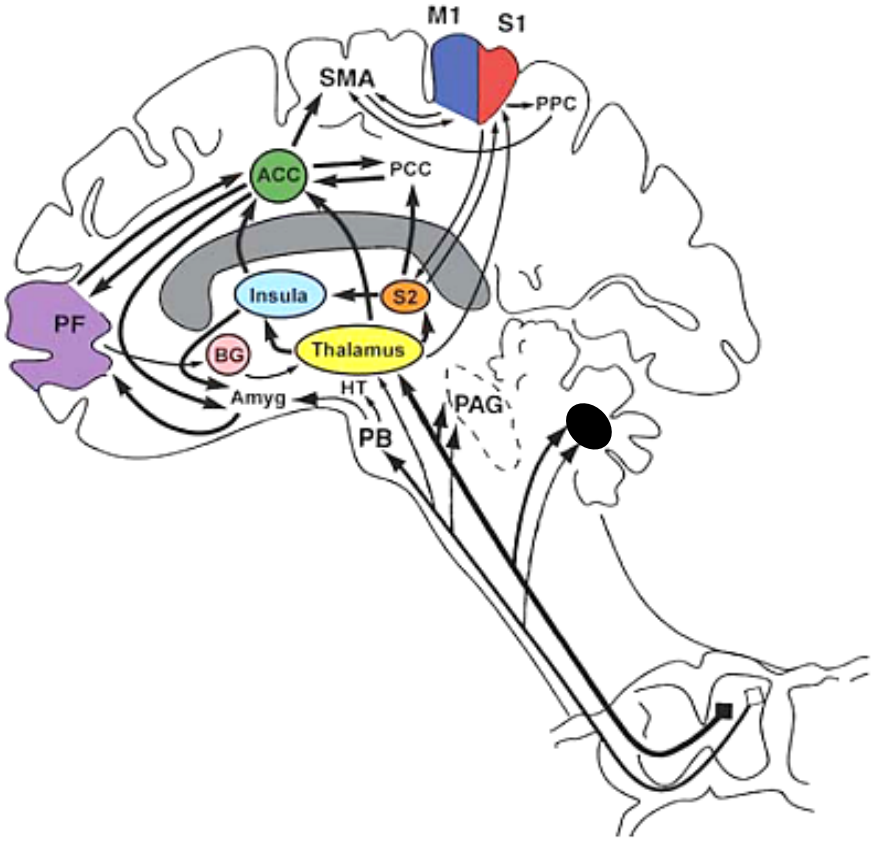

Figure 11: Cortical and subcortical brain structures involved in acute pain perception. Interconnectivity and afferent pathways are illustrated by arrows. S1/S2 = primary/secondary somatosensory cortices, ACC = anterior cingulate, PF = prefrontal cortex. M1 = primary motorcortex, SMA = supplementary motor cortex, PPC = posterior parietal cortex, PCC = posterior cingulate, BG = basal ganglia, HT = hypothalamus, Amyg = amygdala, PB parabrachial nuclei, PAG = periaqueductal gray (Figure from Apkarian et al., 2005, modified by the author).

strongly overlapping activity patterns between nociceptive somatosensory, non-nociceptive somatosensory, auditory and visual stimuli (Mouraux et al., 2011).

Although the pain research community mainly adopted the view of pain sensation being an emergent phenomenon linked to holistic brain activity patterns in the aforementioned brain regions, some researchers continue the quest for areas more specifically involved in the creation of the pain percept. The focus on areas with higher pain specificity is supported by deep brain stimulation

studies, where a vast area of the brain was electrically stimulated. In these studies, the stimulation of many of the above summarized areas failed to induce pain perceptions. The only structures which were associated with the perception of pain when stimulated were the posterior insula and the medial parietal operculum (Mazzola et al., 2012b). These findings have been further validated using fMRI by the same group (Mazzola et al., 2012a), providing evidence for pain specificity in a cytoarchitectonically distinct part of the posterior insula: The posterior granular part of the insula (mostly) contralateral to the stimulation site. The fMRI-study (study 3) conducted in the context of this doctoral thesis addresses this issue by applying a novel pain paradigm. The results provide evidence for a special role of the posterior insula in the percept of pain, hence being in line with the studies from Mazzola et al. (2012, 2012a).

3.1.3 Built-In Loudness Control of Nociceptive Signals: The DPMS

The brain possesses a powerful mechanism capable of modulating afferent nociceptive signals on the spinal cord and TBSNC level. This neural network is called the Descending Pain Modulatory System (DPMS) and is able of modulating the "gain" of nociceptive signals by facilitating or inhibiting signal transmission at the level of the spinal cord and TBSNC (Tracey and Mantyh, 2007; Ren and Dubner, 2011; Denk et al., 2014). The neurocircuitry of the DPMS is schematically depicted in figure 12.

The core structures of the DPMS consist of two regions located in the brainstem: The periaqueductal gray (PAG) and the rostral ventromedial medulla (RVM).

The PAG is considered to be the core structure of the opioid-based top-down pain modulation system, which is well studied on an experimental animal basis (Graeff and Del-Ben, 2008). It is subject to top-down regulation through connections to (sub-)cortical structures of the DPMS , such as areas from the frontal lobe, the thalamus, subregions of the anterior cingulate cortex,

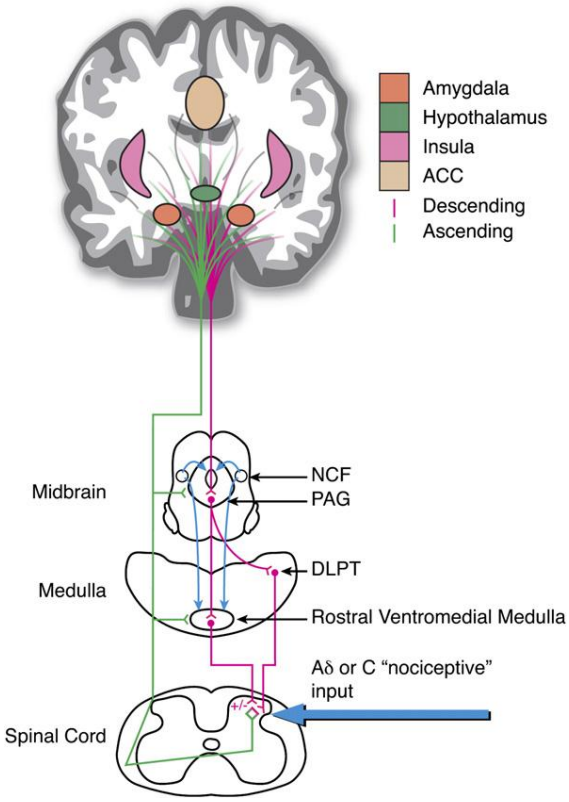

Figure 12: Schematic depiction of the descending pain modulatory system (DPMS). The DPMS consists of a network of brainstem structures: Nucleus cuneiformis (NCF), periaqueductal gray (PAG), dorsolateral pontine tegmentum (DLPT) and rostral ventromedial medulla (RVM). The DPMS is subject to top-down and bottom-up modulation (pink and green lines) and excerts pro- and antinociceptive influences on ascending nociceptive input (indicated by +/- symbols)(Figure from Tracey and Mantyh, 2007; modified by the author).

hypothalamus and amygdala, all structures which also play a role in the formation of pain experiences (Tracey and Mantyh, 2007; Denk et al., 2014).

The PAG projects to the rostral ventromedial medulla (RVM), which inhibits ascending nociceptive signals through its projections to the spinal cord and TBSNC through releases of noradrenaline and 5-hydroxytryptamine (5-HT) (Tracey and Mantyh, 2007; Ren and Dubner, 2011; Linnman et al., 2012; Denk et al., 2014). As previously mentioned, the PAG is also capable of facilitating nociceptive signaling through its projections to the nucleus cuneiformis (NCF)(Tracey and Mantyh, 2007). Pathological imbalances in the inhibitory/facilitatory functions are believed to play an important role in the development and persistence of chronic pain conditions, as shown by various animal studies (Denk et al., 2014).

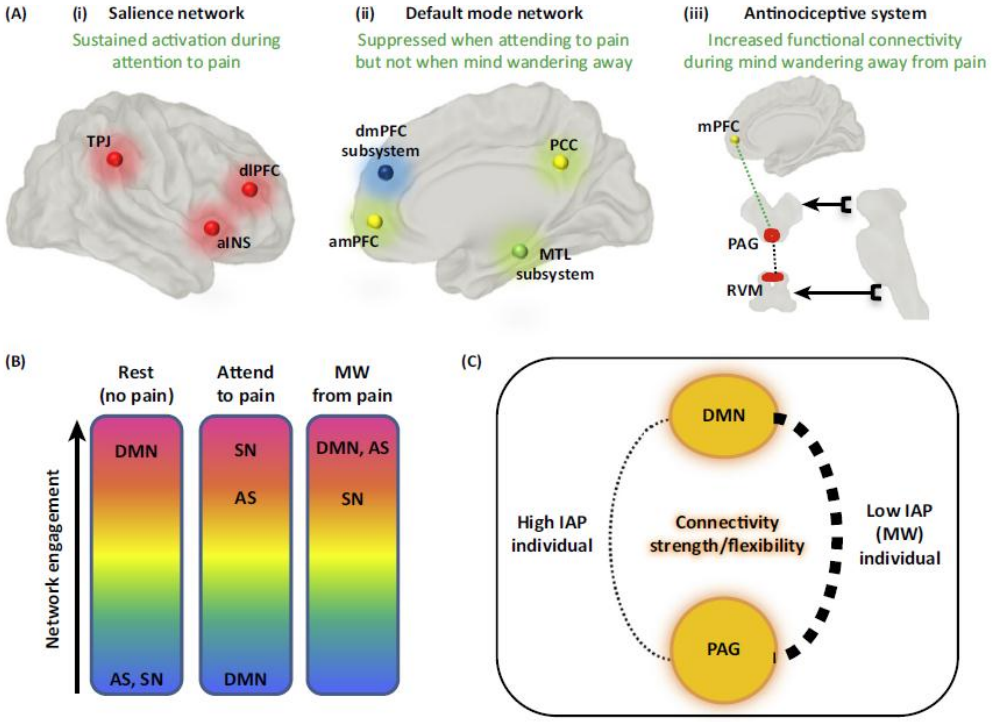

Figure 13: The concept of the dynamic pain connectome. A) Three neural networks are involved in the level of intrinsic attention to pain: The i) salience network (SN), the ii) default mode network (DMN) and iii) the antinociceptive system AS (also termed DPMS by others). B) During rest, attention to pain, or mind wandering away from pain, the three networks are engaged to a different extent. C) People with high or low intrinsic attention to pain (IAP) differ in their functional and structural connectivity between the DMN and AS. (From Kucyi & Davis, 2015)

Top-down regulation of the DPMS is a highly dynamical process. Subjects' participating in our pain studies typically show different levels of fluctuations in perceived pain intensity, despite the administered identical stimulus intensities. I often asked the participants during the psychophysical testing about the thoughts they had during the stimulation procedure. I frequently observed that the phasic changes in mind wandering, distraction, fear etc. reported by the participants correlated with the fluctuations in perceived intensities. Interestingly, a recent line of research has been investigating these effects of sustained attention to and mind-wandering away from pain and identified three neural systems which are key contributors to the ongoing dynamics of pain: The

salience network (SN), the default-mode network (DMN) and the DPMS (Kucyi and Davis, 2015) (see sigure 13). It was found that during the attention to pain, the SN is strongly activated, probably due to the role of the SN in orienting attention towards external stimuli. However, during mind wandering away from pain, the DMN and the DPMS are both stronger engaged and functionally connected (Kucyi and Davis, 2015).

Based on these findings, Kucyi and Davis (2015) developed the concept of "Intrinsic Attention to Pain" (IAP). In their concept, people can be ascribed to low and high IAP groups based on their intrinsic attention levels to pain sensations and their capability to mind wander away from pain sensations (Kucyi and Davis, 2015). Interestingly, people from the low IAP-group show stronger functional and structural connectivity between the DMN and PAG compared to high IAP subjects, hence providing an anatomical and functional basis for their superior capability to disengage from pain perception. These findings provide compelling evidence for the importance of the DPMS in highy dynamic aspects of pain perception (Kucyi and Davis, 2015).

3.1.4 Central Nervous Processes Involved in Chronic Pain

There is no sole mechanism for the cause of chronic pain. In the contrary, chronic pain conditions may be associated with various dysregulatory processes along the whole pain-processing pathway, from the TBSNC/spinal cord to multimodal brain cortices.

<u>Local Aberrant Modulation of Somatosensory Stimuli at the Level of the Dorsal Horn and TBSNC.</u>

As previously mentioned in section 2.1.1, already at the 1st-order synapses in the spinal cord and TBSNC, nociceptive (and innocuous) inputs are subject to modulation. Misregulation including disinhibition and central sensitization can

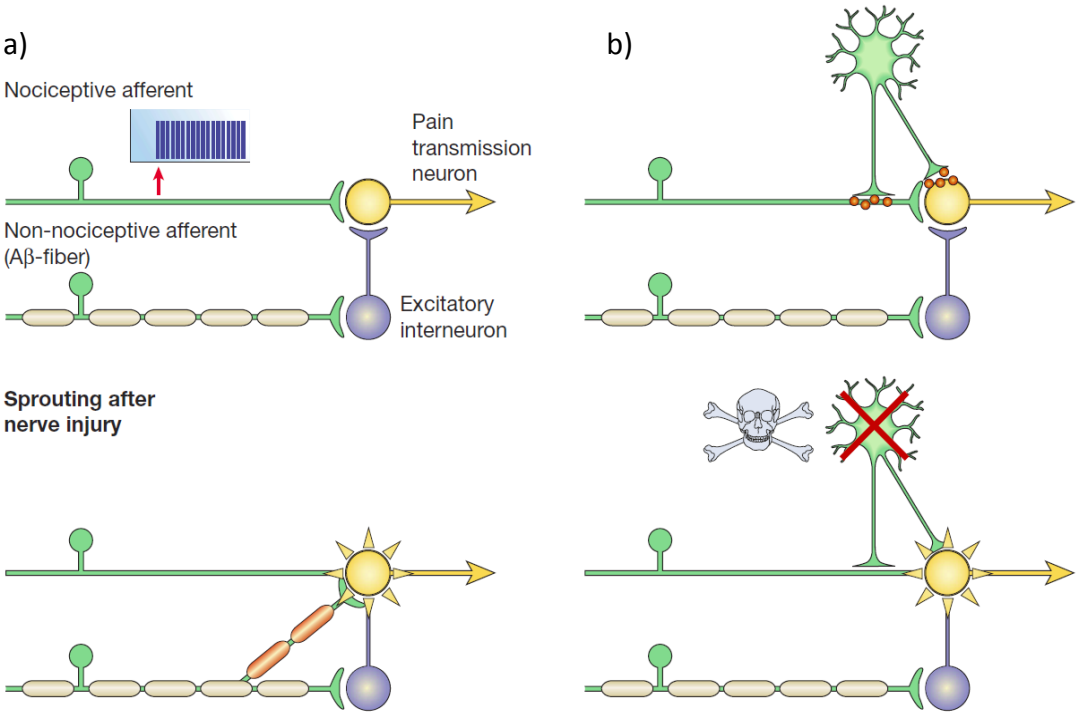

Figure 14: a) Alterations in synaptic connectivity in the spinal cord. Central terminals of myelinated non-nociceptive Aβ-fibers sprout in the dorsal horn and synapse with nociceptive neurons, leading to a painful experience of innocuous afferents. b) Disinhibition. Following peripheral nerve injuries, inhibitory interneurons can be lost due to excessive levels of excitotoxic amino acid glutamate. The loss of interneurons together with reductions in inhibitory neurotransmitter synthesis such as GABA and glycine increases the excitability of pain transmission neurons. As a consequence, these neurons begin to respond to usually innocuous stimuli (Figure from Scholz & Woolf, 2002, modified by the author).

occur at this level (Scholz and Woolf, 2002). Peripheral nerve injuries can result in various aberrant neuroplastic changes in the dorsal horn of the spinal cord and TBSNC which lastly may give rise to chronic neuropathic pain conditions (Sessle, 2000; Scholz and Woolf, 2002). On the one hand, central terminals of myelinated non-nociceptive Aβ-fibres can sprout in the dorsal horn and synapse with nociceptive neurons (Figure 14). The synaptic alterations may result in the painful processing of otherwise innocuous afferents and hence contribute to persistent pain hypersensitivity (Scholz and Woolf, 2002).

On the other hand, examples from animal research show that chronic neuropathic pain resulting from nerve injury can be the consequence of the loss of dorsal horn inhibitory circuits (Figure 14)(Bráz et al., 2012). The loss of GABAergic interneurons leads to a loss of inhibition, manifesting itself as spontaneous pain but also as allodynia and hyperalgesia (Bráz et al., 2012). Further evidence is provided by the study from Bráz et al. (2012). In their study, the transplantation of immature telencephalic GABAergic interneurons from the mouse medial ganglionic eminence (MGE) into the adult mouse spinal cord reversed the mechanical hypersensitivity produced by peripheral nerve injury.

In the same vein, orofacial neuropathic pain has been linked to local changes in the GABAergic inhibitory sytem in the nucleus caudalis of the TBSNC in animal models (Takeda et al., 2011; Sessle, 2016).

DPMS-Mediated Aberrant Regulation of Nociceptive Signaling

During the last decade, the DPMS has become a major research subject in regard to its prominent role in the perpetuation of chronic pain conditions. Under physiological conditions, facilitating and inhibiting efferents of the DPMS are believed to function in concert to create a balance in somatosensory modulation (Denk et al., 2014).

However, different processes have been suggested which are capable of shifting the DPMS towards persisting facilitating mode, thus creating a pathological imbalance. Animal research points towards the loss of inhibitory and facilitatory balance in the DPMS. This loss of inhibition has been linked to plastic changes in its structures as a consequence of ongoing nociceptive signaling. Exemplary are reported plastic changes in the RVM as a result of ongoing afferent input due to peripheral nerve injuries (Porreca et al., 2002). In addition, it has been suggested that enhanced facilitation may be due to an upregulation of NMDA receptors in the RVM due to persisting nociceptive inputs (Terayama et al., 2000).

Hence, a direct baseline assessment of the status of DPMS structures in humans, for example by the characterization of their neurochemical status, may provide important additional information about misregulatory processes in the DPMS. With regard to the PAG, some evidence suggests that glutamatergic and GABAergic systems may distinctively mediate facilitatory and inhibitory processes (Samineni et al., 2017). I hypothesize that the quantification of glutamate and GABA concentration in the human PAG may provide crucial information about the facilitatory/inhibitory balance in humans and should be subject to further ^{1}H-MRS studies.

Yet, there are some studies performed with humans which indirectly investigated the status of the DPMS. For example, studies investigating DMPS-mediated processes such as noxious inhibitory control and pain temporal summation are predictive of the level of postoperative acute pain and of the level of risk for post-surgical chronic pain (Yarnitsky et al., 2008; Weissman-Fogel et al., 2009).

(Sub-) Cortical Processes Involved in Chronic Pain

Neuroimaging studies provided valuable insights regarding the altered connectivity between the DPMS and cortical structures linked to chronic pain patients. A multitude of studies point towards connectivity changes between attention-related cortical structures and the PAG (Kucyi and Davis, 2015). Based on the IAP-concept previously discussed in section 2.1.3, it is conceivable that the level of the intrinsic attention to and within its connectomics may constitute a mechanistic factor that alters structural and functional reorganization over time ultimately leading to misregulation of afferent somatosensory signals (Kucyi and Davis, 2015). In this vein, not only have anatomical changes (gray matter volume and cortical thickness) been found in regions of the DMN, salience network and DPMS in chronic pain populations (May, 2011; Davis and Moayedi,

2013), but also changes in functional connectivity within and between these networks has been identified in chronic pain disorders (Napadow et al., 2010; Baliki et al., 2011; Mainero et al., 2011; Bolwerk et al., 2013; Loggia et al., 2013; Baliki et al., 2014; Yu et al., 2014).

Another (sub-) cortical system that has been linked to the etiology and manifestation of chronic pain is the reward network (Denk et al., 2014). In a longitudinal brain imaging study, subacute back pain patients were examined over the course of one year from the acute pain phase onwards. Pain persisted in 12 patients, whereas pain improved in the other 12. Interestingly, the connectivity strength between the nucleus accumbens (NAc) and the prefrontal cortex (PFC) recorded at the beginning of the study during the acute pain phase, predicted the pain chronification by more than 80%. Furthermore, the increased connectivity between NAc and PFC remained unchanged during the chronification process (Baliki et al., 2012). Altogether, these findings point towards the involvement of the reward-mesolimbic-prefrontal circuitry in the transition to and continuation of chronic pain (Denk et al., 2014).

Another study points towards the involvement of a structure usually associated with declarative memory declaration and consolidation: The hippocampus. The same group that identified the predictive nature of NAc-PFC connectivity in the chronification process also investigated the role of the hippocampus in the same longitudinal brain imaging data and found that the hippocampal-cortical connectivity differed between the pain remission and the pain persisting group. Specifically, the group with persistent pain over the time course of one year showed a large decrease in connectivity between the medial PFC and the hippocampus. Furthermore, the strength in hippocampal-medial PFC connectivity reflected variations in back pain intensity levels over the year (Mutso et al., 2014).

The importance and necessity of a multimodal approach in the investigation of the neural correlates of chronic pain is reflected in the work conducted by Henderson et al. (2013). They investigated the role of the thalamus as a central generator in the formation of neuropathic pain. Patients suffering from trigeminal neuropathic pain (due to nerve lesions caused in chirurgical interventions) and healthy controls were compared using an array of neuroimaging methods such as voxel-based morphometry (VBM), arterial spin labeling (ASL) and ^{1}H-MRS. They found a reduction in the gray matter density accompanied by a decrease in blood perfusion (Henderson et al., 2013). Interestingly, the reduction in gray matter volume and cerebral blood flow in the thalamus was accompanied by a highly significant reduction in GABA concentrations in the thalamus. The combination of the ^{1}H-MRS and ASL data revealed significant changes in the functional connectivity (in primary/somatosensory cortices, anterior insula, primary motorcortex and cerebellum) between the thalamus and cortical pain processing regions in dependence of GABA concentrations, indicating towards a reduction in nociceptive inhibition. These changes were only observed in the neuropathic pain condition, but not in the healthy participants.

4 ^{1}H-MRS in Human Pain Research –Potential and Pitfalls

This chapter aims at discussing the potential and challenges of ^{1}H-MRS for answering important questions in pain research. Firstly, examples are given where ^{1}H-MRS can provide valuable contributions to the field of pain research. And lastly, the pitfalls and challenges of ^{1}H-MRS in pain studies (and studies in general) are discussed.

4.1 Valuable Contributions of ^{1}H-MRS to Pain Research

In the previous chapters, a basic overview was presented about the brain processes underlying physiologic and pathologic pain processing.

When looking at the research conducted at different levels of the CNS, it becomes apparent that types of research are somewhat segregated along the neuraxis. Our knowledge about brainstem processes like neurochemical and cellular mechanisms involved in physiologic nociceptive modulation in health and disease is mostly based on animal research. Few studies on human pain-related structures have been conducted at the level of the brainstem using MR-imaging techniques such as fMRI and DTI (DaSilva et al., 2002; Upadhyay et al., 2008; DaSilva and DosSantos, 2012; Mills et al., 2018). Although these studies provide important insights, the transfer of some of the findings provided by animal-based studies remain unmet regarding humans. Although functional processes between the TBSNC and regions of the DPMS were investigated using fMRI, such investigations still lack the necessary “depth” to elucidate underlying neurochemical processes. The application of ^{1}H-MRS may thus be a viable option to bridge animal and human research on brainstem mechanisms.

In order to clarify this perspective, animal research on the TBSNC shall be taken as an example. Normal nociceptive processing in the TBSNC has been linked to excitatory neurotransmittory processes such the activation of NMDA receptors

via glutamate (Sessle, 2000). On the chronification side, models of trauma, inflammation and nerve constriction injuries point towards the involvement of changes in the GABAergic system. In order to evaluate treatment efficiency and develop new treatment options, it is important to understand how these neurotransmitter systems act in health and in chronic orofacial pain conditions such as trigeminal neuropathic pain. Thus, as ^{1}H-MRS grants access to glutamate and GABA concentrations, it may hold the potential to provide such crucial information and fosters the obtainment of new findings, the prerequisite to more specific treatment development and evaluation.

In the same vein, animal research focusing on the DPMS also suggests the existence of different neurotransmittory systems involved in the facilitatory/inhibitory homeostasis of nociceptive regulation (Samineni et al., 2017). Therefore, the in-vivo assessment of such neurotransmittory systems using ^{1}H-MRS may help shedding light in possible dysfunctional states in the DPMS in humans.

Also regarding the complex functional dynamics of pain processing between (sub-) cortical areas identified with fMRI or ASL, ^{1}H-MRS might be highly auxiliary as a complementary technique for a multimodal investigation of brain dynamics. The previously reported study conducted by Henderson et al. (2013) shall be taken as an example. In their work, they showed that baseline levels of GABA in the thalamus were predictive for the functional connectivity strength between the thalamus and other cortical pain-processing regions. In that vein, ^{1}H-MRS could be applied as a complementary method to explain the nature of functional connectivity patterns by adding a neurochemical component to the fMRI or ASL analysis.

4.2 Pitfalls and Challenges of ^{1}H-MRS in Pain Research

The pitfalls and challenges of ^{1}H-MRS presented in the following sections are not specific to pain research and hence are common to neuroscientific investigations in general.

4.2.1 Anatomical and Functional Specificity

Single-voxel ^{1}H-MRS is usually applied to a-priori defined brain regions based on an underlying scientific question. However, the sensitivity and accuracy to appropriately answer a scientific question strongly depends on the specificity of the voxel.

As an example, the insular cortex as a whole is strongly involved in various aspects of pain processing. Yet, subregions of this cortical structure are distinctively involved in the processing of different pain facets. The insular cortex has been segmented into subregions based on their cytoarchitectonic organization. From these defined subregions, the posterior granular compartment (lg) shows a superior specificity to pain compared to the other types of somatosensory input (Figure 15) (Mazzola et al., 2012a). In that vein, the application of ^{1}H-MRS to the posterior insula could significantly contribute to the question of pain specificity in the posterior by unveiling possible neurochemical underpinnings underlying the observed effects.

However, as previously discussed in section 2.1.2, voxels applied in ^{1}H-MRS investigations have a typical size of 8cm^{3} (Figure 16). In regard to the example with the posterior insular subarea, such voxel dimensions would be impractical as it would include surrounding structures, possibly lacking the same pain specificity. As a consequence, it is conceivable that with such voxel dimensions the results would not provide any evidence for a hypothezized specific role of the posterior insular subarea in pain processing.

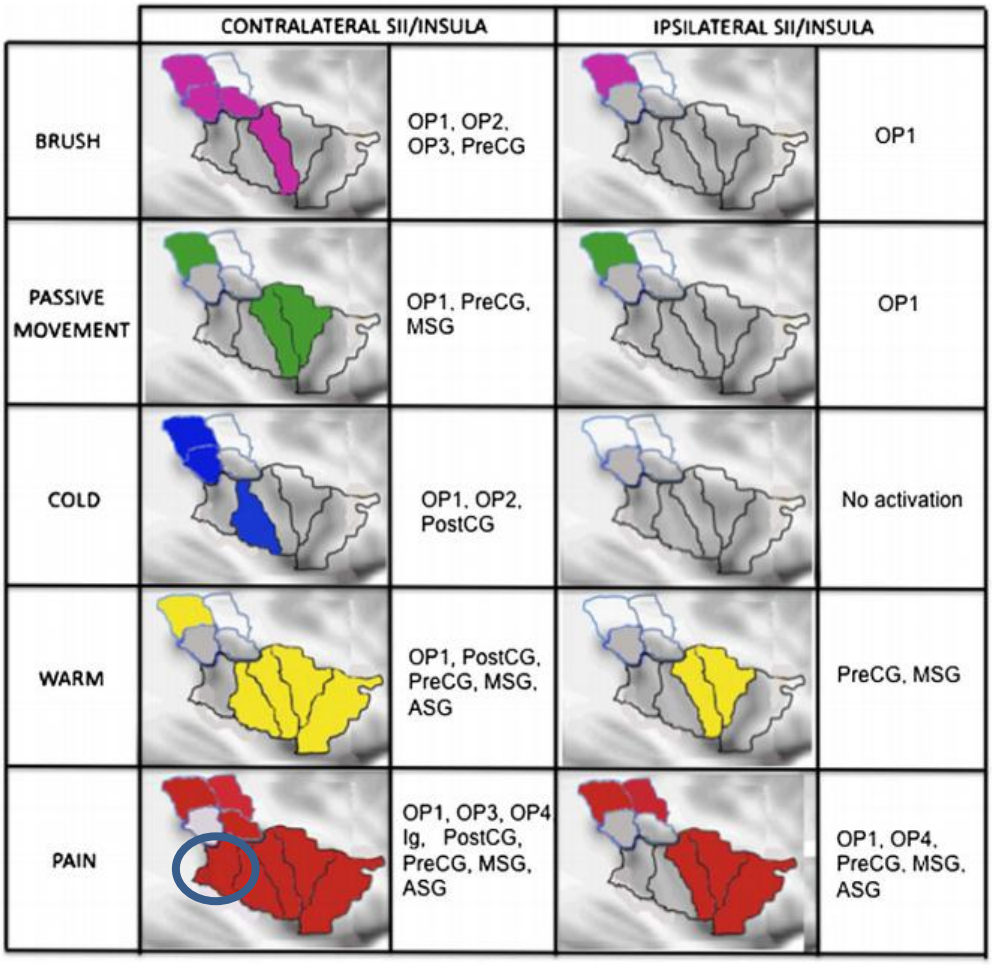

Figure 15: Group activation maps corresponding to various stimulation types applied to the left hand. The insular cortex and adjacent parietal operculum are segmented based on cytoarchitectonical criteria. The only regions showing pain-specificity was the opercular area 3 (OP3) and the posterior granular compartment of the insula contralateral to the stimulation site (blue circle) (Figure from Mazzola et al, 2012a, modified by the author).

During the preparation of such a study, it may be useful to conduct reproducibility analyses in order to determine the impact of optimal voxel dimensions on data quality, fitting errors and the resulting sensitivity of the method in detecting differences in neurochemical compound concentrations. As shown in our reproducibility study (de Matos et al., 2016), the reduction of voxel dimensions to an acceptable specificity level does not have to go along with bad reproducibility.

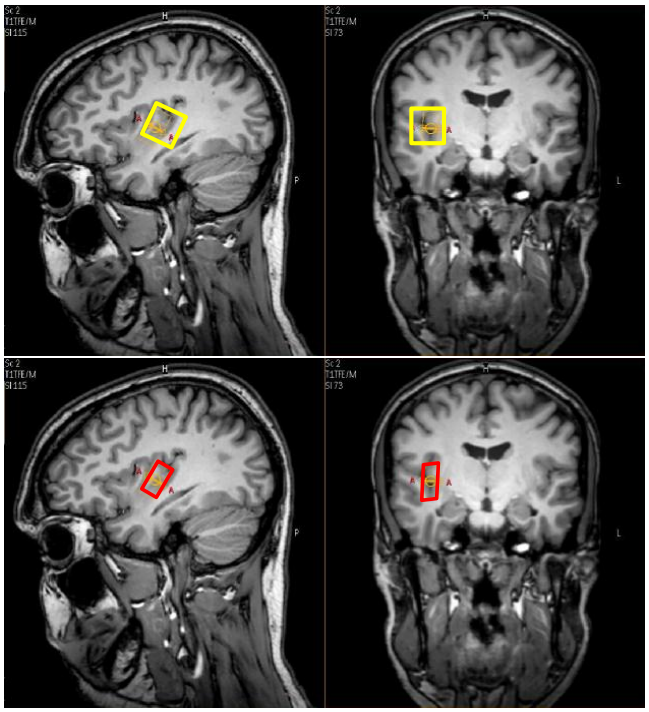

Figure 16: Comparison of voxel specificity in the posterior insula of a typical 8 cm^3 voxel (yellow boxes) and a more specific voxel with a 3 cm^3 volume (red boxes). The 8 cm^3 sized volume shows large levels of partial volume effects due to the inclusion of unwanted regions such as the claustrum, temporal gyri and parietal operculum. Furthermore, the bigger volume contains larger contributions from CSF and white matter, hence further reducing its specificity.

The inclusion of unwanted brain areas and tissue types into the measurement voxel is called partial volume effect (Stagg, 2013). The previous example illustrates possible consequences of the inclusion of areas other than the intended region, which could result in the masking of the effects of interest. Yet, the aspect of the ratio of gray matter (GM), white matter (WM) and cerebrospinal fluid (CSF) in the voxel is also of importance. As most neuroscientific investigations using ^{1}H-MRS focus on GM processes such as neurotransmission, any contribution of WM and CSF to the signal reduces the sensitivity with respect to GM specific processes/mechanisms.

4.2.2 Systematic Errors in Quantification

Variation in SNR and LW can cause systematic errors in the spectrum quantification such as over- and underestimation of neurochemical concentrations in dependence to SNR and LW (Kanowski et al., 2004; Bartha, 2007; Henry et al., 2011; Hong and Pohmann, 2013). Hence, it is of outmost importance to keep differences in SNR and LW between experimental groups and conditions to a minimum. On the one hand, as described in section 2.1.5, the use of thresholds for SNR and LW for data inclusion may be beneficial in reducing such differences due to the exclusion of outlier spectra.

On the other hand, the filtering of spectra in the time domain might be necessary to reduce systematic differences in SNR and LW between conditions. Functional ^{1}H-MRS studies investigating neurochemical responses to a certain task or stimulus (like pain) can be affected by changes in the hemodynamic response.

As described in the introduction of this thesis, neuronal activity modulates local blood perfusion changing the ratio of oxyHb to deoxyHb. A body of evidence suggests that ^{1}H-MRS is also influenced by hemodynamic responses (Zhu and Chen, 2001; Mangia et al., 2007; Koush et al., 2013; Mumuni and McLean, 2017). In fMRI, this process constitutes the underlying mechanism for the identification of brain activity. However, the effect on ^{1}H-MRS is usually less favorable as it directly affects spectral resolution. Changes in the oxyHb/deoxyHb ratios affect the duration of the FID. With the overcompensation in oxyHb due to the hemodynamic response, the FID becomes longer, resulting in reduced LW. As a consequence, spectral resolution may become improved due to increases in blood perfusion, lastly causing differences in spectral LW between experimental conditions. The application of MC-PRESS in functional studies is advantageous due to the conservation of both, the neurochemical and water peaks. As the water signal is acquired simultaneously to the neurochemical signal, it is affected by the same hemodynamic influences. Hence, the water spectrum of one of both

conditions can be filtered to match the water LW of the other condition, automatically removing LW differences in the neurochemical spectrum (Matos et al., 2017).

4.2.3 Physiology-Dependent Signal Disturbances

Structures in the human brainstem are particularly difficult to investigate due to the strong arterial and CSF pulsation arising from surrounding structures. Pulsation causes shifts in B_0, shifting the larmor frequencies of the neurochemicals of interest. As a result, spectral linewidths are reduced.

In addition, as brainstem regions are usually very small in their size, small voxels must be applied to guarantee an acceptable level of anatomical specificity. The downside of the small voxel sizes is that longer measurement times are needed,

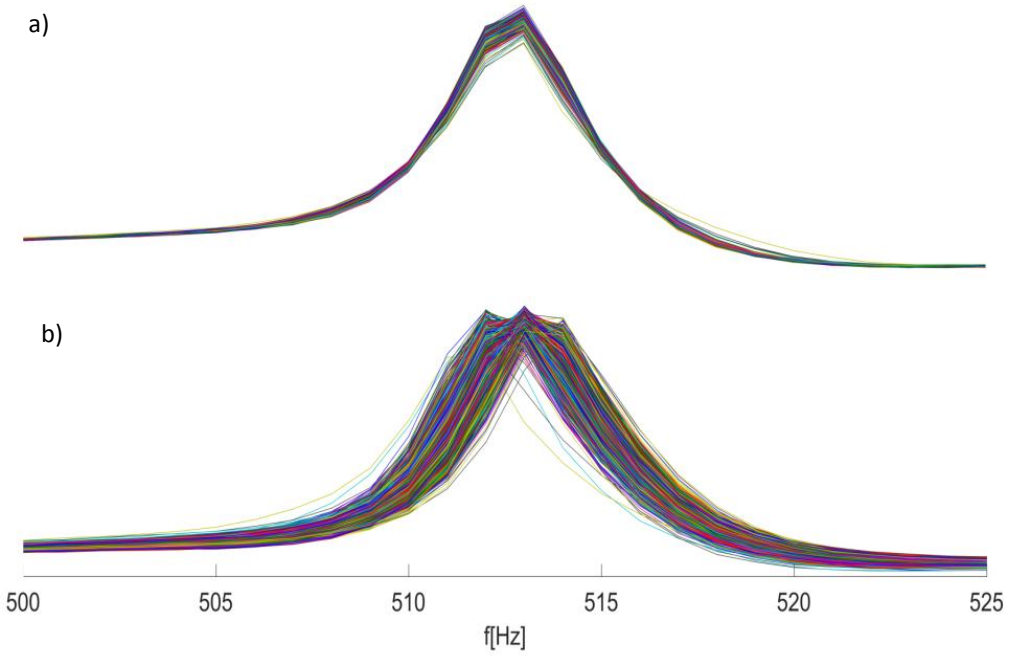

Figure 17: This picture shows the distribution of 512 water peaks from a TBSNC measurement in the brainstem a) after and b) before peak realignment. In b), water peaks are distributed due to frequency shifts caused by various changes in B_0. After realignment, spectral resolution is improved, enabling the quantification of neurochemical information (unpublished data from our TBSNC-^{1}H-MRS study).

thus adding additional B_0-shifts due to B_0-drifts and participant movement. MC-PRESS provides the possibility to align, phase and eddy current correct single spectra before averaging, thus minimizing the impact of these different sources of B_0-changes during the data acquisition (Figure 17). The application of MC-PRESS in our TBSNC-study was the crucial point to accurately obtain important neurochemical effects in the brainstem.

5 Empirical Studies

5.1 Study 1

Reproducibility of neurochemical profile quantification in pregenual cingulate, anterior midcingulate and bilateral posterior insular subdivisions measured at 3 Tesla.

Nuno M. P. de Matos[1,2], Lukas Meier[4], Michael Wyss[3], Dieter Meier[3], Andreas Gutzeit[5], Dominik A. Ettlin[1], Mike Brügger[1,3]

[1]Center of Dental Medicine, University of Zurich, Zurich, Switzerland
[2]Institute for Complementary and Integrative Medicine, University Hospital Zurich and University of Zurich, Zurich, Switzerland
[3]Institute for Biomedical Engineering, University of Zurich and ETH Zurich, Zurich, Switzerland
[4]Seminar for Statistics, ETH Zurich, Zurich, Switzerland
[5]Institute of Radiology and Nuclear Medicine, Hirslanden Hospital St. Anna, Lucerne, Switzerland

Published in Frontiers in Human Neuroscience

5.1.1 Abstract

The current report assessed measurement reproducibility of proton magnetic resonance spectroscopy at 3 Tesla in the left and right posterior insular, pregenual anterior cingulate and anterior midcingulate cortices. 10 healthy male volunteers aged 21 to 30 years were tested at four different days, of which 9 were included in the data analysis.

Intra- and inter-subject variability of myo-inositol, creatine, glutamate, total-choline, total-*N*-acetylaspartate and combined glutamine-glutamate were calculated considering the influence of movement parameters, age, daytime of measurements and tissue composition.

Overall mean intra-/inter-subject variability for all neurochemicals combined revealed small mean coefficients of variation across the four regions: 5.3/9.05% in anterior midcingulate, 6.6/8.84% in pregenual anterior cingulate, 7.3/10.00% in left posterior and 8.2/10.55% in right posterior insula. Head movement, tissue composition and day time revealed no significant explanatory variance contribution suggesting a negligible influence on the data. A strong correlation between Cramer-Rao Lower Bounds (a measure of fitting errors) and the mean intra-subject coefficients of variation ($r=0.799$, $p<0.001$) outlined the importance of low fitting errors in order to obtain robust and finally meaningful measurements.

The present findings confirm proton magnetic resonance spectroscopy as a reliable tool to measure brain neurochemistry in small subregions of the human brain.

5.1.2 Introduction

Neuroimaging taught us a lot about functional principles of the human brain with functional magnetic resonance imaging (fMRI) as leading edge technology. Proton magnetic resonance spectroscopy (^{1}H-MRS) represents another non-invasive magnetic resonance based method. In contrast to fMRI, which relies on relative changes of blood oxygenation, ^{1}H-MRS is able to directly detect and quantify neurochemical components of the living brain. This method provides information about energy metabolism (creatine/phosphocreatine, glucose and lactate), membrane metabolism and integrity (choline) as well as neurotransmission (glutamate, N-acetyl-aspartyl-glutamate, glutamine, GABA, aspartate and glycine). *N*-acetylaspartate and myo-inositol are thought to reflect neuronal and astroglial markers whereas ascorbic acid and gluthatione provide the in-vivo antioxidant profile (Stagg and Rothman, 2013). Compared to fMRI as the mainstay of neuroimaging, ^{1}H-MRS thus holds the potential to provide important and complementary (to fMRI) insights with respect to understanding neurochemical related functional principles of the human brain in both, health and disease.

However, application of ^{1}H-MRS poses several challenges. Generally, the signals are very minute making spectrum quality and succeeding interpretation of acquired data a critical issue (Kreis, 2004). To compensate for this major constraint, frequently applied volumes of interest - termed voxel - are about 8 ml in size. But, such voxel sizes are often too big to optimally capture relevant brain structures considering their functional and anatomical specifications (Stagg and Rothman, 2013). Exemplary are cingulate and insular brain areas with their corresponding subdivisions. They are crucially involved in a multitude of brain functions reflected in high citation rates across the literature by covering an impressive discipline variety. For example, significant functional contributions of these subareas have been demonstrated in chronic (Denk et al., 2014) and acute

pain (Apkarian et al., 2005; Vogt, 2009; Wager et al., 2013), attention deficit hyperactivity disorder (Bush, 2011), anxiety (Damsa et al., 2009), depression (Fountoulakis et al., 2008; Su et al., 2014) and schizophrenia (Takahashi et al., 2003; Haznedar et al., 2004; Costain et al., 2010).

Importantly, a considerable body of literature emphasizes anatomical and functional heterogeneity within those gross cingulate and insular areas. For example, current consensus subdivides the coarse cingulate cortex into six subregions based on cytoarchitectonic and associated functional characteristics (Vogt, 2005, 2009; Dou et al., 2013). In a similar vein, subdividing of the insular cortex into an (at least) anterior and posterior compartment is strongly recommended based on structurally and functionally known attributes (Varnavas and Grand, 1999; Kurth et al., 2010b; Kurth et al., 2010a; Stephani et al., 2011; Mazzola et al., 2012a; Mazzola et al., 2012b; Nieuwenhuys, 2012).

For obtaining more meaningful ^{1}H-MRS measures, voxels should therefore cover functional homogeneous cingulate and insular subregions as distinctly as possible (Dou et al., 2013; Gutzeit et al., 2013).

The critical points are that such subregion dimensions clearly are below 8 ml, and applicable ^{1}H-MRS volumes are limited to cuboid shapes. Those two aspects hamper adequate anatomical coverage of the target areas because gyrification and structure contours are mostly bent. Consequently, voxels should be even smaller than the actual target areas to ensure appropriate anatomical (and functional) specificity.

Additionally, besides covering the desired gray matter (GM), they also include white matter (WM) and cerebrospinal fluid (CSF). Hence, measured signals derived from all these tissue components induce another source of uncertainty regarding meaningful interpretation of the underlying area's specific neurochemistry (Stagg and Rothman, 2013) (in fMRI studies, this issue is circumvented by specific tissue segmentation strategies implemented in all

analysis software packages, but this practice is not yet common in ^{1}H-MRS reports). Therefore, when applying such small voxels in an attempt to optimally capture relevant brain subregions, it must be clarified as to whether quality aspects of ^{1}H-MRS measurements are affected in order to gain the appropriate information with respect to the neurochemical milieu within the target areas.

This study was conceptualized to explore ^{1}H-MRS measurement reproducibility in anatomically and functionally homogenous subregions of cingulate and insular cortices, all substantially below 8ml. Areas investigated were: Pregenual anterior cingulate (pgACC), anterior midcingulate (aMCC), as well as left and right posterior insular cortex (pIL and pIR). Measurements were conducted using standard MR-equipment and ^{1}H-MRS sequences at 3 Tesla in order to allow application and replication in commonly available clinical and research settings.

5.1.3 Materials & Methods

The present study was approved by the local ethics committee and conducted according to the Declaration of Helsinki.

Subjects and Experimental Procedure

10 healthy male volunteers (mean age = 25.3, range: 21-30) were recruited for the study. Exclusion criteria were general contraindications for MR, neurologic and psychiatric diseases as well as any form of pain conditions. Every subject attended four scan visits on different days (mean intersession interval = 11.03 d; SD = 10.98; range = 1-42 d). All acquisitions (except for one measurement which was performed at 2:00 PM) were conducted at one of four time slots in the afternoon and evening (Time slot 1: 4:00 - 5:30 PM; Time slot 2: 5:30 – 7:00 PM; Time slot 3: 7:00 – 8:30 PM; Time slot 4: 8:30 – 10:00 PM). The overall mean starting time was 5:47 PM (SD = 1h 44 min).

Subjects received detailed information about the experimental procedure, aim of the study and provided written informed consent. Participants were informed in detail about the importance of remaining as motionless as possible during the scan sessions. They were further instructed not to consume alcohol, analgesic medication and other drugs on examination days as well as to be fed.

Scanning

Subjects were comfortably positioned in the scanner in a supine position. The Pearltec Crania (Pearltec AG, Schlieren/Zurich, Switzerland) head fixation system was applied for an optimal and comfortable head fixation. MR measurements consisted of a survey scan, a T1-weighted anatomical scan for precise voxel placement and tissue segmentation (duration = 7 min 29 s) followed by four consecutive single-voxel MRS measurements in the four target areas (duration = approximately 6 min each). To consider possible head movements, an adapted short T2-weighted image (duration = 21s) was recorded before and after each MRS sequence in order to estimate the extent of voxel displacements. The measurement order of the brain regions was alternated between the four measurement days to account for measurement order effects and frequency drifts due to heating and other time dependent MR-system changes. The total duration of the MR measurements was approx. 45 min.

MR protocols

MR experiments were performed on a 3-Tesla MR unit (Ingenia, Release 4.1.3, Philips Healthcare, Best, The Netherlands) utilizing a dS-SENSE 15-channel head coil (Philips Healthcare, Best, The Netherlands). Parameter of the T1-weighted turbo gradient echo sequence for voxel placement and segmentation were: TR/TE = 8.1/3.7 ms; flip angle = 8°; FOVFHxAP = 240x240mm; 160 slices; recorded voxel size = 1mm isometric. To calculate possible head movements, a

short T2-weighted turbo spin-echo sequence (<30s) was performed in axial orientation with the following parameters: TR/TE = 3000/80 ms, flip angle = 90°; FOVAPxRL = 230 x 182 mm; resulting voxel size = 1 x 1 x 4 mm.

For the MR spectra acquisition, a conventional single-voxel PRESS (point-resolved spectroscopy) sequence (TR/TE = 2500/32 ms; data points = 1024; sample frequency = 2000 Hz; readout duration = 512 ms; number of acquisitions = 128) was used. A water-unsuppressed spectrum recorded with 16 acquisitions was acquired prior to the main spectrum for post-hoc spectral corrections. Water suppression was achieved using a VAPOR (variable pulse power and optimized relaxation delays) scheme. An implemented automatic second-order projection-based shimming routine (Gruetter, 1993) was used for the reduction of B0-inhomogeneities.

The pgACC and aMCC voxels were carefully placed according to suggestions from specific literature (Vogt, 2005, 2009). The respective dimensions were: pgACC 12 x 16 x 18 mm (AP x LR X FH; 3.46 ml), aMCC 23 x 15 x 12 mm (4.14 ml). Voxel placements for left and right posterior insular subdivisions were based on neuro-anatomic and functional work (Varnavas and Grand, 1999; Kurth et al., 2010a; Mazzola et al., 2012a; Nieuwenhuys, 2012). They were placed posterior and aligned to the insular central sulcus including the gyri longi leading to voxel dimensions of 12 x 11 x 23 mm (3.04ml). Voxel placement was always performed by the same person (NM)(Figure 1).

Quantification of spectroscopic data

Spectroscopic data were quantified with LCModel (Provencher, 1993) using a basis set for an echo time of 32 ms including the following *in vitro* neurochemical model spectra: *N*-acetylaspartate (NAA), *N*-acetyl-aspartyl glutamate (NAAG), glutamate (Glu), glutamine (Gln), γ-aminobutyric acid (GABA), glutathione (GSH), glycerophosphocholine (GPC), phosphocholine (PCh), creatine (Cre), myo-Inositol

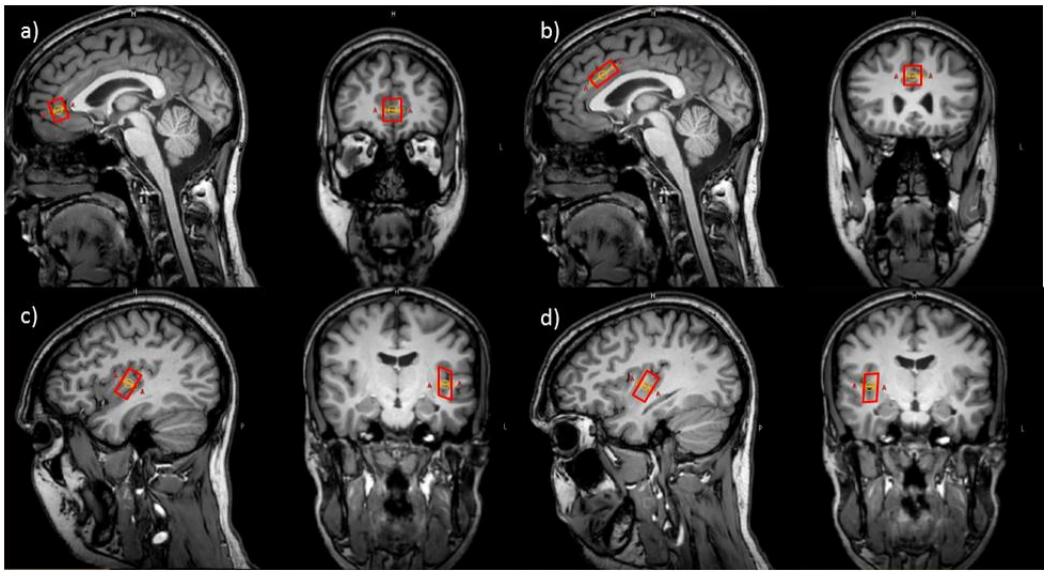

Figure 1: Representative illustration of a voxel positioning on sagittal and coronal plane images in a single subject. a) pregenual anterior cingulate cortex (pgACC), b) anterior midcingulate cortex (aMCC), c) left posterior insula (pIL), d) right posterior insula (pIR).

(mI), ethanolamine and phosphorylethanolamine (PE), aspartate (Asp), glucose (Glc), lactate (Lac), scyllo-inositol (sI) and taurine (Tau). Substances with strongly overlapping spectra were combined to single spectra in order to improve quantification accuracy: Glu + Gln = Glx, GPC + PCh = tCho and NAA + NAAG = tNAA. The chemical shift range for the fitting procedure was set to 4.0-0.2 ppm. Fitted neurochemical concentrations were scaled to the internal water signal obtained from the corresponding water-unsuppressed spectrum acquisition. For all subsequent analysis steps we included the following neurochemicals, which demonstrated Cramér-Rao lower bounds (CRLB) <20%: mI, Cre, Glu, tCho, tNAA, Glx. A correction was applied to account for the fact that metabolic signals originate mainly from WM and GM but not from cerebrospinal fluid (CSF) (McLean et al., 2000). For this purpose, the T1-weighted anatomical images were segmented into brain tissue compartments (GM, WM, CSF) using the segmentation routine included in the SPM8 software package

(http://www.fil.ion.ucl.ac.uk/spm) running on MATLAB 2013b (MathWorks, Natick, USA). The calculation of tissue fractions in the applied spectroscopic voxels were performed using a self-written MATLAB script. The neurochemical concentrations (C_0) were corrected applying the following equation using the estimated fraction of CSF (F_{CSF}) (McLean et al., 2000):

$$C = C_0 * (1/(1 - F_{CSF})).$$

Head movement analysis

Anatomical T2-weighted scans were analyzed to track possible head movements between spectroscopic acquisitions using the realignment function included in the SPM8 software package (http://www.fil.ion.ucl.ac.uk/spm) running on MATLAB 2013b (MathWorks, Natick, USA). Defining the first anatomical scan as reference, following scans were realigned to it providing estimates for translational (mm) and rotational (deg) displacements in the x, y and z-axis over time.

In the next step, maximum displacements in the three translational and rotational orientations were determined for each individual session and then averaged over all sessions. This approach provides a more stringent evaluation of possible movement interference compared to mean intra-session displacements, as it represents more accurate strong head movements.

Statistical and reproducibility analyses

Statistical analyses were carried out with the SPSS Statistics 22 software package (IBM Corp., Armonk NY, USA).

Mean neurochemical concentrations between the four spectroscopy acquisitions were compared with a repeated measure ANOVA (rmA).

In addition, reproducibility was determined by estimating the magnitude of intra- and inter-subject variability by means of coefficients of variation (CV, calculated as SD/Mean*100).

CV is preferable to other dispersion measures due to its independence of the underlying scale (Lovie, 2005).

Measures of reliability like the intraclass correlation (ICC) have also been used in MRS studies. The problem with this measure is its dependence on variation of a trait (like true differences in neurochemical concentrations between persons) in the measured populations, thus impeding a direct comparison of ICC values from different studies (Müller and Büttner, 1994; Henriques et al., 2013). In this vein, a heterogeneous population could yield higher (more reliable) ICC than a homogeneous population despite similar intra-subject variability. We therefore decided not to apply this measure in our study.

Inter-subject variability was calculated by randomly selecting one time point from the four repeated measures of all participants and calculating mean and standard deviation. This step was repeated 5000 times to account for different combination possibilities. Afterwards, the 5000 means and SDs were averaged. The resulting means and SDs were used to calculate the inter-subject CV.

Variations in GM/WM-ratio, daytime of participation and magnitude of between session movements contribute to intra-subject variability (Kreis, 2004; Soreni et al., 2006). Despite the applied precaution to control such effects, they might still have influenced variability. In order to estimate their effects, an ANCOVA with participants and regions as fixed effects (to account for variance attributable to participant and region characteristics) was calculated with GM/WM-ratio, daytime of participation and the absolute voxel displacement (d) as covariates. The vector representing the voxel displacement was calculated as follows:

$$d = \sqrt{X^2 + Y^2 + Z^2}$$

X, Y and Z correspond to the three directions of the voxel displacement; therefore d is the vector of the three displacement directions describing the absolute voxel displacement.

5.1.4 Results

One participant had to be excluded due to problems with the tissue segmentation procedure, resulting in nine full data sets with a total of 36 spectra per region.

Movement

Results from the head movement analysis are summarized in Table 1. The displacement during the sessions was minute, with maximal shifts of 1.5 mm in the X-axis, 1.51 mm in the Y-axis and 1.43 mm in the Z-axis (mean of max. displacements: 0.31±0.23mm (X); 0.43±0.24mm (Y); 0.77±0.37mm (Z)). The estimated maximal rotational changes were negligible with max. rotations of 2.51° in the pitch, 0.79° in the roll and 1.78° in the yaw-angle. We therefore expect head movement to be an insignificant source of variation.

Spectral quality, fitting errors and tissue fractions

One important aspect of chosen voxel dimensions was the maximization of grey matter tissue portion to enhance tissue specificity and account for partial volume

Table 1. Mean, standard deviation (sd) and range of translational (mm) and rotational (deg) movement estimation

	Translation (mm)			Rotation (Degrees)		
	X-axis	Y-axis	Z-axis	Pitch	Roll	Yaw
Mean ± SD	0.31 ± 0.23	0.43± 0.24	0.77 ± 0.37	0.44 ± 0.48°	0.30 ± 0.19°	0.55 ± 0.40°
Range	0.07-1.28	0.08-1.51	0.28-1.43	0.08-2.51°	0.04-0.79°	0.1-1.78°

Table 2. Spectral quality and Tissue fractions in the voxels (Mean ± SD).

	aMCC	pgACC	pIL	pIR
Spectral quality:				
SNR	16 ± 1.79	12.78 ± 1.71	11.94 ± 1.37	11.28 ± 1.43
LW_{H20} (Hz)	0.0532 ± 0.0004	0.0711 ± 0.010	0.0513 ± 0.0025	0.0514 ± 0.0020
Voxel size:	4.14 cc	3.46 cc	3.04 cc	3.04 cc
Tissue composition:				
GM	74.58 ± 2.36%	80.85 ± 2.07%	77.62 ± 2.89%	77.68 ± 4.38%
WM	8.48 ± 3.10%	4.29 ± 1.89%	8.24 ± 2.01%	7.53 ± 1.99%
CSF	16.86 ± 3.58%	14.77 ± 2.98%	14.04 ± 2.75%	14.70.65%

Notes: SNR = signal-to-noise ratio, LW_{H20} = linewidth of the water peak (in Hz), GM = gray matter, WM = white matter, CSF = cerebrospinal fluid, aMCC = anterior midcingulate cortex, pgACC = pregenual anterior cingulate cortex, pIL/pIR = left/right posterior insula.

Table 3. Characteristics of neurochemical concentrations, fitting errors (CRLB) and variability (CV) per region

	aMCC						pgACC					
	mI	Cre	Glu	tCho	tNAA	Glx	mI	Cre	Glu	tCho	tNAA	Glx
Mean CRLB [%][a]	6.7	4.2	6.9	4.5	3.7	6.1	6.5	4.2	6.6	4.9	4.4	6.0
(range)	5-11	4-5	6-8	3-6	3-4	5-7	5-8	3-5	5-8	4-6	4-6	5-7
Mean conc. (A.U.)[d]	4.4	5.3	10.2	1.8	8.1	14.6	4.9	5.7	11.2	2.0	8.0	15.9
Intra-subj SD[b]	0.36	0.25	0.48	0.11	0.27	0.70	0.41	0.32	0.70	0.17	0.36	0.97
(CV%)	8.8	4.7	4.7	5.8	3.4	4.8	8.2	5.8	6.2	8.7	4.4	6.1
Inter-subj-SD	0.63	0.47	0.70	0.16	0.66	1.10	0.58	0.41	1.06	0.18	0.62	1.23
(CV%)	14.3	8.8	6.9	8.7	8.1	7.5	11.8	7.3	9.5	8.9	7.7	7.8

	pIL						pIR					
	mI	Cre	Glu	tCho	tNAA	Glx	mI	Cre	Glu	tCho	tNAA	Glx
Mean CRLB[%][a]	8.7	4.6	8.6	5.7	4.6	7.6	9.1	5.0	9.1	6.6	4.6	8.1
(range)	7-20	4-5	7-12	4-7	4-6	6-9	6-16	4-6	7-12	5-10	4-7	6-11
Mean conc. (A.U.)[d]	4.4	5.9	10.4	1.8	8.2	14.7	4.6	5.9	10.6	1.7	8.3	15.1
Intra-subj SD[b]	0.39	0.27	1.06	0.12	0.35	1.24	0.44	0.48	1.05	0.12	0.47	1.35
(CV%)	9.9	4.5	10.1	6.6	4.2	8.4	9.6	7.9	10.2	7.0	5.7	8.9
Inter-subj-SD	0.74	0.35	1.16	0.18	0.49	1.51	0.65	0.57	1.25	0.17	0.58	1.65
(CV%)	16.7	5.9	11.1	10.1	6.0	10.2	14.0	9.7	11.8	10.0	6.9	10.9%

[a] CRLB = Cramer-Rao Lower Bound. CRLB are estimates of the fitting errors provided by LCModel.
[b] Intra-subject SDs were calculated as the average of individual SD from the four sessions.
[c] Intra-subject CVs were calculated as the average of individual CV from the four sessions.
[d] A.U. = arbitrary units.
aMCC = anterior midcingulate cortex, pgACC = pregenual anterior cingulate cortex, pIL/pIR = posterior insula left/right.
mI = myo-inositol, Cre = creatine, Glu = glutamate, tCho = total choline, tNAA = total *N*-acetyl aspartate, Glx = glutamate + glutamine

effects. The results from the tissue segmentation procedure are shown in table 2. Highest GM contents were found in the pgACC voxels (80.85%), the smallest in the aMCC voxels (74.58%). Accordingly, WM percentages were small with mean values between 8.48% (aMCC) and 4.29% (pgACC). The remaining contributions from CSF were between 16.86% (aMCC) and 14.77% but are insignificant due to the applied CSF-correction.

Differences in tissue percentages between the four sessions could increase intra-subject variability. However, intra-subject differences of GM fractions between the four measurement repetitions were minimal with a mean CV of 1.83% over all participants and regions. We were able to record high quality spectra using small voxel sizes (3.04-4.14 ml) and moderate number of acquisitions (128). The level of SNR in the spectra was between 11.28 (pIR) and 16.00 (aMCC). The mean linewidth of the unsuppressed water signal was <0.054 ppm for allregions except for the pgACC (0.071 ppm).

The good data quality resulted in overall small CRLBs although higher fitting errors were observed in the posterior insulae compared to aMCC and pgACC (Table 3).

Reproducibility

Figure2 provides a descriptive visual illustration of the four repeatedly acquired spectra in a given subject. Figure3 illustrates the overview of intra- and inter-subject variations of neurochemical concentrations over all subjects. Differences in neurochemical concentrations between the four intra-individual measurements were analyzed by means of an ANOVA for repeated measures and no significant differences were found. Estimates of intra-subject and inter-subject variability are summarized in table 3. The overall intra-subject variability was low with mean CV per region over all reported neurochemicals of 5.3%

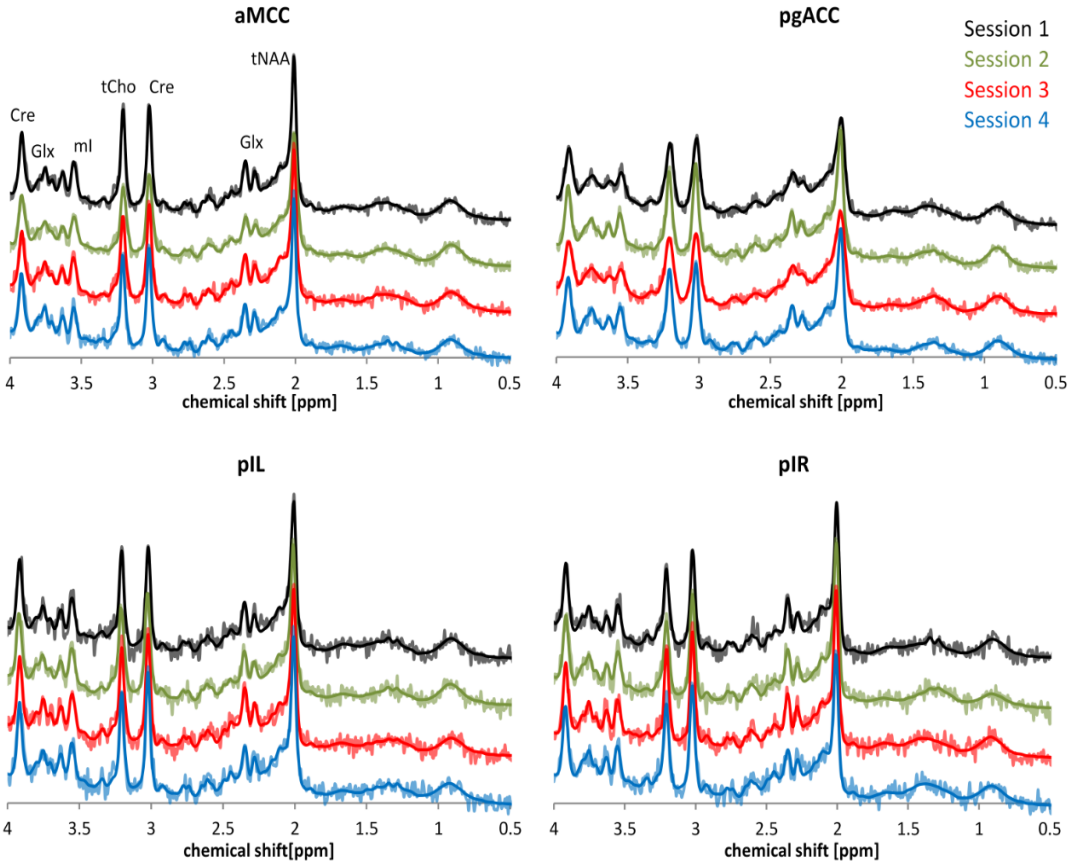

Figure 2: Exemplary depiction of spectral intra-subject variability based on representative spectra of one participant. The time interval between each of the 4 sessions was 7 days. Spectra belonging to the four sessions are illustrated using different colors. Dark lines in the spectra represent the LCModel fit; brighter lines show the underlying raw data.

(aMCC), 6.6% (pgACC), 7.3% (pIL) and 8.2% (pIR). Over all regions, the least variation was observed for tNAA (4.42%) whereas the largest variation was observed for mI (9.12%).

Inter-subject variability showed a similar pattern with mean CV over all reported neurochemicals of 9.05% (aMCC), 8.84% (pgACC), 10.00% (pIL) and 10.55% (pIR). tNAA showed the least mean variability (CV = 7.18%) over all subareas whereas mI had the largest mean dispersion (CV = 14.23%). Differences between intra- and inter-subj. CV were smaller than expected, with a mean difference of just 2.75%, pointing towards minimal subject-specific differences in neurochemical

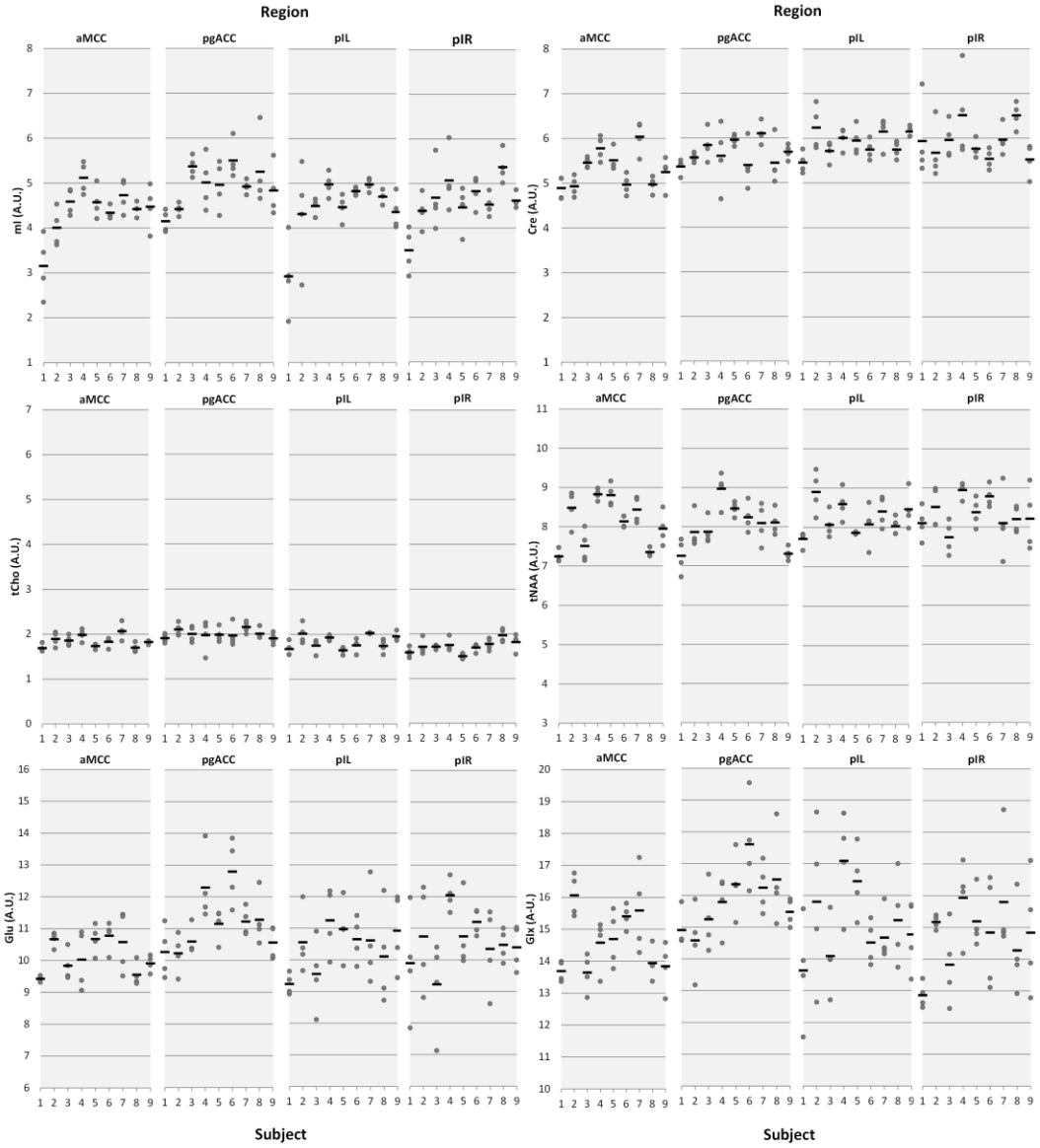

Figure 3: Intra- and inter-subj. variation of neurochemical concentrations illustrated by means of dot plots. Dots represent individual measurements; the horizontal black bars represent the mean of the four measurement days. The X-axis represent the subject number, the Y-axis represent the metabolite concentrations in arbitrary units (A.U.) aMCC = anterior midcingulate cortex, pgACC = pregenual anterior cingulate cortex, pIL/pIR = posterior insula left/right.

concentrations. The small inter-subject effect might be attributable to the homogeneous group of participants tested.

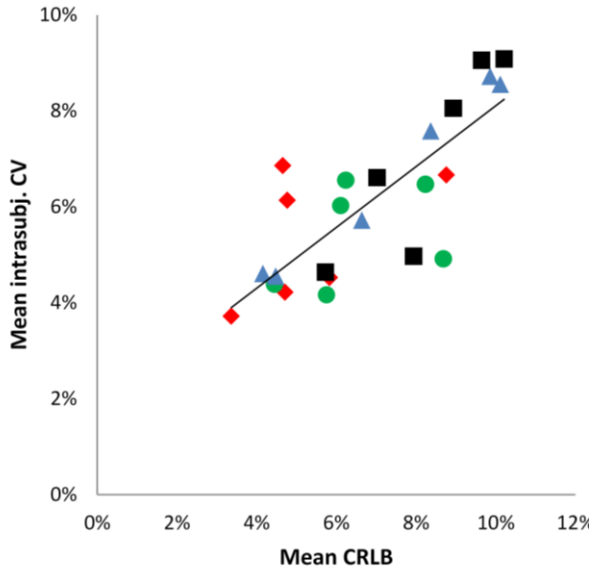

Figure 4: Scatterplot illustrating the positive correlation between mean intrasubject CV and mean CRLBs. Data points represent the six neurochemicals, data point shape and colours correspond to the four brain regions. r = 0.779; R^2 = 0.6382. ◆ = aMCC, ● = pgACC, ▲ = pIL, ■ = pIR.

To test different sources of intra-subject-variability (GM/WM ratio, daytime of participation and head movements), an ANCOVA with participants and regions as fixed effects was conducted using these variables as covariates. This calculation revealed no significant explanatory contribution of variance by the covariates confirming their negligible effect on the data.

In order to estimate the impact of the fitting error expressed as CRLBs, a pearson correlation analysis was performed between mean intra-subject CV and mean CRLB over all neurochemicals for the four regions (figure 4) (according to Geurts et al., 2004), revealing a significant positive correlation ($r=0.799$, $p<0.001$).

5.1.5 Discussion

The current report explored reproducibility of ^{1}H-MRS at 3T in the following subregions of the cingulate and insular cortices: Pregenual anterior cingulate (pgACC), anterior midcingulate (aMCC) cortices as well as left and right posterior insula (pIL and pIR). Results confirm that important neurochemical compounds are reliably quantifiable intra- and inter-subjectively over four measurement sessions on different days. In favor of a better overview, the discussion will be

categorized into four sections: 1) Specificity, 2) data quality, 3) intra-subject variation and 4) inter-subject variation. Afterwards, the results will be discussed in a broader context.

Specificity

In the present context, the term specificity encompasses 1) the accurate positioning of the voxels within the anatomical borders of aMCC, pgACC, pIL and pIR, 2) the achievement of a high gray matter (GM) percentage and 3) is further referred to the exact voxel repositioning across the four measurement days.

Regarding 1), to remain as precise as possible within the regions specific anatomical borders, applied voxel sizes resulted in 3.46/4.14 ml for pgACC/aMCC and 3.04 for pIL/pIR. In terms of both cingulate subareas, we followed the classification scheme suggested by Vogt and colleagues (please see the methods section "Definition and placement of Voxels") as practically as possible. However, note that according to ex-vivo anatomical topography, the unilateral pgACC possesses volumes of about 6.4 ml, and the unilateral aMCC volumes of about 4.3 ml (talairach space)(Vogt, 2009). In order to remain clearly within the anatomical borders together with the limitation of cuboid voxel shapes, the revealed volumes in this report were smaller with 3.46 for the pgACC and 4.14 for the aMCC subareas. Particularly, the pgACC voxel is much smaller than the reported ex-vivo anatomy based volumes reasoning in the contour of this subdivision: it is heavily bent and hence we were coerced to reduce voxel dimensions in order to clearly remain within the pgACC borders. With respect to the aMCC, it was possible to cover the effective shape of this subregion rather accurately as it is a less bent cingulate subarea (see figure 1).

For the pIL and pIR, sizes of 3.04 ml were finally used to approximate the anatomical borders as exactly as possible following several anatomical and functional reports (please see the methods section "Definition and placement of

Voxels"). Please note that the remaining voxels of the posterior insulae contained (however, to a small extent) tissue from surrounding areas (see fig. 1) due to gyrification and anatomical shape of adjacent gyri and temporal located areas. This situation combined with the cuboid voxel issue impeded an even more precise voxel positioning. Higher anatomical specificity might be attainable by further reducing voxel dimensions, however, with critical SNR costs, requiring very long acquisition times hardly applicable for in-vivo measurements. Other specificity enhancement strategies are under development and partly usable i.e. arbitrary voxel shapes. This strategy allows drawing of the region of interest along its exact contours, thus a high spatial selectivity can be theoretically achieved (Weber-Fahr et al., 2009; Snyder et al., 2012).

Regarding 2), results from the tissue segmentation analysis confirmed high GM fractions in our volumes with percentages of 74.58% (aMCC), 80.85% (pgACC), 77.62% (pIL) and 77.68% (pIR). Being able to delineate high GM contents are of particular importance for a multitude of basic neuroscientific/clinical questions as it increases sensitivity for the observation of neurochemical processes associated with neural activity (eg. Synaptic transmission, energy metabolism etc. Mangia et al., 2007b; Mangia et al., 2007a; Gussew et al., 2010) and GM-specific structural changes (eg. loss of neurons indicated by decreases of NAA)(Stagg and Rothman, 2013).

Point 3 can only be indirectly addressed, but small mean GM variations in the voxels (pgACC: 1.61%, aMCC: 1.44%, pIL: 2.15%, pIR: 2.11%) across the four measurement days over all subjects indicate fairly small differences in voxel repositioning.

Data quality

The quality properties of acquired spectra depend on a multitude of variables (for review see Kreis, 2004). Main criteria are peak linewidth and SNR which are

directly linked to voxel sizes. The smaller the voxel, the more negatively SNR is influenced, leading to lower spectral quality. In this report, voxel sizes from 3.04-4-14 ml were applied and revealed acceptable to good spectral quality reflected in SNRs from 11.28 (pIR) to 16.00 (aMCC). On the contrary, spectral resolution can benefit from reduced voxel dimensions by a facilitation of B0-shimming. An enhanced shim allows for narrower and higher peaks enhancing neurochemical peak discrimination and resulting in better SNR (Kreis, 2004).Therefore, SNR loss due to reduced voxel dimensions can be partly compensated by improved shimming (Hock et al., 2013a).

In our study, the revealed spectra resolution (reflected by mean water peak linewidths) was excellent within aMCC (0.0532 ppm) pIL (0.0513 ppm) and pIR (0.0514 ppm) but less within pgACC (0.0711 ppm). pgACC water peak linewidths were more than 25% broader compared to the other three regions. Similar observations have been reported by Dou et al. (2013), using an almost identical pgACC voxel positioning and size. We hypothesize that this concomitant observation might be attributed to interfering effects caused by arteria cerebri anterior (subcallosal artery) pulsation, clearly affecting the accurate shimming of the small pgACC voxel. Furthermore, varying frequency changes in local static magnetic field (B_0) during spectral acquisition, mainly evoked by arterial pulsation, could additionally cause broadening of the peak linewidths (Hock et al., 2013b; Stagg and Rothman, 2013). In this context, techniques applied in spinal cord 1H-MRS – such as frequency alignment of single free induction decays before averaging, or cardiac triggering – can improve spectral resolution obtained from pgACC and other critically located brain areas (Hock et al., 2013a; Hock et al., 2013b).

Generally, the good spectral quality resulted in low overall estimated fitting errors for the reported neurochemicals and regions. Mean CRLB were below 10% (thus lower than the typical consensus of 20%), although the fitting errors were

larger for insular cortex subregions (table 3). This dissimilarity is probably due to the smaller voxel sizes (3.04ml) and therefore slightly lower signal intensities compared to the cingulate subregions (3.46/4.14ml). Important to mention is that higher number of averages per region (although resulting in a longer acquisition time, which is not always feasible) results in increased SNR. This approach could compensate for signal drop accompanied by small voxel sizes thus lowering CRLB values. In this vein, to enhance spectral quality (and therefore reproducibility) it is favorable to combine small voxel dimensions and increased numbers of averages (instead of the usage of big voxels) to get both, narrow peak linewidths and high SNR (Kreis, 2004; Nacewicz et al., 2012).

Intra-subject variability

Results showed small intra-subject variation with mean CVs of 5.3% (aMCC), 6.6% (pgACC), 7.3% (pIL) and 8.2% (pIR) over all reported neurochemicals, indicating robust within-subject measurement reproducibility. Intra-subject variability is a conglomerate of various variance sources. It can be influenced by the software quantification error, inaccurate voxel positioning/repositioning, individual biological variation between measurements (as daytime of participation) and head movement (Kreis, 2004; Stagg and Rothman, 2013). Thus considerable effort was put into controlling variance from the aforementioned factors. As a consequence, head movements were minute, variation of daytime of participation was acceptable. An ANCOVA with participants and region as fixed effects and GM/WM ratio, daytime of participation and head movements as covariates showed no significant explanatory contribution (by the covariates), confirming their rather negligible impact on the data. Otherwise, the fitting error (expressed as CRLB) seems to be a crucial source of intra-subject variance in our data demonstrated by a strong positive correlation ($r = 0.799$) between mean intra-subject CV and mean CRLB over all neurochemicals/regions.

An extreme example for the relationship between intra-subject CV and CRLB can be found in the dot-plot illustrating each single neurochemical concentration (Figure 3). Focusing on the first two participants, obviously higher intra-subject variation of pIL mI concentrations compared to the other subjects is depicted. Analysis of fitting errors showed the highest CRLB exactly for these two subjects (subj. 1 [mean, range]: 13.5%, 9-20%); subj. 2: 10.5%, 7-16%; group average of subj. 3-9: 8%, 7-10%); corroborating our suggestion that CRLB mainly accounts for measured fluctuations in some neurochemicals/regions. We do not have a concise explanation for the outcome of these two participants as all assessed co-variables were unobtrusive.

Inter-subject variability

Inter-subject variations with mean CVs of 9.05% (aMCC), 8.85% (pgACC), 10.00% (pIL) and 10.55% (pIR) were observed. Surprisingly, presented data indicate small differences between inter- and intra-subject CVs with mean CV-difference of 2.75%. We think that the main reason for this observation is the homogeneous sample tested as all participants were male and between 20 and 30 years old. Previous studies showed significant age and gender effects on neurochemical concentrations (Grachev and Apkarian, 2000; Grachev and Apkarian, 2001; Haga et al., 2009), thus our approach in keeping age and gender within a tight range provides a probable explanation for the small differences in present data. This factor should generally be taken into account more rigorously in experimental settings, as effects can be attributed to age dependent alterations in neurochemical signatures rather than to the experimental variation itself (Gutzeit et al., 2013; Stagg and Rothman, 2013).

General discussion of the results within the literature context

In principle, each 1H-MRS reproducibility study is inherently unique due to differences in applied MR scanner equipment and sequences, brain areas measured, number or participants tested, number of measurement sessions performed and the type of statistics finally reported. It is thus advisable to cautiously compare results across publications as no conclusive reproducibility criteria exist (Stagg and Rothman, 2013). Here, we opted to focus on studies investigating insular and cingulate cortex in order to remain within a comparable framework in terms of investigated brain areas. In this report, considerable effort was put into a correct anatomical classification of the regions of interest and the corresponding voxel positioning. Unfortunately, in neuroimaging studies, there is still no overarching rationale that supports identical basic definition regimes with respect to a distinct classification of cortical and subcortical subunits. This fact is reflected even in actual reports as rather imprecise anatomical descriptions are used (e.g. reported is "insula activity" despite the activity is clearly located in "anterior insula subdivision"). The importance of a correct sub-classification was demonstrated by a study conducted by (Gutzeit et al., 2013) showing significant differences in basic neurochemical concentrations between left and right lateralized anterior/posterior insular subdivisions. The differences were robust during acute dental pain stimulation, presumably reflecting inherent functional specificities of these insular subareas.

With respect to the cingulate areas, our approach is based on extensive anatomical and cytoarchitectonic work (see introduction and methods section for all references incorporated). We consider that Dou et al. (2013) are partly in line with the presented anatomical definition, meaning that their investigated cingulate subareas, namely pgACC and aMCC, are almost identical to ours. Yet, the difficulty in comparing the works refers to the fact that they utilized ultra-high fields at 7-Tesla and opted to calculate intraclass-correlations (ICC, instead

of coefficients of variation CV). This value represents a measure of reliability (instead of reproducibility) and therefore depends on population heterogeneity which makes it rather difficult to compare between studies (Müller and Büttner, 1994; Henriques et al., 2013). It has to be clearly noted here that based on their reported ICC values they were able to reach high reliability values as well, however, reporting other neurochemicals as glutamine and GABA. Both components are tedious to detect without applying specific imaging regimes at 3-Tesla.

Venkatraman et al, (2006) estimated 1H-MRS reproducibility aspects in left and right anterior cingulate and hippocampus at 4-Tesla. Their voxel sizes were 6ml (compared to our 4.14ml), thus substantially larger. Based on the information provided (transversal section of voxel positioning scheme), it is not clear how specifically they defined their investigated cingulate subarea. Interestingly, they revealed slightly higher intra-subject CVs compared with our results despite using larger voxels and higher field strengths (Mean CV (right/left hemisphere): tNAA = 10.0/7.2%; tCho = 12.8/9.1%; Cre = 9.5/6.6%; mI = 23.2/12.2%; Glu = 11.8/14.1%; Glx = 17.4/13.3%). In addition to the different sequence parameters and water suppression scheme applied, differences in the CVs could be due to their used variability measure. Venkatraman et al. (2006) reported precision as a measure of reproducibility which was based on 10 repetitive measurements of the same subject (compared to our 9 subjects and 4 repetitive measurements. The differences in the CVs of Venkatraman et al. and our report could be further rooted in their broader linewidth of the right cingulate spectra (ca. 0.068 ppm (right hemisphere) vs our 0.0532 ppm), or that two different cingulate subareas were partly included, namely pgACC and aMCC. Due to variations in their cytoarchitectural structure, related neurochemistry might also differ what could be reflected in the differences reported by Venkatraman and colleagues.

Jang et al. (2005) did reproducibility analyses in the cingulate (similar to our pgACC-volume) and insular cortices using a 3T-scanner and voxel sizes of 4 ml. Contrary to the rationale of the present study, they did not separate between anterior and posterior segments of the insular cortex, thus, their results have to be compared to ours with caution. They revealed CV values for the inter-subject variability (tNAA (pgACC/Insula) = 8.7/9.4%; Cre = 7.6/11.4%; tCho = 11.8/13.1; mI = 13.8/15.9; Glu = 11.0/13.1; Glx = 7.2/11.2). Interestingly, despite applying larger insular cortex voxels, the characteristic reproducibility values were slightly higher than those of our study. It can only be speculated whether this fact results from not accounting for the cytoarchitectonic differences between anterior/posterior insular compartments or due to a more heterogenous study population. Considering the pgACC, their results indicate slightly lower inter-subject variability which might be rooted either in the larger voxel (4 ml to 3.46ml) or attributed to the fact that they measured the pgACC of each of the 21 persons twice and averaged the intra-subj. data thus reducing the intra-subject variance component in the inter-subject variability measures.

Altogether, bearing in mind differences in methodology and voxel definition, our work suggest comparable or slightly superior levels of variability in comparison to studies testing reproducibility of 1H-MRS in the cingulate and insular cortex (Jang et al., 2005; Venkatraman et al., 2006). These results are particularly remarkable regarding the applied voxel sizes which were used for neurochemical quantification in our regions of interest. Therefore, the present report suggests that pgACC, aMCC, pIL/pIR can well be targeted in clinical and scientific questions even using standard MR-equipment and 1H-MRS sequences at 3 Tesla. As pointed out in the introduction section, those areas play pivotal roles in a multitude of brain functions that are predominantly known from fMRI studies. In our opinion, 1H-MRS provides a complementary option by gaining information regarding neurochemical milieus. Knowing such baseline neurochemistry allows

for a more thorough understanding in both, healthy and disease conditions, as in the latter, neurochemical alterations are frequently reported.

Limitations

This report has limitations to consider. Beginning with our primary aim to assess spectra from anatomical/functional homogenous brain areas, we would like to emphasize existing differences across subjects' individual anatomy. The study sample consisted exclusively of 21-30 aged male participants. An adaptation of voxel dimensions may be necessary for the investigation of pgACC, aMCC pIL/pIR in female volunteers or populations with pathological brain conditions due to different brain sizes and pathology-rooted anatomical deviations. Thus, our results may not be generalizable to studies investigating such populations and further studies might be necessary.

In the same vein, the narrow age range could represent a further limitation. Studies have shown that metabolite concentrations are subject to change over the life span (Haga et al., 2009). Our results may therefore not be generalizable to studies using a study sample with different age ranges or/and age groups due to differences in the magnitude of inter-subject variability.

A clear limitation has to be allocated in possible movement influences especially when small areas are targeted. Although using a fixations system (Pearltec Crania) we additionally quantified head movements to estimate voxel displacement between the spectroscopic acquisitions only, hence, intra-measurement movements were not accessible with this approach. However, the small peak linewidths combined with related minute variation indicate rather small movements during acquisitions, possibly related with the choice and positioning of the voxels clearly within the anatomical borders of the targeted brain subareas.

Conclusions

Our study provides information regarding measurement reproducibility of the neurochemical milieu within strictly determined cingulate and insular subareas, namely: pregenual anterior/anterior midcingulate as well and left and right posterior insular cortices. All areas were defined according to anatomical/cytoarchitectonic work to guarantee the best possible within region homogeneity as well as an optimal agreement according to their functional specificity. It can be concluded, that the reported neurochemicals are reliably measurable in those areas as reflected in small intra/inter subject variations. We therefore think that based on the presented rationale, it is possible to conduct 1H-MRS studies in small and functional homogenous – and often critically located – brain areas. When applied with the necessary diligence, we think that profound insights of the neurochemical status in both, health and disease can be obtained, possibly even on single-subject level.

Author Contributions

Conceived and designed the study: NM, MB, MW, DM. Performed the experiments: NM, MB. Analyzed the data: NM, MB, LM, DM. Discussed and interpreted the data: NM LM MW DM AG DE MB. Wrote first draft of the paper: NM, MB. Revised the manuscript and approved the final version: NM LM MW DM AG DE MB.

Funding

This study was funded by the “Forschungskredit” of the University of Zurich (Grant number: 8436).

Acknowledgements:

We thank Niklaus Zölch (Institute for Biomedical Engineering, University of Zurich and ETH Zurich, Zurich, Switzerland) for providing his expertise and help for the tissue segmentation procedure.

5.1.6 References

Apkarian, A. V., Bushnell, M. C., Treede, R.-D., and Zubieta, J.-K. (2005). Human brain mechanisms of pain perception and regulation in health and disease. Eur J Pain 9, 463–484. doi: 10.1016/j.ejpain.2004.11.001

Bush, G. (2011). Cingulate, frontal, and parietal cortical dysfunction in attention-deficit/hyperactivity disorder. Biological Psychiatry 69, 1160–1167. doi: 10.1016/j.biopsych.2011.01.022

Costain, G., Ho, A., Crawley, A. P., Mikulis, D. J., Brzustowicz, L. M., Chow, Eva W C, et al. (2010). Reduced gray matter in the anterior cingulate gyrus in familial schizophrenia: a preliminary report. Schizophrenia research 122, 81–84. doi: 10.1016/j.schres.2010.06.014

Damsa, C., Kosel, M., and Moussally, J. (2009). Current status of brain imaging in anxiety disorders. Current opinion in psychiatry 22, 96–110. doi: 10.1097/YCO.0b013e328319bd10

Denk, F., McMahon, S. B., and Tracey, I. (2014). Pain vulnerability: a neurobiological perspective. Nature neuroscience 17, 192–200. doi: 10.1038/nn.3628

Dou, W., Palomero-Gallagher, N., van Tol, M.-J., Kaufmann, J., Zhong, K., Bernstein, H.-G., et al. (2013). Systematic regional variations of GABA, glutamine,

and glutamate concentrations follow receptor fingerprints of human cingulate cortex. J. Neurosci. 33, 12698–12704. doi: 10.1523/JNEUROSCI.1758-13.2013

Fountoulakis, K. N., Giannakopoulos, P., Kövari, E., and Bouras, C. (2008). Assessing the role of cingulate cortex in bipolar disorder: neuropathological, structural and functional imaging data. Brain research reviews 59, 9–21. doi: 10.1016/j.brainresrev.2008.04.005

Geurts, Jeroen J G, Barkhof, F., Castelijns, J. A., Uitdehaag, Bernard M J, Polman, C. H., and Pouwels, Petra J W (2004). Quantitative 1H-MRS of healthy human cortex, hippocampus, and thalamus: metabolite concentrations, quantification precision, and reproducibility. J Magn Reson Imaging 20, 366–371. doi: 10.1002/jmri.20138

Grachev, I. D., and Apkarian, A. (2000). Chemical Heterogeneity of the Living Human Brain: A Proton MR Spectroscopy Study on the Effects of Sex, Age, and Brain Region. NeuroImage 11, 554–563. doi: 10.1006/nimg.2000.0557

Grachev, I. D., and Apkarian, A. V. (2001). Aging alters regional multichemical profile of the human brain: an in vivo1 H-MRS study of young versus middle-aged subjects. Journal of Neurochemistry 76, 582–593. doi: 10.1046/j.1471-4159.2001.00026.x

Gruetter, R. (1993). Automatic, localizedin Vivo adjustment of all first-and second-order shim coils. Magn. Reson. Med. 29, 804–811. doi: 10.1002/mrm.1910290613

Gussew, A., Rzanny, R., Erdtel, M., Scholle, H. C., Kaiser, W. A., Mentzel, H. J., et al. (2010). Time-resolved functional 1H MR spectroscopic detection of glutamate concentration changes in the brain during acute heat pain stimulation. NeuroImage 49, 1895–1902. doi: 10.1016/j.neuroimage.2009.09.007

Gutzeit, A., Meier, D., Froehlich, J. M., Hergan, K., Kos, S., V Weymarn, C., et al. (2013). Differential NMR spectroscopy reactions of anterior/posterior and

right/left insular subdivisions due to acute dental pain. European radiology 23, 450–460. doi: 10.1007/s00330-012-2621-0

Haga, K. K., Khor, Y. P., Farrall, A., and Wardlaw, J. M. (2009). A systematic review of brain metabolite changes, measured with 1H magnetic resonance spectroscopy, in healthy aging. Neurobiology of Aging 30, 353–363. doi: 10.1016/j.neurobiolaging.2007.07.005

Haznedar, M. M., Buchsbaum, M. S., Hazlett, E. A., Shihabuddin, L., New, A., and Siever, L. J. (2004). Cingulate gyrus volume and metabolism in the schizophrenia spectrum. Schizophrenia research 71, 249–262. doi: 10.1016/j.schres.2004.02.025

Henriques, T., Antunes, L., Bernardes, J., Matias, M., Sato, D., and Costa-Santos, C. (2013). Information-based measure of disagreement for more than two observers: a useful tool to compare the degree of observer disagreement. BMC Med Res Methodol 13, 47. doi: 10.1186/1471-2288-13-47

Hock, A., Fuchs, A., Boesiger, P., Kollias, S. S., and Henning, A. (2013a). Electrocardiogram-triggered, higher order, projection-based B0 shimming allows for fast and reproducible shim convergence in spinal cord 1 H MRS. NMR Biomed. 26, 329–335. doi: 10.1002/nbm.2852

Hock, A., MacMillan, E. L., Fuchs, A., Kreis, R., Boesiger, P., Kollias, S. S., et al. (2013b). Non-water-suppressed proton MR spectroscopy improves spectral quality in the human spinal cord. Magnetic resonance in medicine 69, 1253–1260. doi: 10.1002/mrm.24387

Jang, D.-P., Lee, J.-M., Lee, E., Park, S., Kim, J.-J., Namkoong, K., et al. (2005). Interindividual reproducibility of glutamate quantification using 1.5-T proton magnetic resonance spectroscopy. Magn Reson Med 53, 708–712. doi: 10.1002/mrm.20387

Kreis, R. (2004). Issues of spectral quality in clinical 1H-magnetic resonance spectroscopy and a gallery of artifacts. NMR Biomed 17, 361–381. doi: 10.1002/nbm.891

Kurth, F., Eickhoff, S. B., Schleicher, A., Hoemke, L., Zilles, K., and Amunts, K. (2010a). Cytoarchitecture and probabilistic maps of the human posterior insular cortex. Cereb. Cortex 20, 1448–1461. doi: 10.1093/cercor/bhp208

Kurth, F., Zilles, K., Fox, P. T., Laird, A. R., and Eickhoff, S. B. (2010b). A link between the systems: functional differentiation and integration within the human insula revealed by meta-analysis. Brain Struct Funct 214, 519–534. doi: 10.1007/s00429-010-0255-z

Lovie, P. (2005). “Coefficient of Variation,” in Encyclopedia of Statistics in Behavioral Science, eds B. S. Everitt, and D. C. Howell (Chichester, UK: John Wiley & Sons, Ltd).

Mangia, S., Tkác, I., Gruetter, R., Van De Moortele, Pierre-Francois, Maraviglia, B., and Uğurbil, K. (2007a). Sustained neuronal activation raises oxidative metabolism to a new steady-state level: evidence from 1H NMR spectroscopy in the human visual cortex. Journal of cerebral blood flow and metabolism : official journal of the International Society of Cerebral Blood Flow and Metabolism 27, 1055–1063. doi: 10.1038/sj.jcbfm.9600401

Mangia, S., Tkác, I., Logothetis, N. K., Gruetter, R., Van De Moortele, Pierre-Francois, and Uğurbil, K. (2007b). Dynamics of lactate concentration and blood oxygen level-dependent effect in the human visual cortex during repeated identical stimuli. Journal of neuroscience research 85, 3340–3346. doi: 10.1002/jnr.21371

Mazzola, L., Faillenot, I., Barral, F.-G., Mauguière, F., and Peyron, R. (2012a). Spatial segregation of somato-sensory and pain activations in the human operculo-insular cortex. Neuroimage 60, 409–418. doi: 10.1016/j.neuroimage.2011.12.072

Mazzola, L., Isnard, J., Peyron, R., and Mauguière, F. (2012b). Stimulation of the human cortex and the experience of pain: Wilder Penfield's observations revisited. Brain 135, 631–640. doi: 10.1093/brain/awr265

McLean, M. A., Woermann, F. G., Barker, G. J., and Duncan, J. S. (2000). Quantitative analysis of short echo time (1)H-MRSI of cerebral gray and white matter. Magn Reson Med 44, 401–411.

Müller, R., and Büttner, P. (1994). A critical discussion of intraclass correlation coefficients. Stat Med 13, 2465–2476.

Nacewicz, B. M., Angelos, L., Dalton, K. M., Fischer, R., Anderle, M. J., Alexander, A. L., et al. (2012). Reliable non-invasive measurement of human neurochemistry using proton spectroscopy with an anatomically defined amygdala-specific voxel. Neuroimage 59, 2548–2559. doi: 10.1016/j.neuroimage.2011.08.090

Nieuwenhuys, R. (2012). The insular cortex: a review. Progress in brain research 195, 123–163. doi: 10.1016/B978-0-444-53860-4.00007-6

Provencher, S. W. (1993). Estimation of metabolite concentrations from localizedin vivo proton NMR spectra. Magn. Reson. Med. 30, 672–679. doi: 10.1002/mrm.1910300604

Snyder, J., Haas, M., Dragonu, I., Hennig, J., and Zaitsev, M. (2012). Three-dimensional arbitrary voxel shapes in spectroscopy with submillisecond TEs. NMR in biomedicine 25, 1000–1006. doi: 10.1002/nbm.2764

Soreni, N., Noseworthy, M. D., Cormier, T., Oakden, W. K., Bells, S., and Schachar, R. (2006). Intraindividual variability of striatal (1)H-MRS brain metabolite measurements at 3 T. Magn Reson Imaging 24, 187–194. doi: 10.1016/j.mri.2005.10.027

Stagg, C., and Rothman, D. L. (2013). Magnetic resonance spectroscopy: Tools for neuroscience research and emerging clinical applications. Amsterdam: Academic Press.

Stephani, C., Fernandez-Baca Vaca, G., Maciunas, R., Koubeissi, M., and Lüders, H. O. (2011). Functional neuroanatomy of the insular lobe. Brain structure & function 216, 137–149. doi: 10.1007/s00429-010-0296-3

Su, L., Cai, Y., Xu, Y., Dutt, A., Shi, S., and Bramon, E. (2014). Cerebral metabolism in major depressive disorder: a voxel-based meta-analysis of positron emission tomography studies. BMC psychiatry 14, 321. doi: 10.1186/s12888-014-0321-9

Takahashi, T., Suzuki, M., Kawasaki, Y., Hagino, H., Yamashita, I., Nohara, S., et al. (2003). Perigenual cingulate gyrus volume in patients with schizophrenia: a magnetic resonance imaging study. Biological Psychiatry 53, 593–600. doi: 10.1016/S0006-3223(02)01483-X

Varnavas, G. G., and Grand, W. (1999). The insular cortex: morphological and vascular anatomic characteristics. Neurosurgery 44, 127-36; discussion 136-8.

Venkatraman, T. N., Hamer, R. M., Perkins, D. O., Song, A. W., Lieberman, J. A., and Steen, R. G. (2006). Single-voxel 1H PRESS at 4.0 T: precision and variability of measurements in anterior cingulate and hippocampus. NMR Biomed 19, 484–491. doi: 10.1002/nbm.1055

Vogt, B. A. (2005). Pain and emotion interactions in subregions of the cingulate gyrus. Nat. Rev. Neurosci. 6, 533–544. doi: 10.1038/nrn1704

Vogt, B. A. (2009). Cingulate neurobiology and disease. Oxford, New York: Oxford University Press.

Wager, T. D., Atlas, L. Y., Lindquist, M. A., Roy, M., Woo, C.-W., and Kross, E. (2013). An fMRI-based neurologic signature of physical pain. N. Engl. J. Med. 368, 1388–1397. doi: 10.1056/NEJMoa1204471

Weber-Fahr, W., Busch, M. G., and Finsterbusch, J. (2009). Short-echo-time magnetic resonance spectroscopy of single voxel with arbitrary shape in the living human brain using segmented two-dimensional selective radiofrequency excitations based on a blipped-planar trajectory. Magn Reson Imaging 27, 664–671. doi: 10.1016/j.mri.2008.10.004

5.2 Study 2

Neurochemical dynamics of acute orofacial pain in the human trigeminal brainstem nuclear complex

Nuno M. P. de Matos[1,2], Andreas Hock[3,4], Michael Wyss[3], Dominik A. Ettlin[1], Mike Brügger[1,3]

[1]Center of Dental Medicine, University of Zurich, Zurich, Switzerland
[2]Institute for Complementary and Integrative Medicine, University Hospital Zurich and University of Zurich, Zurich, Switzerland
[3]Institute for Biomedical Engineering, University of Zurich and ETH Zurich, Zurich, Switzerland
[4]Philips Healthcare, Hamburg, Germany

Published in Frontiers in NeuroImage

5.2.1 Abstract

The trigeminal brainstem sensory nuclear complex is the first central relay structure mediating orofacial somatosensory and nociceptive perception. Animal studies suggest a substantial involvement of neurochemical alterations at such basal CNS levels in acute and chronic pain processing. Translating this animal based knowledge to humans is challenging. Human related examining of brainstem functions are challenged by MR related peculiarities as well as applicability aspects of experimentally standardized paradigms.

Based on our experience with an MR compatible human orofacial pain model, the aims of the present study were twofold: 1) from a technical perspective, the evaluation of proton magnetic resonance spectroscopy at 3 Tesla regarding measurement accuracy of neurochemical profiles in this small brainstem nuclear complex and 2) the examination of possible neurochemical alterations induced by an experimental orofacial pain model.

Data from 13 healthy volunteers aged 19 to 46 years were analyzed and revealed high quality spectra with significant reductions in total N-acetylaspartate (N-acetylaspartate + N-acetylaspartylglutamate) (-3.7%, $p = 0.009$) and GABA (-10.88%, $p = 0.041$) during the pain condition. These results might reflect contributions of N-acetylaspartate and N-acetylaspartylglutamate in neuronal activity-dependent physiologic processes and/or excitatory neurotransmission, whereas changes in GABA might indicate towards a reduction in tonic GABAergic functioning during nociceptive signaling.

Summarized, the present study indicates the applicability of 1H-MRS to obtain neurochemical dynamics within the human trigeminal brainstem sensory nuclear complex. Further developments are needed to pave the way towards bridging important animal based knowledge with human research to understand the neurochemistry of orofacial nociception and pain.

5.2.2 Introduction

Pain in general and orofacial pain in particular are complex multifaceted phenomena encompassing sensory, affective, cognitive and motor processes. Worldwide costs, suffering and psychosocial distress especially in chronic forms are immense (Maixner et al., 2011; Murray and Lopez, 2013). Related brain mechanisms have been disentangled up to a certain degree, with several (predominantly cortical) areas being involved in decoding specified information from the underlying pain cascade (Peyron et al., 2000; Wager et al., 2013; Denk et al., 2014). In contrast to these quite well described (pain related) neuronal correlates, the brainstem still remains scarcely characterized, particularly in humans (Beissner and Baudrexel, 2014).

As neuronal gate to and from the cortex, this structure is involved in a multitude of vital functional processes and of crucial importance for our daily survival. The functional spectrum of this area covers co-control of breathing, sleep-wake rhythms, blood pressure, heart rate, pain modulation and even higher cognitive and psychological functions (Sessle, 2005; Fairhurst et al., 2007; Hurley et al., 2010).

Listed as one of the most prevalent pain conditions, orofacial pain seems strongly associated with maladaptive brainstem processing (Sessle, 2000; Maixner et al., 2011). The collective term “orofacial pain” encompasses a variety of pain types perceived in the face, jaw and oral cavity including acute (eg. dental pain) and chronic conditions (eg. trigeminal neuralgia; trigeminal neuropathic pain; burning mouth syndrome; temporomandibular disorders) (Zakrzewska, 2013). One commonality of these different pain types is that their nociceptive information is exclusively transmitted to the brain via the trigeminal brainstem sensory nuclear complex (TBSNC) (Sessle, 2000). This intricate nuclear cluster represents the first relay station in the brain for peripheral somatosensory afferents from the trigeminal nerve (and to a smaller extent from the facial and

glossopharyngeal nerves) (Sessle, 2000; DaSilva and DosSantos, 2012). It consists of three nuclei ranging from the mesencephalon down to the cervical dorsal horn, namely: mesencephalic, principal and spinal trigeminal nucleus (Nieuwenhuys et al., 2008). The spinal trigeminal nucleus (Sp5) is further subdivided into three subnuclei in a rostral to caudal fashion: Subnuclei pars oralis, pars interpolaris and pars caudalis (Dubner and Bennett, 1983; Beck et al., 1997; Nieuwenhuys et al., 2008). The TBSNC (Sp5 in particular) receives nociceptive signals from the ipsilateral site of the face and mouth via Aδ and C-fibers and forwards them via 2nd-order neurons to the contralateral ventral posteromedial nucleus (VPM) of the thalamus from which the stimuli are further projected to several cortical structures (Nieuwenhuys et al., 2008).

Based on animal studies, cellular and neurochemical alterations in the TBSNC were suggested being crucially involved in processing acute pain as well as in maladaptation mechanisms leading to pain chronification. Neurochemicals released in the TBSNC by afferents, interneurons and (pain) modulatory pathways – most notably GABA, 5-HT and opioids – alter the processing of nociceptive input on that basal CNS level (Sessle, 2000). Exemplary are various investigations demonstrating changes in GABAergic neurotransmission associated with trauma, inflammation and partial deafferentation (Sessle, 2000; Viggiano et al., 2004; Takeda et al., 2011). Additionally, evidence is given by chronic neuropathic pain models. Using a constriction injury model of the rat infraorbital branch of the trigeminal nerve (CCI-ION), only baclofen (a $GABA_B$-receptor agonist) but not carbamazepine, morphine or tricyclic antidepressants were able to reduce the allodynia-like behavior (Idänpään-Heikkilä and Guilbaud, 1999). Using a similar model, Martin et al. (2010) found a decrease in GAD65 immunoreactivity in the caudal nucleus of the Sp5 suggesting a disruption in GABA-mediated inhibitory circuits.

Few human neuroimaging studies addressed the specific functional/anatomical contributions of the TBSNC in acute and chronic orofacial pain by applying functional magnetic resonance imaging (fMRI) (DaSilva et al., 2002), diffusion tensor imaging (DTI) and voxel-based morphometry (VBM) (Wilcox et al., 2015). However, none of the performed neuroimaging studies provided insights regarding neurochemical alterations in the human TBSNC thus corroborating some results provided by animal studies. But this question could be addressed by proton magnetic resonance spectroscopy (^{1}H-MRS), a powerful method able to simultaneously quantify neurochemical compounds in a defined brain region. Typically measured neurochemicals provide for example information about neuronal density and viability (*N*-acetylaspartate), energy metabolism (creatine/phosphocreatine), membrane turnover and integrity (choline), antioxidant status (glutathione), glial cell proliferation (Myo-inositol) or neurotransmission (Glutamate, GABA, N-acetyl-aspartyl-glutamate)(Stagg, 2013). Theoretically, ^{1}H-MRS allows observing neurochemical processes and alterations associated with acute and chronic (orofacial) pain conditions within relevant brainstem nuclei. Thus a bridge from human research to the animal studies on TBSNC might be in reach.

However, in-vivo measurements on brainstem levels face a series of significant challenges as technical, structural and physiological characteristics of the brainstem and spinal cord impede proper MR acquisitions. Blood flow in adjacent arteries/venes and CSF pulsation in and around the brainstem induce inhomogeneity in the static magnetic field (B_0) thus causing frequency shifts resulting in poor spectral resolution (Brooks et al., 2013; Beissner and Baudrexel, 2014; Hock et al., 2013). Furthermore, the signal obtained by ^{1}H-MRS is in general very minute, demanding large measurement volumes (usually voxel sizes of 8 ml) in order to achieve sufficient signal-to-noise ratios (SNR) in a reasonable acquisition time (Kreis, 2004; de Matos et al., 2016). But, measuring the TBSNC

with the adequate anatomical and functional specificity demands smaller voxel sizes and hence requires adaptations towards long acquisition times. Those, in turn enhance the likelihood for temporal changes in the B_0 field caused by subject motion and B_0 drifts resulting in frequency and phase shifts between single free induction decays (FIDs). All these facets hamper spectral quality aspects and require careful planning and adequate measurement strategies (Hock et al., 2013c).

In this feasibility study, we provide a brainstem optimized ^{1}H-MRS sequence and data post processing scheme in combination with a reliable experimental dental pain model in healthy volunteers. The following two questions were pursued: 1) ^{1}H-MRS measurability aspects of a small brainstem area from a technical perspective and 2) possible alterations in the neurochemical milieu induced by experimental dental pain.

5.2.3 Materials and Methods

The present study was conducted from March 2015 to December 2015 according to the Declaration of Helsinki and was approved by the local ethics committee.

Subjects

26 healthy males (mean age: 27.35 ± 6.84, range: 19-46) were recruited for the study. Inclusion criteria required the test tooth (right upper canine) to be vital, caries free, sensorically intact and free of previous dental treatments. Exclusion criteria were psychiatric and neurologic diseases, regular pain medication intake, pain syndromes, claustrophobia and general contra-indications for MR. No female volunteers were recruited due to possible variability in pain perception caused by menstrual cycle associated variation in hormonal levels (Wiesenfeld-Hallin, 2005).

All subjects received detailed information about the experimental procedure, aim of the study and provided their written informed consent before any procedure was performed. Subjects were instructed not to consume alcohol, analgesic medication and other drugs 24h before the start of the MR experiment and to be fed before participation. Participants were explicitly informed to have the possibility to terminate participation and withdraw from the study at any time. They were financially compensated (40 Swiss francs/hour) for the effective time of participation.

From the initial 26 recruited participants, 8 were excluded after the test session due to insufficient and/or inconstant pain intensity perception; therefore 18 subjects were included in the study. Two subjects had to be excluded due to spectral artifacts and two others due to insufficient spectral resolution ($FWHM_{NAA}$ > 10Hz). An additional subject had to be excluded due to strong movements during the experimental conditions, resulting in a total of 13 (mean age: 27.69 ± 7.89, range: 19-46) data sets for analysis.

Dental Stimulation Setup

Dental stimulation was administered to the right upper canine. For this purpose, individual dental splints with non-ferromagnetic stainless steel electrodes embedded directly at the center of labial and palatal surfaces were fabricated. To reduce electrical resistance, small portions of hydrogel (size ca. 3x3mm) covering the electrodes were applied before splint insertion.

In addition to the tooth stimulating electrodes, a small 2 MΩ resistor (surface-mount device, SMD, KOA Corporation, Tokyo, Japan) was placed on the left side of the dental splint over the second left incisor tooth and sealed with Blu-Mousse (thixotropic vinyl polysiloxane; Parkell, Edgewood, USA). This resistor served as “dummy tooth” enabling running of the stimulation procedure during

the baseline measurements without evoking sensory perceptions. This approach allowed for identical conditions during baseline and pain ^{1}H-MRS measurements. For details regarding splint fabrication and stimulation equipment specs, please see Gutzeit et al., 2013.

Psychophysical testing and familiarization

Subjects were invited to a test session 1-2 weeks prior to the MR-experiment. The aim of this preceding visit was fourfold: 1) Check of inclusion/exclusion criteria, 2) manufacturing of the dental splint, 3) psychophysical testing of the subjects' sensory and pain thresholds and 4) familiarization of the participant with the dental stimulation procedure and equipment.

The psychophysical testing consisted of the administration of electrical pulses of 1 ms duration with linearly increasing electrical currents and randomized inter-stimulus-intervals (ISI) 5-8s long. The procedure started at an imperceptible intensity of 1 mA; the intensity was then increased in steps of 1 mA. Thresholds for sensory detection (SDT), pain detection (PDT), and a stimulus intensity corresponding to the subjects' individual rating of 4-5 (moderately painful) on a NRS were obtained. 4-5 was the target pain intensity for the pain stimulation condition in the MR-experiment. Subjects indicated the SDT, PDT and 4-5 by hand signs. This procedure was repeated 3 times to assure the stability of individual sensory thresholds as well as account for novelty effects and potential initial feelings of uneasiness associated with the dental stimulation.

Experimental Procedure

At the beginning of the MR-experiment, psychophysical testing (procedure identical to the test session) was performed and the SDT, PDT and intensity of 4-5 was evaluated outside the scanner to test the participants' current perceptual characteristics.

The subjects were then positioned in the 3-Tesla MR unit (Philips Healthcare, Best, The Netherlands) in a supine position. Since small voxel dimensions were applied in an anatomical localization difficult to investigate, it was crucial to keep head movements at a minimum. Multipad positioning cushions (Pearltec AG, Schlieren / Zurich, Switzerland) were used for this purpose. Two were bilaterally placed between the temple and the coil, and a third was positioned under the participant's neck/occipital head. Subjects adjusted the cushion inflation for optimal comfort which is essential considering the extended measurement durations. Participants were instructed to press the alarm button in case of discomfort caused by the head fixation system.

After acquisition of anatomical sequences and placement of the MRS-voxel, the baseline MRS measurement was obtained. During this baseline condition, dummy stimulation was applied. Psychophysical testing was then repeated inside the scanner to adjust, if necessary, the electrical current strength evoking a 4-5/10 pain intensity. Prior to the painful measurement sequence, correct voxel placement was verified on another set of anatomical images and adjusted if necessary. Electrical stimulation during the baseline and pain stimulation block consisted of 128 short pulses (1 ms, identical characteristics as during the psychophysical testing) administered with an ISI of 10-12.5s (block duration: approx. 21 minutes). Previous work demonstrates that the applied dental stimulation paradigm is not prone to sensitization and habituation effects during long measurement periods (Brügger et al., 2012). The total duration of the MR measurement was approx. 60 min.

MR protocol

The integrated body coil was used for transmission (maximum B1 = 13.5 µT); a receive-only 8 channel head coil array (Philips Healthcare, Best, NL) was applied for signal reception. Anatomical high-resolution T2-weighted turbo spin-echo

sequences were performed in axial and sagittal orientations (TR/TE = 3000/120; Flip-angle = 90°; voxel size 0.8x1x3.2mm3) to ensure precise voxel planning and positioning.

For the MR spectra acquisition, an inner-volume saturated (IVS)(Edden et al., 2006; Hock et al., 2013), non-water suppressed PRESS (point-resolved spectroscopy) sequence (TR/TE = 2500/32 ms; data points = 1024; sample frequency = 2000 Hz; readout duration = 512 ms; number of averages = 512) was used via the metabolite cycling (MC) technique (MC-PRESS) (Dreher and Leibfritz,

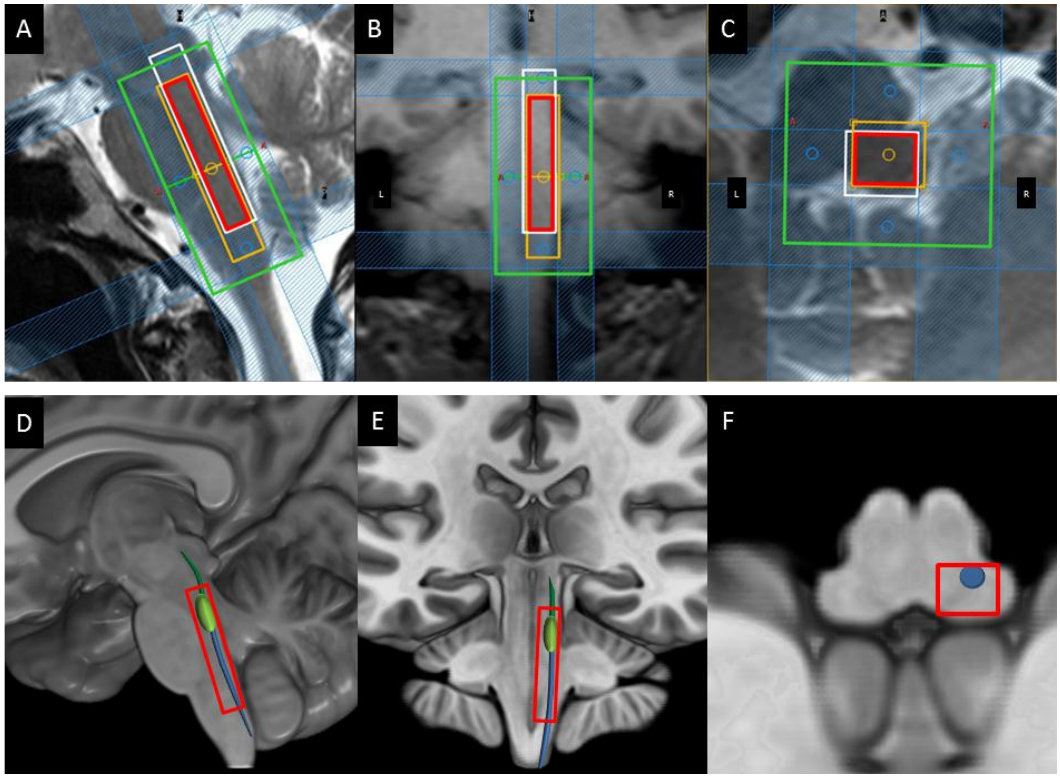

Figure 1: Panels A-C illustrate the MRS voxel placement on sagittal (A), coronal (B) and transversal (C) anatomical images. Orange and white boxes represent the acquisition volumes of lactate (orange) and myo-inositol (white) which are shifted relative to each other due to the chemical shift artifact. This artifact is reduced by the use of inner-volume saturation (IVS) bands. The red box corresponds to the resulting excitation volume generating the MRS signal. In addition, the shim box is represented by the green box. Panels D-F illustrate the position of the excitation volume (red) in relation to the schematically represented TBSNC with the associated mesencephalic (dark green), primary (light green) and spinal trigeminal nuclei (blue) on sagittal, coronal and transversal images.

2005; Hock et al., 2013). This enables a simultaneous recording of water and neurochemical signals, by adding or subtracting consecutively acquired echoes modulated via alternate up- or downfield inversion pulses which do not affect the water signal (Dreher and Leibfritz, 2005; Hock et al., 2013). Therefore, MC-PRESS allows the acquisition of high SNR water-peaks from single FIDs, permitting frequency alignment, phase and eddy current correction before averaging of neurochemical spectra. Hence, MC-PRESS provides the potential to reduce frequency shifts caused by pulsatile effects of blood vessels/CSF and B0 drifts. Furthermore, the simultaneous acquisition of both water and neurochemical signals means that both are subject to the same MR-specific and physiologic influences thus optimizing the use of the water peak as an internal reference during neurochemical quantification.

To optimally cover the region of interest, the MRS voxel was carefully placed along the transition zone to the 4th ventricle. Important to note: due to individual shapes and contours of the volunteers' brainstem, the placements were adjusted to avoid contamination of the MRS voxel with CSF from the 4th ventricle, central canal and cisterna magna. The voxel was placed on the ipsilateral side in reference to the stimulated tooth using following dimensions: 37.6 x 8.5 x 7.6 mm (2.4ml, Fig. 1).

MRS data post processing

MRS data were post-processed according to Hock et al. (2013; 2016). The individual 512 FIDs were truncated after 100ms and zero-filled to 1024 points, followed by frequency alignment, phase and eddy current correction of individual FIDs before averaging. These steps were performed using in-house scripts running on MATLAB 2013b (MathWorks, Natick, MA, USA).

In case of a significant mismatch of spectral linewidth estimates between both conditions, filtering by means of an exponential multiplication was performed to

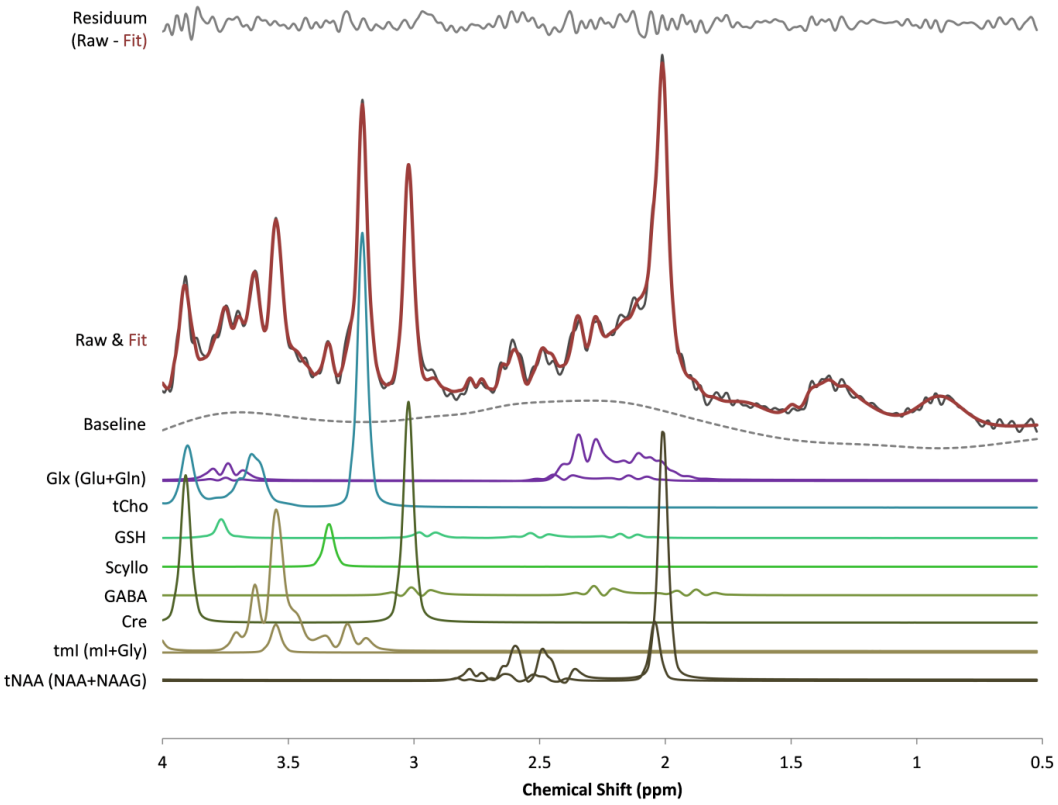

Figure 2: Exemplary spectrum fitted with LCModel. The fitted spectum (red) is superimposed on the raw spectrum (grey). The difference of raw and fitted spectrum is displayed by the residuum which is an indicator for the goodness-of-fit. The spectral baseline is delineated by the dashed grey line. The fits of the reported neurochemicals are displayed below the baseline.

minimize systematic errors in neurochemical quantification. This approach prevents false neurochemical differences between the conditions (Mangia et al., 2007). The correction was done by matching the water peak linewidth to the water peak linewidth of the pain spectrum. Individual filter parameters were chosen to ensure the best match possible for each participant.

Quantification of Neurochemicals

Neurochemicals were quantified with LCModel (Provencher, 1993) using a set of basis spectra which were simulated using the GAMMA Simulation Package (Smith et al., 1994). The basis set included the following components: N-acetyl

aspartate (NAA), N-acetyl-aspartyl glutamate (NAAG), glycerophosphocholine (GPC), phosphocholine (PCh), creatine (Cre), myo-Inositol (mI), glycine (gly), alanine (Ala), ascorbic acid (Asc), aspartate (Asp), ethanolamine and phosphorylethanolamine (PE), glutamine (Gln), glutamate (Glu),
glutathione (GSH), glucose (Glc), γ-aminobutyric acid (GABA), lactate (Lac), taurine (Tau) and scyllo-inositol (sI). The chemical shift range was set to 4.0-0.5 ppm. Following neurochemicals with strongly overlapping spectra were combined to one single spectrum: Glu + Gln = Glx, GPC + PCh = tCho, mI + Gly = tmI and NAA + NAAG = tNAA.

With respect to neurochemical related inclusion criteria, we followed the suggestions provided by De Graaf (2007): Neurochemicals with CRLB<10% count as measured with sufficient precision, neurochemicals with CRLB <20-30% should be considered with caution whereas neurochemicals with CRLB >30% are deemed unreliable and should therefore be excluded from the analysis. Hence, the following neurochemicals were included: tNAA, tCho, tmI, Cre, Glx, GSH, Scyllo and GABA.

We decided to use water (from the simultaneously acquired water spectra) as internal reference instead of Cre due to the following reasons:

1. Previous pain MRS studies observed significant alterations in Cre concentrations (see Gutzeit et al., 2013).
2. Reduced sensitivity due to combined quantification errors of Cre and the other neurochemicals (resulting in higher variation).
3. Unspecific Cre signal changes could either under- or overestimate "true" effects in other neurochemicals evoked by the experimental conditions.

Movement

Two navigator sequences were performed during both conditions. This procedure enables two different approaches to reduce the impact of motion on

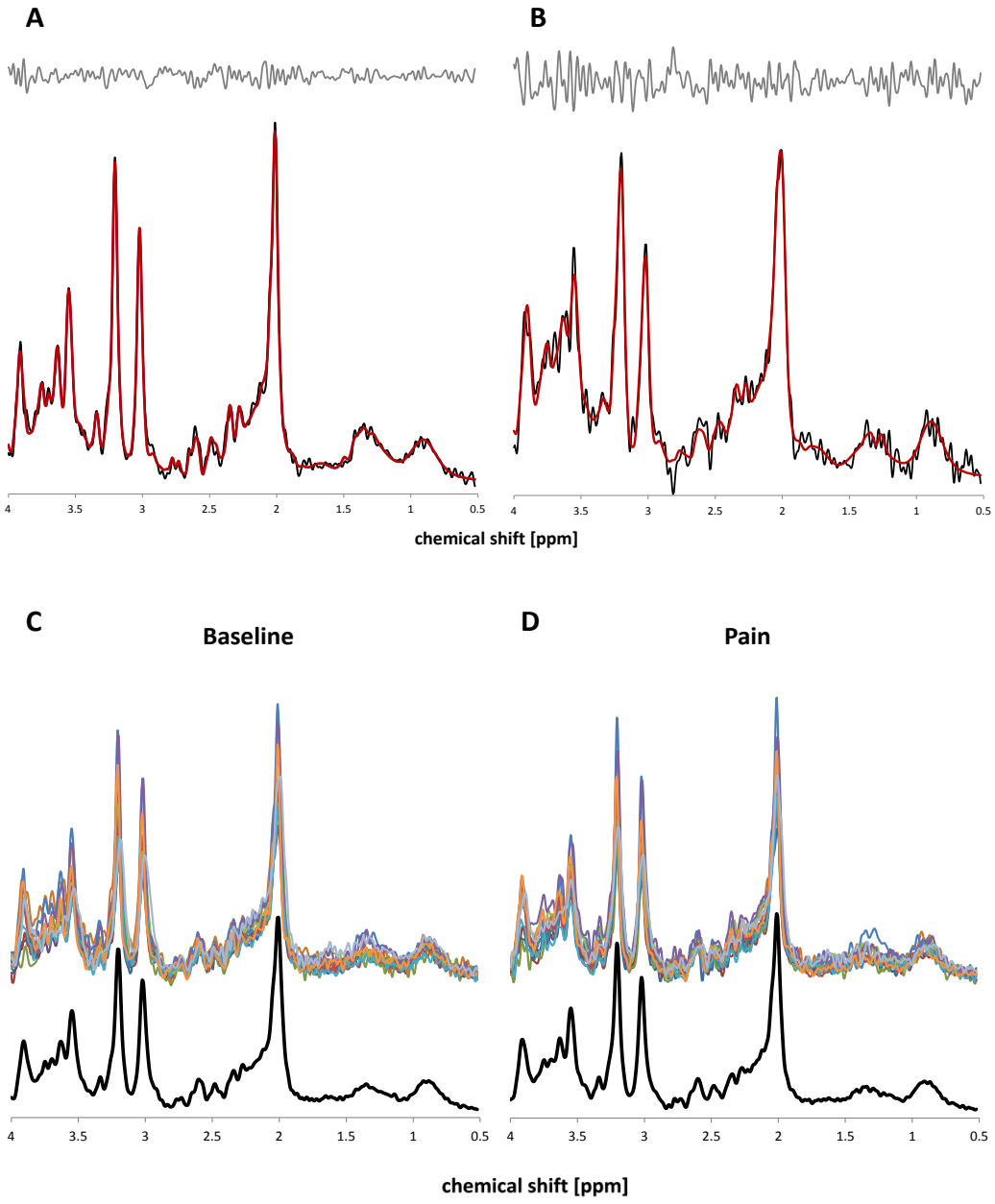

Figure 3: Overview of the spectral quality range of included spectra. Quality estimates (from LCModel) of the best spectrum (A) were: SNR = 23, Linewidth = 4.85 Hz. Estimates of the worst (B) were: SNR = 12, Linewidth = 7.79 Hz. Mean spectral quality over all spectra: SNR = 19.08, Linewidth = 6.41 Hz. Panels C and D illustrate the spectral variability as overlay of all 13 included spectra (colored lines) with the corresponding averaged spectrum (black) for the baseline (C) and

the neurochemical data: Firstly, real time feedback to instruct the volunteers not to move and secondly, rejecting data sets with excessive levels of motion.

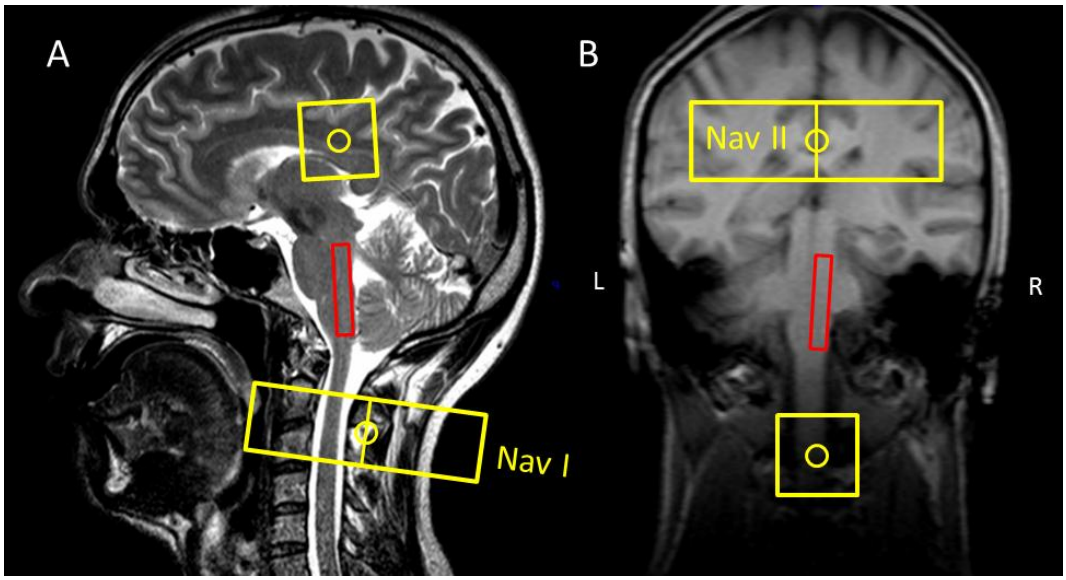

Figure 4: Placement of the two navigators (orange) shown on sagittal (A) and coronal (B) images. The lower navigator (Nav I) measured movement in the anterior-posterior axis, he upper navigator (Nav II) measured movement in the left-right axis. The red box corresponds to the MRS excitation volume.

Navigator sequences were carried out in the dead time before the inner-volume saturation (IVS) pulses of each single MRS acquisition (pencil-beam excitation with radius r = 30mm and length l = 100mm; flip-angle = 15°, acquisition duration = 2.9ms) (Hock and Henning, 2016).

The first navigator (Nav I, anterior-posterior axis) was positioned ventral to the MRS voxel perpendicularly oriented to the medulla. The second one (Nav II, left-right axis) was placed dorsally to the MRS-voxel covering corpus callosum and occipital areas (Fig. 4).

Navigator positions were extracted from the raw MR data using MRecon (GyroTools, Zurich, Switzerland). The extracted movement data was used for the calculation of relative movement during individual scans using the first navigator acquisition as reference. A gating window of ±1mm was used to identify echoes associated with significant movement. Navigator data demonstrating excessive noise were excluded (See excluded data sets in supplementary material).

Spectra from individual participants were excluded from the analysis based on their movement estimates if more than 10% of the individual spectral acquisitions were shifted outside the gating window.

Statistical analysis

SPSS 22 (IBM Corp., Armonk, NY, USA) was used to perform the statistics; the significance threshold was set at $p < 0.05$. First, data were tested for normal distribution by means of the Shapiro-Wilk test. Differences between both experimental conditions regarding neurochemical concentrations were tested using a paired t-test, whereas comparison of SNR and linewidth was tested using a Wilcoxon signed-rank. In order to estimate reproducibility, inter-scan variability (variability between baseline and pain condition for each participant) was estimated by means of coefficient of variation (CV, calculated as SD/Mean*100).

5.2.4 Results

Data quality

Mean spectral quality and fitting error estimates for both conditions are shown in table 1.Linewidth estimates provided by LCModel differed significantly between both conditions ($Z = -2.670$, $p = 0.008$). In order to minimize linewidth differences, individual baseline spectra were filtered resulting in negligible linewidth differences ($Z = -0.509$, $p = 0.611$).

Mean SNR was 19.1 for both conditions and thus not significant ($Z = 0.000$, $p = 1.000$).

The good data quality is also reflected by the low CRLB over all spectra and all subjects (Baseline: 9.6%; Pain: 11.1%). As a consequence, resulting inter-scan CV

Table 1: Estimates of spectral quality and fitting errors (CRLB) of the included spectra from the baseline and pain conditions. In addition, inter-scan variation estimates are presented as coefficients of variation (CV). Values are reported as means ± SD.

	Baseline	Pain	P
Spectral quality:			
$FWHM_{NAA}$[Hz] [a]	6.6 ± 1.7	5.8 ± 1.6	**0.008**
$FWHM_{NAA}$[Hz] [b]	6.5 ± 1.6	6.3 ± 1.4	0.611
SNR_{NAA}	19.1 ± 2.7	19.1 ± 2.3	1.000
CRLB [%]:			Inter-scan CV [%]:
tCho	3.2 ± 0.7	3.0 ± 0.6	2.7 ± 1.6
tNAA	2.8 ± 0.4	3.2 ± 0.8	3.4 ±2.1
tml	3.4 ± 0.5	3.3 ± 0.5	2.4 ± 2.3
Cre	3.4 ± 1.1	3.3 ± 0.5	2.6 ± 2.0
Glx	9.3 ± 1.7	11.0 ± 5.2	12.6 ± 12.7
Scyllo	18.6 ± 7.4	19.3 ± 7.3	13.72 ± 10.6
GSH	21.9 ± 7.8	23.8 ± 11.3	25.3 ± 26.5
GABA	23.4 ± 6.3	26.5 ± 8.4	16.1 ± 15.9

[a] Linewidth estimates provided by LCModel without linewidth-matching of the water peaks
[b] Linewidth estimates provided by LCModel with linewidth-matching of the water peaks (by means of exponential filtering)

Table 2: Water peak area (mean ± SD; area under the curve, AUC) and absolute neurochemical concentrations (mean ± SD; institutional units) of included metabolites from both conditions. Significance levels of the paired t-test between both conditions are represented under p.

	Baseline	Pain	Abs. Change	Rel. Change [%]	p
$H2O_{AUC}$	47.48 ± 4.75	47.58 ± 4.39	0.10 ± 0.61	0.29 ± 1.52	0.580
tCho	6.50 ± 0.75	6.44 ± 0.75	-0.06 ± 0.30	-0.78 ± 4.50	0.515
tNAA	22.89 ± 2.54	22.01 ± 2.35	-0.87 ± 1.01	-3.70 ± 4.11	**0.009**
tml	21.73 ± 2.70	21.55 ± 2.25	-0.18±1.05	-0.50 ± 4.73	0.552
Cre	15.31 ± 1.56	15.13 ± 1.56	-0.18 ± 0.74	-1.07±4.51	0.404
Glx	19.28 ±4.09	18.17 ± 5.55	-1.10 ± 3.81	-3.67 ± 25.35	0.317
Scyllo	1.28 ± 0.44	1.18 ± 0.41	-0.10 ± 0.26	-3.93 ± 22.73	0.206
GSH	3.57 ± 1.33	3.35 ± 1.42	-0.23 ± 1.57	2.02 ± 44.85	0.612
GABA	6.29 ± 1.79	5.40 ± 1.63	-0.89 ± 1.41	-10.88 ± 24.47	**0.041**

Table 3: Movement analysis results. Mean displacement (±SD), and the mean percentage of MRS acquisitions (Range) exceeding the gating-window (±1mm). Significance levels of the wilcoxon-test between both conditions are represented under p.

Group analysis	Nav I (anterior-posterior axis)			Nav II (left-right axis)		
	Baseline	Pain	p	Baseline	Pain	p
Mean [mm]	-0.19 ±0.25	-0.25 ± 0.22	0.60	-0.27 ± 0.28	-0.23 ± 0.26	0.42
Echoes > ±1mm [%]	0.50 (0-3.13)	0.90 (0-7.81)	0.55	0.57 (0-4.30)	1.05 (0-9.57)	1.00

Excluded Participant	Nav I		Nav II	
	Baseline	Pain	Baseline	Pain
Mean[mm]	-0.41	-1.50	-0.07	-0.19
Echoes > ±1mm [%]	0.00	**73.83**	0.00	0.00

were low with mean CV of 9.85% over all participants and included neurochemicals (see Table 1).

Movement

Two movement datasets from navigator 2 had to be excluded due to excessive noise, resulting in a complete data set of 13 movement profiles for navigator 1 (anterior-posterior, AP) and 11 movement profiles for navigator 2 (left-right, LR; Illustrations of the individual movement profiles are provided in the supplementary material). Spectra from one participant had to be excluded due to a significant drift movement in the anterior-posterior direction.

The movement quantification results are summarized in table 3. The overall movement was negligible with mean displacements of -0.22 mm (AP) and -0.25 (LR). Accordingly, the percentages of navigator echoes exceeding displacements of ±1mm were minute with mean percentages of 0.70% (AP) axis and 0.81% (LR). No significant differences were observed in mean displacement magnitudes between baseline and pain conditions for Nav I ($Z = 0.52$, $p = 0.60$) and Nav II ($Z = 0.80$, $p = 0.42$). In the same vein, the count of single navigator echoes lying

outside gating window were also not significant between the baseline and pain condition for both navigators (Nav I: Z = -0.60, p = 0.55; Nav II: Z = 0.00, p = 1.00).

Neurochemical concentrations:

Table 2 shows absolute neurochemical concentrations and the resulting changes with corresponding paired t-test results. Figure 2 graphically illustrates the intra-individual neurochemical differences as boxplots. tNAA and GABA revealed significant alterations during the pain condition. tNAA showed the most significant differences with a consistent drop during pain (T = 3.130(12); p = 0.009). Also GABA demonstrated a significant concentration drop during pain (T = 2.286(12); p = 0.041).

5.2.5 Discussion

In the present study, neurochemical changes within the human TBSNC during experimental orofacial pain were assessed by brainstem-optimized functional ^{1}H-MRS. To our knowledge, this is the first human study which quantified neurochemical alterations at anatomically distinct brainstem level in response to experimental nociception. The combination of MC-PRESS ^{1}H-MRS-sequences and dedicated spectral post-processing enabled the acquisition of high quality spectra in spite of the present technical challenges inherent to the brainstem, long measurement times and small voxel dimensions. Eight neurochemicals were quantified with good reproducibility as indicated by overall low CRLBs and inter-scan CV (Table 1).

From these eight neurochemicals, significant decreases were observed for tNAA and GABA during the pain application.

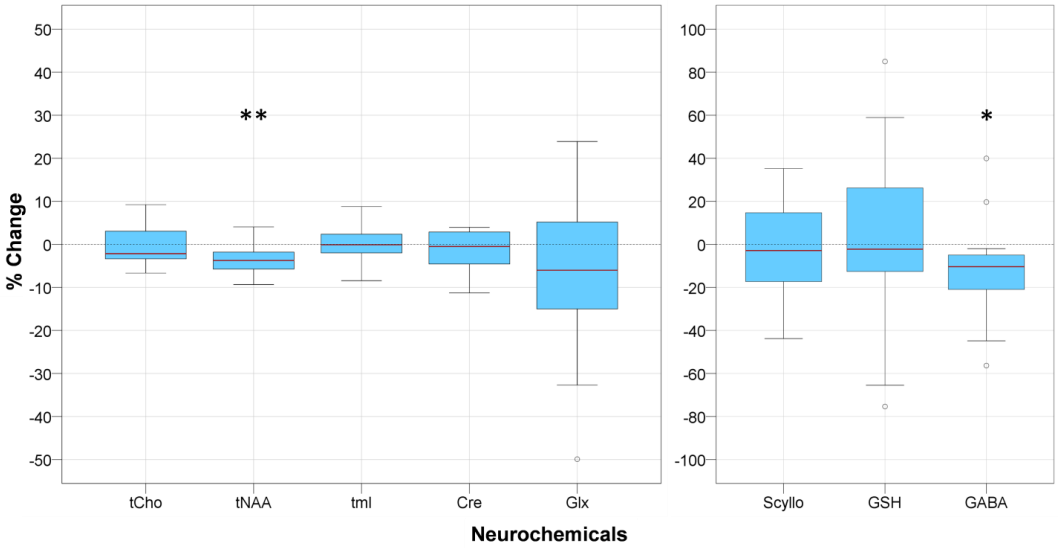

Figure 5: Boxplots of the percent changes in neurochemical concentrations between baseline and pain condition. tNAA and GABA showed a statistically significant reduction during pain stimulation. *p<0.05; **p<0.01

Mechanisms underlying NAA and NAAG decreases with an emphasis on nociception

NAA is one of the most abundant neurochemicals in the human nervous system reaching high concentrations of approx. 10mM (Moffett et al., 2007). In ^{1}H-MRS, this neurochemical is typically represented by the highest peak in the spectrum which originates from three nearly equivalent methyl hydrogen atoms on the acetate group resonating with a frequency shift of 2.02 ppm relative to the MRS standard tetramethylsilane (De Graaf, 2007). NAA is specific to neurons, being predominantly synthesized in neuronal mitochondria from aspartate and acetyl-coenzyme A by the enzyme L-aspartate N-acetyltransferase (Asp-NAT) (Stagg, 2013). NAA synthesis has been shown to be coupled to oxygen consumption and adenosine triphosphate (ATP) production, thus linking NAA to mitochondrial activity and associated neuronal energy metabolism (Benarroch, 2008). NAA

counts as a reliable marker of neuronal health and integrity (Rae, 2014). Pursuant to, a variety of clinical conditions demonstrate transient or permanent decreases, confirmed in stroke, Alzheimer's disease, epilepsy, brain tumors, multiple sclerosis, schizophrenia, chronic low back and orofacial pain (Moffett et al., 2007; Benarroch, 2008; Gussew et al., 2011; Gustin et al., 2011). These results point towards an indubitably important role of NAA in those pathological conditions. However, it should be emphasized that its utility as marker for general neuronal health is primarily based on empirical evidence and not on a profound understanding of its specific neuronal functions, in particular during neuronal activity (Moffett et al., 2007; Stagg, 2013; Rae, 2014).

A variety of functional roles of NAA have been suggested in animal and human research. Baslow and coworkers (Baslow, 2002; Baslow et al., 2007; Baslow et al., 2016) proposed that NAA might additionally function as molecular water pump (MWP), able of removing excess water produced by increased glucose respiration during neuronal activation. According to this hypothesis, NAA is actively transported to the extracellular space in conjuction with bound water molecules. Subsequently, NAA is catabolized by aspartoacyclase (ASPA) in oligodendrocytes, releasing the bound water molecules and thus allowing water removal from the extracellular space by astrocytes. Although intriguing, the MWP-theory remains hypothetical as to date no key transport protein has been identified. Another possible mechanism for a controlled release of NAA during neuronal activation has been suggested by experiments performed on organotypic hippocampal slices. Tranberg et al. (2004) observed a NAA release during a 20 min period after a transient 5 min activation of NMDA-receptors. Importantly, the NAA efflux was not due to potassium depolarization, but to a NMDA-mediated influx of Ca^{2+}.

Such NMDA-mediated releases of NAA could function as an activity-driven mechanism for metabolic water removal thus supporting neurophysiological

processes proposed by Baslow et al. (Baslow, 2002). In addition, this NMDA-mediated release could constitute a regulation mechanism for axon-glial signaling, which has been proposed by others (Moffett et al., 2007).

Widely accepted is the role of NAA as precursor for *N*-acetylaspartylglutamate (NAAG), the highest concentrated neuropeptide in the human CNS (Benarroch, 2008). NAAG is synthesized in neurons from NAA and glutamate and is then synaptically (calcium mediated) released. NAAG is predominately converted by glutamate carboxypeptidase II (GCPII) located on the surface of astrocytes. GPCII hydrolyzes NAAG back to NAA and glutamate which are taken up by astrocytes. Glutamate is then converted to glutamine and transported back to neurons. NAA, however, is most likely released to the blood stream by astrocytes (Moffett et al., 2007).

It has been suggested that NAAG binds to the metabotropic glutamate receptor 3 (mGluR3) located on presynaptic endings thus enabling a modulation of neurotransmitter release (Zhao et al., 2001; Zhong et al., 2006). Due to the co-localization of NAAG with major neurotransmitters (including glutamate, GABA, acetylcholine and serotonin, dopamine and norepinephrine), it possibly modulates their release from synapses (Moffett et al., 2007). It has been further proposed that NAAG could function as modulatory pro-transmitter. In this view, NAAG would act as a glutamate carrier, releasing glutamate at sites where active GCPII enzymes are present, therefore promoting focal glutamatergic neurotransmission (Stagg, 2013).

Functional ^{1}H-MRS (fMRS) studies have been conducted in the past to investigate neurochemical dynamics of acute experimental pain processing in cortical regions (anterior/posterior insular cortex, pregenual anterior cingulate cortex) of healthy volunteers (Mullins et al., 2005; Kupers et al., 2009; Gussew et al., 2010; Gutzeit et al., 2011; Gutzeit et al., 2013). Indeed, none of the performed studies reported significant changes in tNAA. Most interestingly, Gutzeit et al. (2011,

2013) applied the identical stimulation paradigm to investigate acute dental pain processing in the insular cortex and neither observed significant alteration regarding tNAA.

What could be possible reasons for the discrepancy between the presented work and previous fMRS pain studies? On one hand, the TBSNC represents the first CNS relay area, processing "pure" somatosensory input, thus reflecting basic nociception in contrast to multifaceted "pain" processing in cortical regions. And with respect to brainstem neurochemical characteristics and compositions, various features are evident compared to cortical regions, especially regarding NAA and NAAG. Based on animal studies it has been stated that Asp-NAT enzyme activity increases from rostral to caudal brain structures with brainstem and spinal cord exhibiting the highest activity levels (Truckenmiller et al., 1985; Moffett et al., 2007). Interestingly, the expression of NAAG has been suggested to follow an analogue rostral-to-caudal pattern, being present at highest concentrations in the brainstem and spinal cord (Moffett and Namboodiri, 2006; Lodder-Gadaczek et al., 2011). Considering the reports on the absence of a similar concentration gradient of NAA (Tallan, 1957; Miyake et al., 1981), the elevated levels of NAAG may be linked to higher NAA synthesis rates in brainstem structures. In parallel to high NAAG concentrations, high densities of GCPII enzymes and mGluR2/3 were documented for the Sp5 in animal immunocytochemistry studies (Slusher et al., 1992; Tang et al., 2001), both closely interacting with NAAG (Zhao et al., 2001; Zhong et al., 2006). Under the consideration of suggested interactions between GCPII and neuropathic pain (Zhang et al., 2002; Zhang et al., 2006; Yamada et al., 2012) and mGlu2/3 receptors involved in orofacial pain at brainstem levels (Tang et al., 2001), our results provide evidence regarding NAAG release and catabolism in acute nociceptive pain processing in the human TBSNC.

Altogether, the observed tNAA reduction during the pain condition may reflect enhanced nociceptive-related NAAG neurotransmission in the TBSNC. The released NAAG would be degraded by GCPII releasing glutamate and NAA. The subsequent removal of NAA would finally result in a reduction of NAA signals in the spectrum. Hence, such a nociception/pain associated involvement of NAAG in the TBSNC could result in the observed reductions of tNAA. Furthermore, as NMDA likely plays a major role in nociceptive processing within the TBSNC (Sessle, 2000), activated NMDA receptors (either by direct glutamate release or indirect via NAAG) possibly lead to NAA efflux, thus further reducing the observable amount of NAA in the MRS signal.

Mechanisms underlying GABA decreases with an emphasis on nociception

GABA has two main roles within the CNS: On one side, it acts as neuronal metabolite throughout the cytoplasm and reflects the largest pool of GABA (Stagg, 2013). On the other hand, it is best known as main inhibitory neurotransmitter in the CNS (Stagg et al., 2011a). It binds to two main types of receptors, both widely distributed over the brain, namely the ionotropic receptors $GABA_A$ and metabotropic $GABA_B$. They are located pre/post and extrasynaptically, hence underlying its comprising role to extensively alter neural activation (Rae, 2014). GABA is thus involved in the modulation of a variety of physiological processes (motor control, pain, sleep) and is supposed to be dysfunctional in several pathological conditions (epilepsy, anxiety, wake-sleep disturbances, schizophrenia) as well as developmental and neurodegenerative disorders (Rae, 2014).

However, to describe distinct roles of GABA within this functional diversity is challenging. Exemplary is the study of Jasmin et al. (2003). By selectively modulating GABAergic mechanisms within a distinct posterior insula subarea of freely moving rats, they evoked either analgesia by general GABAergic mediated

down regulation via brainstem areas or hyperalgesia by specific $GABA_B$ receptor mediated amygdala projections. In this vein, further evidence is given by studies examining the link between animal (chronic) orofacial pain models and GABA alterations in the TBSNC, indicating generally reduced GABA levels within these pathological conditions (Idänpään-Heikkilä and Guilbaud, 1999, Sessle, 2000; Takemura et al., 2001; Viggiano et al., 2004; Martin et al., 2010; Takeda et al., 2011). Also, a recent animal study by François et al. (2017) proposed a crucial role of GABAergic neurons, however, within the rostral ventromedial medulla (RVM) in integrating sensory inputs together with internal state information, which finally leads to a gatekeeper function for mechanically evoked pain. They further suggest "that multiple parallel GABAergic systems may exist for independent descending control of distinct somatosensory modalities".

In addition to evidence provided by animal research, human resting-state and functional ^{1}H-MRS studies suggest GABA involvement in clinical and acute experimental pain conditions. Henderson et al. (2013) examined GABA resting-state concentrations in the thalamus of patients with painful trigeminal neuropathy (PTN, a form of chronic orofacial pain) compared to healthy volunteers and found significant GABA decreases in patients only. Additionally, they measured volumetric gray matter reductions in the thalamus of PTN patients but not in controls. In our opinion, a conclusive interpretation of their findings as either chronic pain related down-regulated GABAergic neurotransmission or neuronal loss including GABAergic neurons is challenging and needs further investigation. More closely related to our study is the experiment performed by Cleve et al. (2015). Experimental thermal pain was administered to healthy volunteers and GABA alterations in the anterior cingulate and occipital cortex were quantified. In accordance with our results, they observed a GABA associated significant mean drop of 15.1% during pain stimulation (we observed a drop of 10.88%). They argued that the observed

drops could reflect a down-regulation of inhibitory neurotransmission associated with neuro-regulatory processes. Opposed to Cleve et al. and to the study presented here, Kupers et al. (2009) compared neurochemical alterations in the pregenual anterior cingulate cortex associated with tonic heat stimulation and found increases in GABA concentration. A reason for this discrepancy could be rooted in the different regions examined as well as the variety of MRS-sequences applied. Likely most important are differences in the type of pain stimulus and application site used: As we and Cleve et al. (2015) applied a repetitive short phasic stimulus, Kupers et al. utilized tonic heat lasting throughout the whole MRS measurement. It is highly probable that different neurochemical pain processing dynamics are engaged in the measured regions, especially considering the functional diversity of brainstem compared to insular/cingulate/frontal areas.

Despite robust evidence provided for GABA involvement in neurophysiologic and pathologic pain processing (derived from animal and human studies), the question still remains about which underlying neuronal processes may have given rise to the observed reduction in GABA in our study. First of all, the GABA-signal obtained by means of ^{1}H-MRS reflects all GABA in a defined voxel. Therefore, it is not possible to directly ascribe our observed concentration changes to specific GABA pools such as metabolic, vesicular and extrasynaptic compartments (GABA distributed in the extracellular fluid) (Stagg et al., 2011a). Also considerable is the fact that some of the pools are more tightly bound to macromolecules, thus reducing their contribution to the acquired GABA-signal (Stagg et al., 2011a). Animal ^{1}H-MRS studies further suggest that the GABA-signal predominately reflects extrasynaptic GABA (which binds to extrasynaptic $GABA_A$ receptors) and therefore determines a general non-synaptic GABAergic tone (Stagg et al., 2011b). It is also important to mention that levels of measured GABA are not simplistically linked to excitatory activity and that an increase in

GABA concentration does not necessarily correspond to increased neuronal inhibition (Rae, 2014). It has generally been proposed that overall GABA levels rather reflect a gross GABAergic tone instead of specific inhibitory activity per se. In that vein, the GABA reduction observed in our study does not need to directly mirror increases in excitatory neurotransmission within the TBSNC due to nociceptive processing (coupled with glutamatergic excitatory neurotransmission). The applied dental stimuli were of 1 ms duration giving rise to associated short dental pain perceptions. In case of induced GABAergic neurotransmission, potentially released GABA into the synaptic cleft would probably be quickly taken up by astrocytes and neurons due to the short stimulation applied. Considering the timespan between excitation of the MRS volume until the end of the signal readout of approx. 572 ms, it is rather unlikely that such short neurotransmittory processes are measurable with the applied ^{1}H-MRS sequence. In this view, the presented results correspond to the view that the observed decrease in GABA levels may reflect changes in a general GABAergic tone rather than specific and direct GABAergic neurotransmission.

Limitations:

Several limitations need to be considered. Starting with the voxel placement, measuring the TBSNC with ideal anatomical and functional specificity proved to be highly demanding. This circumstance is attributable to the shape of the TBSNC and brainstem in general impeding measurability accuracy using the available cuboid voxel shape. Higher anatomical specificity might be attainable by applying other specificity enhancement strategies currently under development and partly applicable, like the use of arbitrary voxel shapes. This technique enables an exact drawing of the region of interest according to its structural contours thus theoretically achieving higher levels of spatial selectivity (Weber-Fahr et al., 2009; Snyder et al., 2012). However, the lack of contrast of structural MRI in the

brainstem hampers the visual identification of TBSNC structures. This circumstance further aggravates the achievement of optimal specificity and resulting increase of sensitivity to neurochemical processes in the TBSNC.

The exclusive assessment of the neurochemical milieu of the TBSNC ipsilateral to the stimulated tooth could represent a further limitation. An additional measurement of the contralateral TBSNC in rest and during dental stimulation could provide valuable insights regarding the lateralization specificity of the observed neurochemical alterations. In the same vein, an additional recovery phase after the pain condition could provide further information on the dynamics of the recorded neurochemical effects. Such examinations are planned.

A possible limitation could be rooted in the exclusive participation of healthy male volunteers. The testing of a female population may demand an adaptation of voxel dimensions due to different brain sizes thus impeding a generalization of our results to the female population and further studies might be necessary.

Further on, we would like to comprehensively address possible limitations regarding the observed changes in GABA.

At 3 Tesla, detection and quantification of GABA is challenging as the signal significantly overlaps with resonances from other neurochemicals. Several approaches have been developed to improve the quantification of GABA at this field strength (Mescher et al., 1998; Schulte and Boesiger, 2006; Stagg, 2013). The most commonly and widely accepted gold-standard of GABA quantification at 3 Tesla is a spectral editing technique named MEGA-PRESS. This method allows the separation of the $^{4}CH_2$-GABA multiplet from the overlapping resonances (Mescher et al., 1998). MEGA-PRESS is a two-step approach which requires the acquisition of “on and off” spectra to calculate the edited spectrum. To date, with respect to our paradigm and the neurochemical quantification within the TBSNC, this method is not applicable due to required voxels sizes and measurement time (high volunteer stress).

Another technique able to improve GABA quantification is 2D *J*-resolved MRS in combination with two-dimensional fitting procedures (Schulte and Boesiger, 2006; Stagg, 2013). However, this approach is also limited within the frame of the present study as significantly larger voxel sizes and longer scan times are required to achieve sufficient SNR.

In this report, MRS sequences and post-processing techniques are based on spinal cord MRS Hock et al., 2013; Hock et al., 2013a; Hock et al., 2016) and are optimized for quantification of neurochemical profiles in the TBSNC. Although methodological work suggests that unedited short-TE MRS measurements at 3 Tesla can yield relatively reliable GABA quantification, distinct caution must be applied regarding the spectral quality between conditions, as differences in linewidth and SNR systematically bias GABA quantification and fitting error estimates (Near et al., 2013). In that sense, special care was applied to ensure comparable spectral quality estimates (linewidth and SNR) between the baseline and pain condition, hence minimizing systematic quantification biases between both conditions (reported in table 1). Another consequence of the resonance overlaps from GABA and other neurochemicals are increased GABA fitting errors. As rule of thumb, neurochemicals determined with CRLB < 20-30% are not considered unreliable, but should be interpreted with caution (De Graaf, 2007). Although mean CRLB for GABA in both conditions meet this criterion, it is important to emphasize that CRLB only reflect lower bounds and therefore may underestimate the actual magnitude of fitting errors. To overcome mentioned limitations we are working on the adaptation of the metabolic cycling technique for the use at 7 Tesla. Additionally, we are working on optimized coil designs to maximize SNR as successfully shown for the spinal cord (Hock et al., 2016).

Conclusion

Conceptualized as a feasibility study, this ^{1}H-MRS investigation provides first evidence of neurochemical alterations in the human TBSNC during experimental orofacial pain. Yet, the findings need to be cautiously interpreted, replication as well as expanding the research focus is indispensable.

We would like to note that the application of ^{1}H-MRS at the level of the TBSNC is possible, allowing the study of neurochemical compositions also in other brainstem subareas. Important in this regard is the measurement quality of tNAA, GABA and the six other quantified neurochemicals (table 1 and 2). Important, since we think that orofacial pain is mediated not only by tNAA and GABA. We rather hypothesize that the general neurochemical composition is somehow involved to code all complex intertwined facets of the human neural pain circuits. This has to be explored in following studies.

This study provides first indications of human brainstem neurochemical nociceptive mechanisms. Hence, it complements identified neurochemical aberrations in animal models of acute/chronic orofacial pain. Thus, bridging both research fields might be in reach and offers hope for successful new treatment opportunities.

Acknowledgements

This study was funded by the Olga-Mayenfisch science foundation.

5.2.6 Supplementary Material

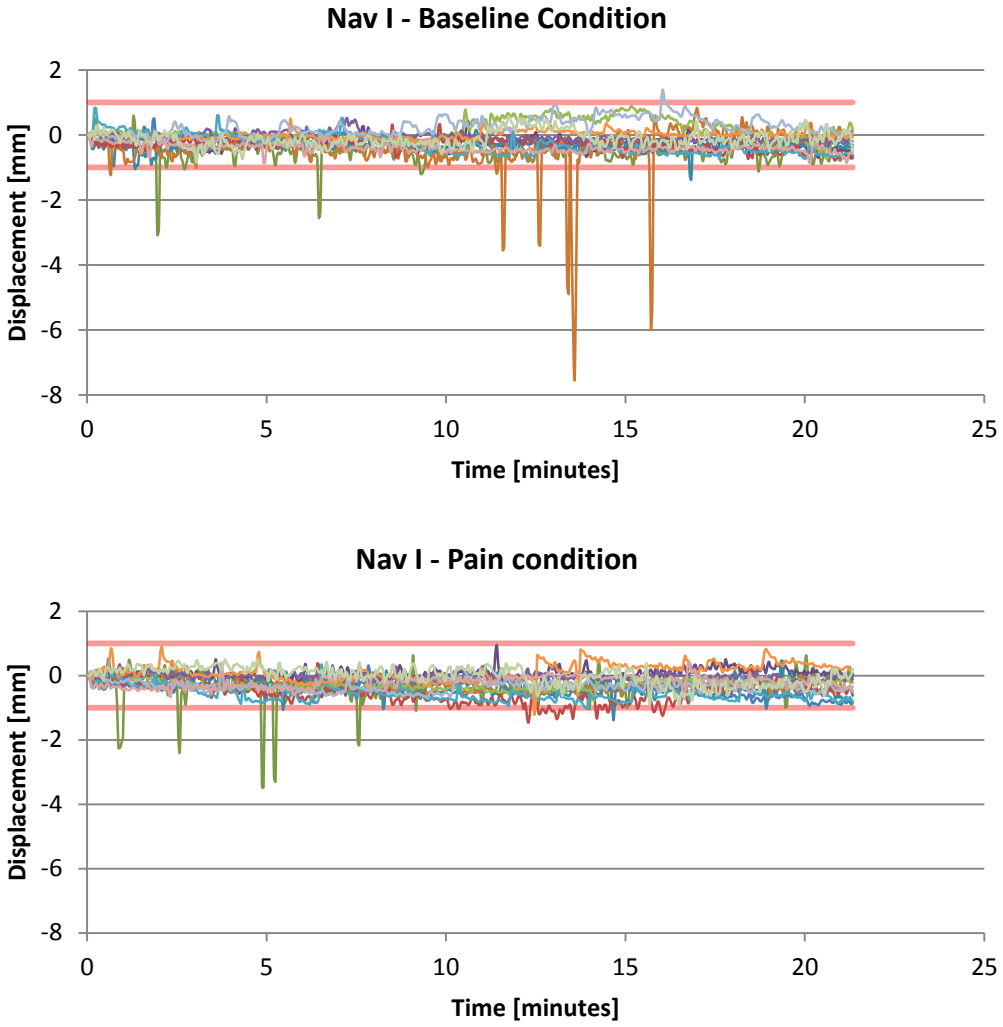

Figure 1: Graphical illustration of movement estimates of all volunteers from navigator 1 (Nav I; anterior-posterior, AP) recorded during baseline and pain conditions. The gating window of ± 1mm is represented by the red lines.

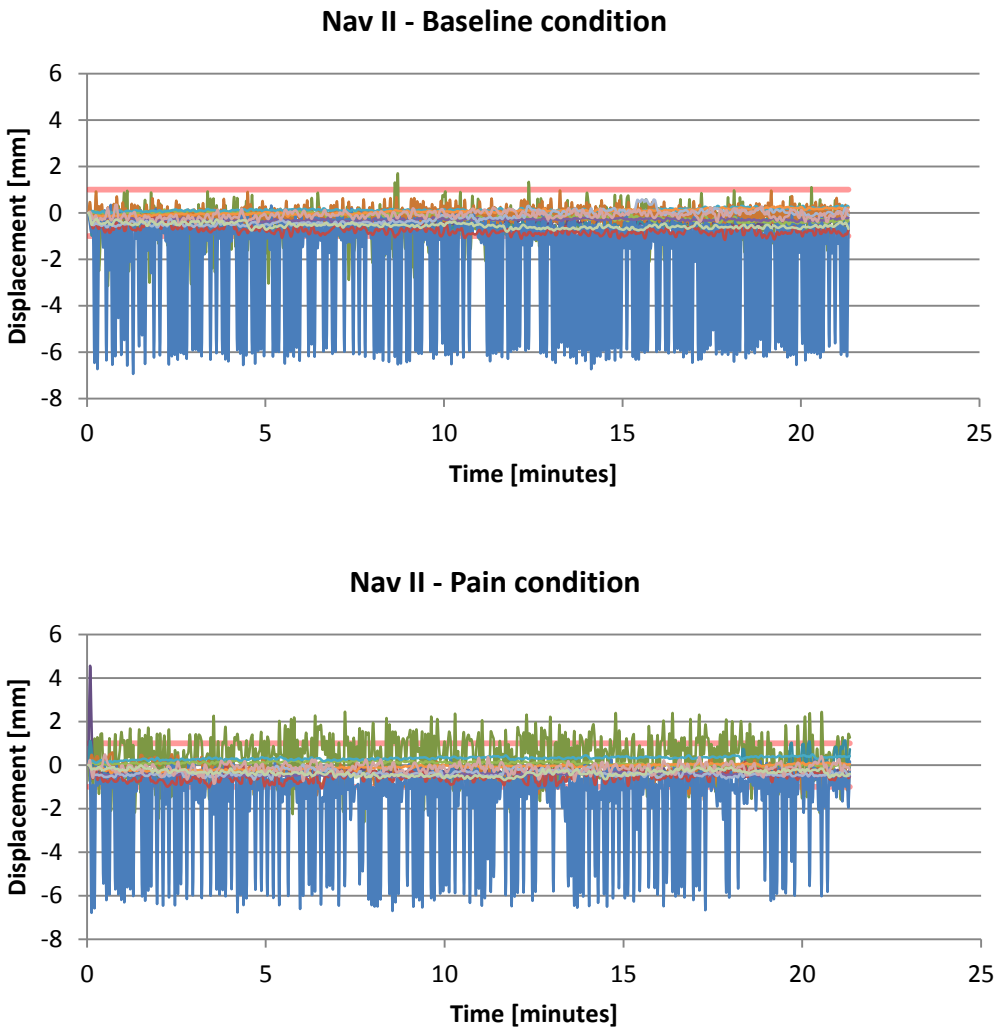

Figure 2: Graphical illustration of movement estimates of all volunteers from navigator 2 (Nav II; left-right, LR) recorded during the baseline and pain condition. The gating window of ± 1mm is represented by the red lines. The movement time-series of two participants (blue and green) showed excessive noise levels, thus were excluded from the movement group analysis.

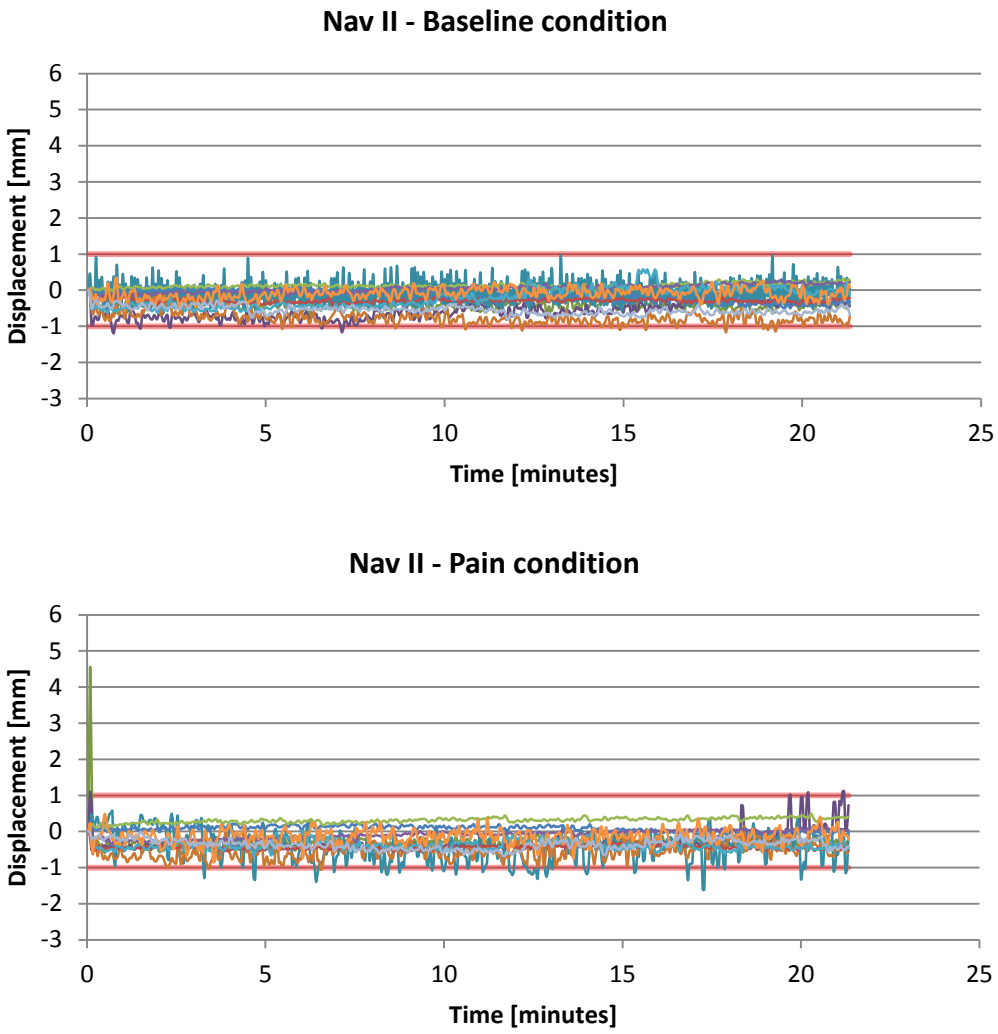

Figure 3: Depiction of movement estimates from Nav II (LR) recorded during the baseline and pain condition. The gating window of ± 1mm is represented by the red lines. This is the same illustration as shown in figure 2 without the two noisy movement profiles.

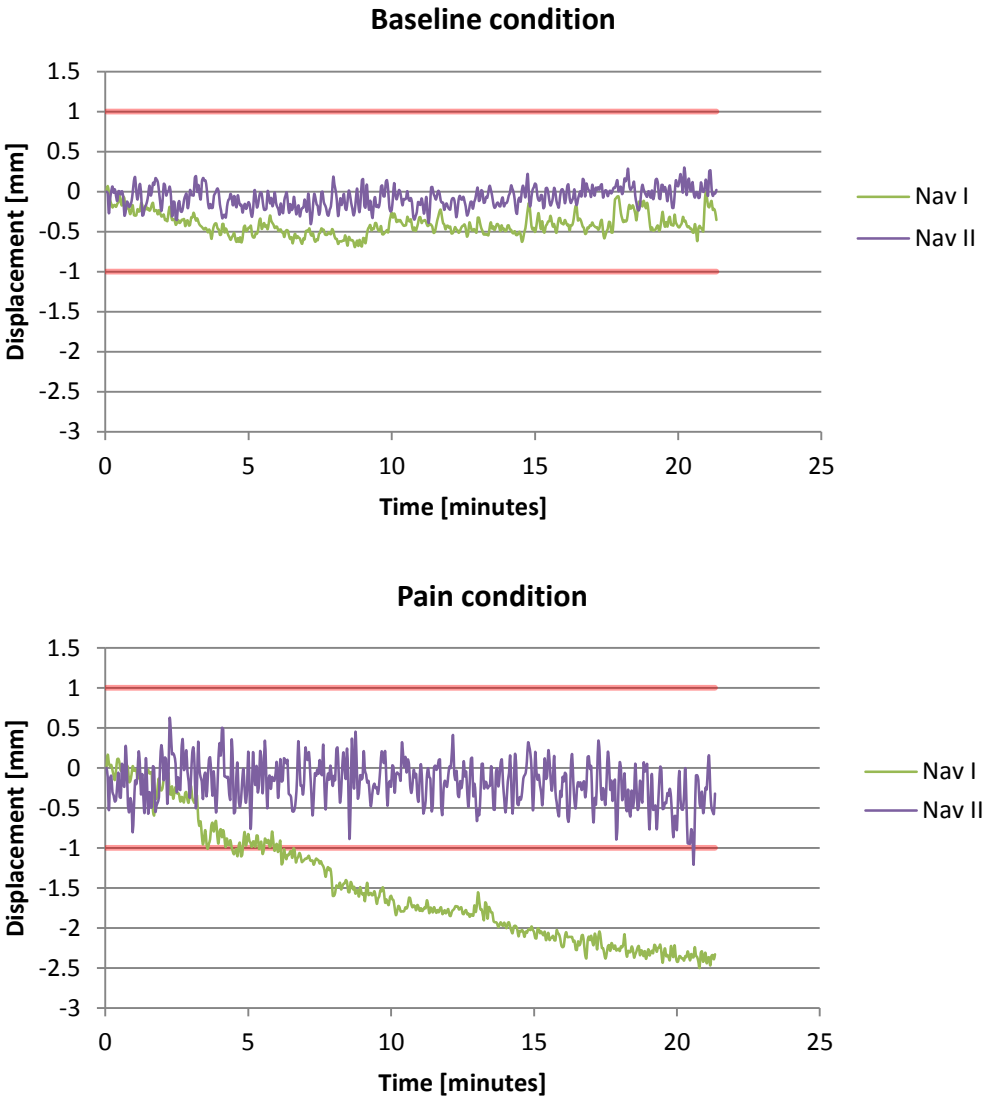

Figure 4: Exemplary, the movement profiles from one excluded participant. The gating window of ± 1mm is represented by the red lines. The exclusion decision was based on the prominent AP drift during the pain-condition (Nav I in panel 2), shifting over 73% of the navigator echoes outside the gating window (Respective information provided in table 3 of the main manuscript).

5.2.7 References

Baslow, M.H. (2002). Evidence supporting a role for N-acetyl-L-aspartate as a molecular water pump in myelinated neurons in the central nervous system. An analytical review. Neurochemistry international 40, 295–300.

Baslow, M.H., Cain, C.K., Sears, R., Wilson, D.A., Bachman, A., Gerum, S., and Guilfoyle, D.N. (2016). Stimulation-induced transient changes in neuronal activity, blood flow and N-acetylaspartate content in rat prefrontal cortex: a chemogenetic fMRS-BOLD study. NMR in biomedicine 29, 1678–1687.

Baslow, M.H., Hrabe, J., and Guilfoyle, D.N. (2007). Dynamic Relationship Between Neurostimulation and N-Acetylaspartate Metabolism in the Human Visual Cortex. J Mol Neurosci 32, 235–245.

Beck, F., Brown, D., Christ, B., Kriz, W., Marani, E., Putz, R., Sano, Y., Schiebler, T.H., Zilles, K., Usunoff, K.G., Marani, E., and Schoen, J.H.R. (1997). The Trigeminal System in Man (Springer Berlin Heidelberg: Berlin, Heidelberg).

Beissner, F., and Baudrexel, S. (2014). Investigating the human brainstem with structural and functional MRI. Frontiers in human neuroscience 8, 116.

Benarroch, E.E. (2008). N-acetylaspartate and N-acetylaspartylglutamate: neurobiology and clinical significance. Neurology 70, 1353–1357.

Brooks, J.C.W., Faull, O.K., Pattinson, K.T.S., and Jenkinson, M. (2013). Physiological noise in brainstem FMRI. Frontiers in human neuroscience 7, 623.

Brügger, M., Lutz, K., Brönnimann, B., Meier, M.L., Luechinger, R., Barlow, A., Jäncke, L., and Ettlin, D.A. (2012). Tracing toothache intensity in the brain. Journal of dental research 91, 156–160.

Cleve, M., Gussew, A., and Reichenbach, J.R. (2015). In vivo detection of acute pain-induced changes of GABA+ and Glx in the human brain by using functional 1H MEGA-PRESS MR spectroscopy. NeuroImage 105, 67–75.

DaSilva, A.F., and DosSantos, M.F. (2012). The role of sensory fiber demography in trigeminal and postherpetic neuralgias. Journal of dental research 91, 17–24.

DaSilva, A.F., Becerra, L., Makris, N., Strassman, A.M., Gonzalez, R.G., Geatrakis, N., and Borsook, D. (2002). Somatotopic activation in the human trigeminal pain pathway. The Journal of neuroscience : the official journal of the Society for Neuroscience 22, 8183–8192.

De Graaf, R.A. (2007). In vivo NMR spectroscopy. Principles and techniques (John Wiley & Sons: Chichester, West Sussex, England, Hoboken, NJ).

de Matos, N.M.P., Meier, L., Wyss, M., Meier, D., Gutzeit, A., Ettlin, D.A., and Brügger, M. (2016). Reproducibility of Neurochemical Profile Quantification in Pregenual Cingulate, Anterior Midcingulate, and Bilateral Posterior Insular Subdivisions Measured at 3 Tesla. Frontiers in human neuroscience 10, 300.

Denk, F., McMahon, S.B., and Tracey, I. (2014). Pain vulnerability: a neurobiological perspective. Nature neuroscience 17, 192–200.

Dreher, W., and Leibfritz, D. (2005). New method for the simultaneous detection of metabolites and water in localized in vivo 1H nuclear magnetic resonance spectroscopy. Magnetic resonance in medicine 54, 190–195.

Dubner, R., and Bennett, G.J. (1983). Spinal and trigeminal mechanisms of nociception. Annual review of neuroscience 6, 381–418.

Edden, R.A.E., Schär, M., Hillis, A.E., and Barker, P.B. (2006). Optimized detection of lactate at high fields using inner volume saturation. Magnetic resonance in medicine 56, 912–917.

Fairhurst, M., Wiech, K., Dunckley, P., and Tracey, I. (2007). Anticipatory brainstem activity predicts neural processing of pain in humans. Pain 128, 101–110.

François, A., Low, S.A., Sypek, E.I., Christensen, A.J., Sotoudeh, C., Beier, K.T., Ramakrishnan, C., Ritola, K.D., Sharif-Naeini, R., Deisseroth, K., Delp, S.L., Malenka, R.C., Luo, L., Hantman, A.W., and Scherrer, G. (2017). A Brainstem-Spinal Cord Inhibitory Circuit for Mechanical Pain Modulation by GABA and Enkephalins. Neuron 93, 822-839.e6.

Gussew, A., Rzanny, R., Erdtel, M., Scholle, H.C., Kaiser, W.A., Mentzel, H.J., and Reichenbach, J.R. (2010). Time-resolved functional 1H MR spectroscopic detection of glutamate concentration changes in the brain during acute heat pain stimulation. NeuroImage 49, 1895–1902.

Gussew, A., Rzanny, R., Güllmar, D., Scholle, H.-C., and Reichenbach, J.R. (2011). 1H-MR spectroscopic detection of metabolic changes in pain processing brain regions in the presence of non-specific chronic low back pain. NeuroImage 54, 1315–1323.

Gustin, S.M., Peck, C.C., Wilcox, S.L., Nash, P.G., Murray, G.M., and Henderson, L.A. (2011). Different pain, different brain: thalamic anatomy in neuropathic and non-neuropathic chronic pain syndromes. The Journal of neuroscience : the official journal of the Society for Neuroscience 31, 5956–5964.

Gutzeit, A., Meier, D., Froehlich, J.M., Hergan, K., Kos, S., Weymarn, C., Lutz, K., Ettlin, D., Binkert, C.A., Mutschler, J., Sartoretti-Schefer, S., and Brügger, M. (2013). Differential NMR spectroscopy reactions of anterior/posterior and right/left insular subdivisions due to acute dental pain. European radiology 23, 450–460.

Gutzeit, A., Meier, D., Meier, M.L., Weymarn, C. von, Ettlin, D.A., Graf, N., Froehlich, J.M., Binkert, C.A., and Brügger, M. (2011). Insula-specific responses induced by dental pain. A proton magnetic resonance spectroscopy study. European radiology 21, 807–815.

Henderson, L.A., Peck, C.C., Petersen, E.T., Rae, C.D., Youssef, A.M., Reeves, J.M., Wilcox, S.L., Akhter, R., Murray, G.M., and Gustin, S.M. (2013). Chronic pain: lost inhibition? The Journal of neuroscience : the official journal of the Society for Neuroscience 33, 7574–7582.

Hock, A., and Henning, A. (2016). Motion correction and frequency stabilization for MRS of the human spinal cord. NMR in biomedicine 29, 490–498.

Hock, A., Henning, A., Boesiger, P., and Kollias, S.S. (2013a). (1)H-MR spectroscopy in the human spinal cord. AJNR. American journal of neuroradiology 34, 1682–1689.

Hock, A., MacMillan, E.L., Fuchs, A., Kreis, R., Boesiger, P., Kollias, S.S., and Henning, A. (2013). Non-water-suppressed proton MR spectroscopy improves spectral quality in the human spinal cord. Magnetic resonance in medicine 69, 1253–1260.

Hurley, R.A., Flashman, L.A., Chow, T.W., and Taber, K.H. (2010). The brainstem: anatomy, assessment, and clinical syndromes. The Journal of neuropsychiatry and clinical neurosciences 22, iv, 1-7.

Idänpään-Heikkilä, J.J., and Guilbaud, G. (1999). Pharmacological studies on a rat model of trigeminal neuropathic pain: baclofen, but not carbamazepine, morphine or tricyclic antidepressants, attenuates the allodynia-like behaviour. Pain 79, 281–290.

Jasmin, L., Rabkin, S.D., Granato, A., Boudah, A., and Ohara, P.T. (2003). Analgesia and hyperalgesia from GABA-mediated modulation of the cerebral cortex. Nature 424, 316–320.

Kreis, R. (2004). Issues of spectral quality in clinical 1H-magnetic resonance spectroscopy and a gallery of artifacts. NMR in biomedicine 17, 361–381.

Kupers, R., Danielsen, E.R., Kehlet, H., Christensen, R., and Thomsen, C. (2009). Painful tonic heat stimulation induces GABA accumulation in the prefrontal cortex in man. Pain 142, 89–93.

Lodder-Gadaczek, J., Becker, I., Gieselmann, V., Wang-Eckhardt, L., and Eckhardt, M. (2011). N-acetylaspartylglutamate synthetase II synthesizes N-acetylaspartylglutamylglutamate. The Journal of biological chemistry 286, 16693–16706.

Maixner, W., Diatchenko, L., Dubner, R., Fillingim, R.B., Greenspan, J.D., Knott, C., Ohrbach, R., Weir, B., and Slade, G.D. (2011). Orofacial pain prospective

evaluation and risk assessment study--the OPPERA study. The journal of pain : official journal of the American Pain Society 12, T4-11.e1-2.

Mangia, S., Tkác, I., Gruetter, R., Van De Moortele, Pierre-Francois, Maraviglia, B., and Uğurbil, K. (2007). Sustained neuronal activation raises oxidative metabolism to a new steady-state level: evidence from 1H NMR spectroscopy in the human visual cortex. Journal of cerebral blood flow and metabolism : official journal of the International Society of Cerebral Blood Flow and Metabolism 27, 1055–1063.

Martin, Y.B., Malmierca, E., Avendaño, C., and Nuñez, A. (2010). Neuronal disinhibition in the trigeminal nucleus caudalis in a model of chronic neuropathic pain. The European journal of neuroscience 32, 399–408.

Mescher, M., Merkle, H., Kirsch, J., Garwood, M., and Gruetter, R. (1998). Simultaneous in vivo spectral editing and water suppression. NMR in biomedicine 11, 266–272.

Miyake, M., Kakimoto, Y., and Sorimachi, M. (1981). A gas chromatographic method for the determination of N-acetyl-L-aspartic acid, N-acetyl-alpha-aspartylglutamic acid and beta-citryl-L-glutamic acid and their distributions in the brain and other organs of various species of animals. Journal of neurochemistry 36, 804–810.

Moffett, J.R., and Namboodiri, A.M.A. (2006). Expression of N-acetylaspartate and N-acetylaspartylglutamate in the nervous system. Advances in experimental medicine and biology 576, 7-26; discussion 361-3.

Moffett, J.R., Ross, B., Arun, P., Madhavarao, C.N., and Namboodiri, A.M.A. (2007). N-Acetylaspartate in the CNS: from neurodiagnostics to neurobiology. Progress in neurobiology 81, 89–131.

Mullins, P.G., Rowland, L.M., Jung, R.E., and Sibbitt, W.L. (2005). A novel technique to study the brain's response to pain: proton magnetic resonance spectroscopy. NeuroImage 26, 642–646.

Murray, C.J.L., and Lopez, A.D. (2013). Measuring the global burden of disease. The New England journal of medicine 369, 448–457.

Near, J., Andersson, J., Maron, E., Mekle, R., Gruetter, R., Cowen, P., and Jezzard, P. (2013). Unedited in vivo detection and quantification of γ-aminobutyric acid in the occipital cortex using short-TE MRS at 3 T. NMR in biomedicine 26, 1353–1362.

Nieuwenhuys, R., Voogd, J., and van Huijzen, C. (2008). The human central nervous system (Springer: Berlin, New York).

Peyron, R., Laurent, B., and García-Larrea, L. (2000). Functional imaging of brain responses to pain. A review and meta-analysis (2000). Neurophysiologie Clinique/Clinical Neurophysiology 30, 263–288.

Provencher, S.W. (1993). Estimation of metabolite concentrations from localized in vivo proton NMR spectra. Magnetic resonance in medicine 30, 672–679.

Rae, C.D. (2014). A guide to the metabolic pathways and function of metabolites observed in human brain 1H magnetic resonance spectra. Neurochemical research 39, 1–36.

Schulte, R.F., and Boesiger, P. (2006). ProFit. Two-dimensional prior-knowledge fitting of J-resolved spectra. NMR in biomedicine 19, 255–263.

Sessle, B.J. (2000). Acute and chronic craniofacial pain: brainstem mechanisms of nociceptive transmission and neuroplasticity, and their clinical correlates. Critical reviews in oral biology and medicine : an official publication of the American Association of Oral Biologists 11, 57–91.

Sessle, B.J. (2005). Peripheral and central mechanisms of orofacial pain and their clinical correlates. Minerva anestesiologica 71, 117–136.

Slusher, B.S., Tsai, G., Yoo, G., and Coyle, J.T. (1992). Immunocytochemical localization of the N-acetyl-aspartyl-glutamate (NAAG) hydrolyzing enzyme N-acetylated alpha-linked acidic dipeptidase (NAALADase). The Journal of comparative neurology 315, 217–229.

Smith, S.A., Levante, T.O., Meier, B.H., and Ernst, R.R. (1994). Computer Simulations in Magnetic Resonance. An Object-Oriented Programming Approach. Journal of Magnetic Resonance, Series A 106, 75–105.

Snyder, J., Haas, M., Dragonu, I., Hennig, J., and Zaitsev, M. (2012). Three-dimensional arbitrary voxel shapes in spectroscopy with submillisecond TEs. NMR in biomedicine 25, 1000–1006.

Stagg, C.J. (2013). Magnetic resonance spectroscopy. Tools for neuroscience research and emerging clinical applications (Academic Press: Amsterdam).

Stagg, C.J., Bachtiar, V., and Johansen-Berg, H. (2011a). What are we measuring with GABA magnetic resonance spectroscopy? Communicative & integrative biology 4, 573–575.

Stagg, C.J., Bestmann, S., Constantinescu, A.O., Moreno, L.M., Allman, C., Mekle, R., Woolrich, M., Near, J., Johansen-Berg, H., and Rothwell, J.C. (2011b). Relationship between physiological measures of excitability and levels of glutamate and GABA in the human motor cortex. The Journal of physiology 589, 5845–5855.

Takeda, M., Matsumoto, S., Sessle, B.J., Shinoda, M., and Iwata, K. (2011). Peripheral and Central Mechanisms of Trigeminal Neuropathic and Inflammatory Pain. Journal of Oral Biosciences 53, 318–329.

Takemura, M., Shimada, T., and Shigenaga, Y. (2001). GABA B receptor-mediated effects on expression of c-Fos in rat trigeminal nucleus following high- and low-intensity afferent stimulation. Neuroscience 103, 1051–1058.

Tallan, H.H. (1957). Studies on the distribution of N-acetyl-L-aspartic acid in brain. The Journal of biological chemistry 224, 41–45.

Tang, F.R., Yeo, J.F., and Leong, S.K. (2001). Qualitative light and electron microscope study of glutamate receptors in the caudal spinal trigeminal nucleus of the rat. Journal of dental research 80, 1736–1741.

Tranberg, M., Stridh, M.H., Guy, Y., Jilderos, B., Wigström, H., Weber, S.G., and Sandberg, M. (2004). NMDA-receptor mediated efflux of N-acetylaspartate: physiological and/or pathological importance? Neurochemistry international 45, 1195–1204.

Truckenmiller, M.E., Namboodiri, M.A.A., Brownstein, M.J., and Neale, J.H. (1985). N-Acetylation of L-Aspartate in the Nervous System: Differential Distribution of a Specific Enzyme. J Neurochem 45, 1658–1662.

Viggiano, A., Monda, M., Viggiano, A., Chiefari, M., Aurilio, C., and Luca, B. de (2004). Evidence that GABAergic neurons in the spinal trigeminal nucleus are involved in the transmission of inflammatory pain in the rat: a microdialysis and pharmacological study. European journal of pharmacology 496, 87–92.

Wager, T.D., Atlas, L.Y., Lindquist, M.A., Roy, M., Woo, C.W., and Kross, E. (2013). An fMRI-based neurologic signature of physical pain. The New England journal of medicine 368, 1388–1397.

Weber-Fahr, W., Busch, M.G., and Finsterbusch, J. (2009). Short-echo-time magnetic resonance spectroscopy of single voxel with arbitrary shape in the living human brain using segmented two-dimensional selective radiofrequency excitations based on a blipped-planar trajectory. Magn Reson Imaging 27, 664–671.

Wiesenfeld-Hallin, Z. (2005). Sex differences in pain perception. Gender Medicine 2, 137–145.

Wilcox, S.L., Gustin, S.M., Macey, P.M., Peck, C.C., Murray, G.M., and Henderson, L.A. (2015). Anatomical changes within the medullary dorsal horn in chronic temporomandibular disorder pain. NeuroImage 117, 258–266.

Yamada, T., Zuo, D., Yamamoto, T., Olszewski, R.T., Bzdega, T., Moffett, J.R., and Neale, J.H. (2012). NAAG peptidase inhibition in the periaqueductal gray and rostral ventromedial medulla reduces flinching in the formalin model of inflammation. Molecular pain 8, 67.

Zakrzewska, J.M. (2013). Multi-dimensionality of chronic pain of the oral cavity and face. The journal of headache and pain 14, 37.

Zhang, W., Murakawa, Y., Wozniak, K.M., Slusher, B., and Sima, A A F (2006). The preventive and therapeutic effects of GCPII (NAALADase) inhibition on painful and sensory diabetic neuropathy. Journal of the neurological sciences 247, 217–223.

Zhang, W., Slusher, B., Murakawa, Y., Wozniak, K., Tsukamoto, T., Jackson, P., and Sima, A. (2002). GCPII (NAALADase) inhibition prevents long-term diabetic neuropathy in type 1 diabetic BB/Wor rats. Journal of the neurological sciences 194, 21–28.

Zhao, J., Ramadan, E., Cappiello, M., Wroblewska, B., Bzdega, T., and Neale, J.H. (2001). NAAG inhibits KCl-induced [(3)H]-GABA release via mGluR3, cAMP, PKA and L-type calcium conductance. The European journal of neuroscience 13, 340–346.

Zhong, C., Zhao, X., Van, K.C., Bzdega, T., Smyth, A., Zhou, J., Kozikowski, A.P., Jiang, J., O'Connor, W.T., Berman, R.F., Neale, J.H., and Lyeth, B.G. (2006). NAAG peptidase inhibitor increases dialysate NAAG and reduces glutamate, aspartate and GABA levels in the dorsal hippocampus following fluid percussion injury in the rat. Journal of neurochemistry 97, 1015–1025.

5.3 Study 3

Brain activity and connectivity attributable to nociceptive signal block

Michael L. Meier[1,2], Sonja Widmayer[3], Nuno M.P. de Matos[1,4], Jetmir Abazi[1], Dominik A. Ettlin[1]

[1]Center of Dental Medicine, University of Zurich, Zurich, Switzerland
[2]Balgrist University Hospital, Zurich, Switzerland
[3]Department of Psychiatry (UPK), University of Basel, Basel, Switzerland
[4]Institute for Complementary and Integrative Medicine, University Hospital Zurich and University of Zurich, Zurich, Switzerland

Published in bioRxiv

5.3.1 Abstract

Converging lines of evidence indicate that the pain experience emerges from distributed cortical nodes that share nociceptive information. While the theory of a single pain center is still not falsifiable by current neuroimaging technology, the validation of distinct brain mechanisms for acute pain and its relief is ongoing and strongly dependent on the employed experimental design. In the current study including a total of 28 subjects, a recently presented, innovative experimental approach was adopted that is able to clearly differentiate painful from non-pain perceptions without changing stimulus strength and while recording brain activity using functional magnetic resonance imaging (fMRI). Namely, we applied a repetitive and purely nociceptive stimulus to the tooth pulp with subsequent suppression of the nociceptive barrage via a regional nerve block. The study aims were 1) to replicate previous findings of acute pain demonstrating a fundamental role of the operculo-insular region and 2) to explore its functional connectivity during pain and subsequent relief. The brain activity reduction in the posterior insula (pINS) due to pain extinction was confirmed. In addition, the posterior S2 region (OP1) showed a similar activity pattern, thus confirming the relevance of the operculo-insular cortex in acute pain processing. Furthermore, the functional connectivity analysis yielded an enhanced positive coupling of the pINS with the cerebellar culmen during pain relief, whereas the OP1 demonstrated a positive coupling with the posterior midcingulate cortex during pain. The current results support the conceptual synthesis of localized specialization of pain processing with interactions across distributed neural targets.

5.3.2 Introduction

Ronald Melzack proposed that each bodily sensation is reflected in the human brain as a result of characteristic neural impulse patterns, and accordingly, he coined the term “neurosignature pattern for pain” (Melzack 1990). The brain regions concomitantly activated by noxious stimuli collectively have been named the “pain matrix” or “pain signature”. These include the thalamus, primary and secondary somatosensory cortices (S1 and S2), insular cortices, the anterior cingulate cortex (ACC), frontal cortices and the cerebellum (Peyron et al. 2000; Apkarian 2013; Moulton et al. 2010; Duerden and Albanese 2013). Increased activity in these areas does not necessarily imply pain selectivity but likely reflects additional unrelated processes. Regardless of whether it is nociceptive in nature, the pain matrix activity can be evoked by any salient or behaviorally relevant stimulus and might not reflect the qualitative change from non-painful to painful perception (Mouraux et al. 2011). Furthermore, accumulating evidence indicates that the pain experience is not dedicated to a specific “pain center” but rather is constructed from distributed nodes that share (anti)nociceptive information (Mano and Seymour 2015; Davis et al. 2015; Kucyi and Davis 2015). Recent advances led to a synthesis of perspectives that reconciles the localized specialization of pain processing with an appreciation for properties that emerge from interactions across distributed brain sources (Matthews and Hampshire 2016; Davis et al. 2015). Wager and colleagues convincingly demonstrated the existence of a “neural pain signature (NPS)” that discriminates between painful and non-painful brain states across many task conditions and subjects (Wager et al. 2013). However, because the NPS incorporates brain regions that are likely unrelated to nociception proper, e.g., the primary visual cortex, it raised questions about nociceptive specificity owing to a lack of evidence for nociceptive input to those brain areas (Apkarian 2013). Converging evidence from animal and human studies using central (intracortical)

and peripheral stimulation suggests the existence of nociceptive afferents passing the thalamus, the cerebellum, the S1 and S2, the midcingulate cortex and the posterior insula (pINS) (Kenshalo et al. 2000; Moulton et al. 2010; Shyu et al. 2010; Garcia-Larrea 2012b; Mazzola et al. 2012a; Vierck et al. 2013; Craig 2014). In humans, the pINS and the adjacent parietal operculum (S2 region) show the uppermost preference for nociceptive signal processing, constituting a promising "core nociceptive node" (Eickhoff et al. 2006a; Garcia-Larrea 2012a; Mazzola et al. 2012b; Mazzola et al. 2012a; Segerdahl et al. 2015; Cowan 1977; Mano and Seymour 2015; Meier et al. 2015; Davis et al. 2015). Yet, while the theory of a single pain center is still not falsifiable by current neuroimaging technology, the validation of distinct brain mechanisms for acute pain and its relief is ongoing and highly dependent on the employed experimental design. Various confounding and pain-unrelated effects, such as the magnitude estimation associated with the cognitive and/or motor aspects of pain intensity rating, might blur the pain-associated neural effects (Baliki et al. 2009). Additionally, most pain studies performed categorical comparisons among different stimulus strengths, covering noxious and non-noxious stimulus ranges (Coghill et al. 1999; Brugger et al. 2012; Meier et al. 2012; Wager et al. 2013). Therefore, the neural substrate of such comparisons might be influenced by the diversity of stimulus strengths. Although efforts have been made to control for such effects by means of advanced statistical modeling (Oertel et al. 2012), it is challenging to design a proper experimental paradigm with the aim of enhancing the pain-related attribution of neuroimaging findings. Recently, we opted for an alternative approach to clearly differentiate painful from non-pain perceptions without changing stimulus strength (Meier et al. 2015). In this approach, the noxious stimulus intensity applied to a tooth was kept constant whereas the nociceptive signaling was interrupted by a local analgesic during functional magnetic resonance imaging (fMRI). In support of the current pain neuroimaging

literature, a significant and exclusive reduction in brain activity in the pINS, after blocking the nociceptive barrage, was observed. The current report is based on an identical approach, but it additionally includes a placebo condition to replicate or dismiss the presumed pain processing preference of the operculo-insular cortex. Furthermore, its potential neural interactions with other brain regions were assessed during pain and its relief using generalized psychophysical interactions (gPPI). Herein, we expected to find novel and distinct functional connectivity measures that are strongly related to pain and its relief.

5.3.3 Methods

Subjects

In addition to the 14 subjects described in our previous report (Meier et al. 2015), the current report involves data from a total of 28 subjects (mean age = 27.32, SD = 7.43). The right-handed male subjects were recruited by an advertisement published on an online marketplace (www.marktplatz.uzh.ch) and were enrolled after having given informed written consent. The subjects were randomly assigned (using the random function implemented in Microsoft Excel) to two groups: one group (Group A) received a dental anesthetic (see 2.2.3), whereas the other group (Group P) served as a control by receiving a placebo (NaCl). The groups were age-matched (independent two-Sample t-test, $t = 1.36$, $p = 0.18$). The subjects received 50 Swiss francs per hour. The study was conducted according to the Declaration of Helsinki and was approved by the Ethics Committee Zurich, Switzerland.

The exclusion criteria were systemic disease, a history of allergy to the components of the local anesthetic solutions, local anesthesia at least 2 weeks before the experiment, caries, large restorations, periodontal disease, dental anxiety or a history of trauma or sensitivity of the mandibular canines. Dental

anxiety was assessed by the Dental Anxiety Scale (DAS) questionnaire (Corah 1969). The mean DAS score was 6.57 (score range [4-11], SD = 1.95), indicating no dental anxiety in any subject, and did not differ between the groups (independent two-sample t-test, t = 0.08, p = 0.93). Alcohol was prohibited for 12 h before the experiment. The fMRI measurements were performed between 1 p.m. and 9 p.m.

Materials

Dental Splint

The mandibular splints were constructed from impressions made of Blu-Mousse (Blu-Mousse is a fast- setting vinyl polysiloxane material produced by Parkell, Inc., 300 Executive Drive, Edgewood, NY 11717, USA). Stainless steel electrodes were embedded in each splint at the labial and palatal centers (they served as anode and cathode) of the left and right mandibular canine. A small portion of a specifically prepared contact hydrogel was placed on the anode and cathode to minimize electrical resistance during stimulation. Furthermore, particular care was taken that the splints did not evoke pain or discomfort (Meier et al. 2015).

Electrical Stimulation

The “Compex Motion” system has been proven to evoke reliable sharp and pricking pain sensations and is described in details elsewhere (Keller et al. 2002; Brugger et al. 2012; Brugger et al. 2011; Meier et al. 2014; Meier et al. 2015). The Presentation® software (http://www.neurobs.com/presentation) was used to control the experimental protocol. Shielded wires were used to avoid the radiofrequency contamination by the stimulation current.

Dental Anesthetic and Placbo

For the anesthetic mental nerve block, articaine was used, which is currently the most common local dental anesthetic in Europe and has a long history of success (Cowan 1977). Articaine (4-methyl-3-[2- (propylamino)-propionamido]-2-thiophene-carboxylic acid, methyl ester hydrochloride) blocks nociceptive input by binding reversibly to sodium channels and subsequently reducing sodium influx (Becker and Reed 2012). The pulp analgesia lasts for one to two hours. Since small trigeminal fibers are generally more susceptible to local anesthetic solutions than thickly myelinated fibers, differential sensitivities are commonly observed in clinical dentistry as patients may remain disturbed by a sense of pressure despite complete analgesia (Becker and Reed, 2012). The pain offset times reported in the current study are in line with other studies reporting pulpal anesthesia onsets and the related inter-subject variability (Chumbley and Friston 2009; Kambalimath et al. 2013). In the current study, 0.6 ml of 4% solution containing 1:100,000 epinephrine was injected at the left mental foramen by a single trained and blinded dentist (JA) according to the technique described by Schwenzer and Ehrenfeld (Schwenzer and Ehrenfeld 2009). For the placebo, an equal amount of 0.9% saline solution (NaCl) was used.

Psychophysical Assessment

Outside MR Scanner

Within 3-6 weeks prior to the fMRI experiment, the noxious intensity (NI) was determined and the dental anesthetic was injected. Subsequent stimulations were performed in separate sessions where subject reports regarding stimulus perception were recorded. Accompanied by detailed instructions, this procedure allowed for familiarizing the subjects with the anesthetic injection to minimize any arousal/anxiety effects and to guarantee a timely synchronized procedure across all subjects during the fMRI measurements.

Inside MR Scanner

While the subjects were positioned in the MR scanner, the sensory detection threshold (SDT), pain detection threshold (PDT) and NI were individually determined by applying an ascending method of limits. The left lower canine was stimulated with increasing intensity (1-mA steps) at randomized intervals between 8 and 12 s with a duration of 1 ms. The subjects were asked to indicate the SDT and PDT by pressing the alarm bell of the MR system. The NI was determined by further increasing the stimulus strength until the subject rated a "5" (corresponding to a painful, but tolerable perception) on a verbally instructed 11-point numeric rating scale (NRS) by pressing the alarm bell. The instructed NRS endpoints were "no pain" and "worst pain imaginable." All threshold determinations (SDT, PDT and NI) were repeated three times, and the mean NI was applied in the subsequent stimulation paradigm. Furthermore, the pain quality was assessed by the verbal descriptors of "pricking," "dull" and "pressing." These three descriptors have demonstrated discriminative properties to distinguish between A-delta- and C-fiber-mediated pain (Beissner et al. 2010).

In a first phase (phase 1), the lower left canine was stimulated 30 times with the predefined NI at randomized intervals of 8 to 12 s. Afterwards, the subjects were instructed that they would receive either a dental anesthetic or a saline solution with no anesthetic effects (placebo). For the purpose of the injection, the original MR scanner bed position was memorized by the MR system and subsequently modified for an optimal local anesthesia setting followed by a submucosal injection (Figure 1) of either 4% articaine (Group A) or 0.9% NaCl (Group P). At the same time, the duration of the injection, including the exact re-positioning of the scanner bed, was maintained below one minute.

Immediately following the injection of articaine or placebo, the subjects continued to receive repetitive electrical stimuli with equal strength as in phase 1. In the course of this second stimulation phase (phase 2), the subjects were

asked to report the possible pain offset (analgesia) by pressing the MR alarm bell once. In case of reporting pain offset, subjects subsequently received 30 stimuli with predefined NI. In the case of no further perception (complete anesthesia), the subjects were asked to press the alarm bell twice.

Image Acquisition

Functional and anatomical scans were obtained using a 3-T Phillips Ingenia scanner with a 15-channel receive-only head coil. The functional blood oxygenation level-dependent (BOLD) time series were recorded with a single-shot echo-planar imaging sequence (SENSE-sshEPI) to acquire 33 axial whole brain slices. The following acquisition parameters were used: echo time (TE) = 30 ms, repetition time (TR) = 2524 ms, FOV = 22 cm, acquisition matrix = 128 x 128, voxel size: 2.75 x 2.75 x 4.00 mm3, flip angle = 78° and SENSE acceleration factor R = 2.0. Using a mid-sagittal scout image, we placed 33 contiguous axial slices at 20-degree angles to the anterior-posterior commissure (AC-PC) plane, covering the whole brain. The first stimulation phase consisted of 120 functional volumes. After injection, the second stimulation phase consisted of 400 volumes in Group A and 120 volumes in Group P. A high-resolution T1-weighted anatomical image (field of view [FOV] = 22 cm, voxel size = 2.00 x 2.00 x 2.00 mm3, 170 slices) was recorded for each subject.

Preprocessing

Preprocessing of the functional brain images was conducted with the statistical parametric mapping software program SPM12 (release 6685, Wellcome Department of Imaging Neuroscience, London, UK; http://www.fil.ion.ucl.ac.uk/spm/). All volumes of the EPI sequence were corrected for slice timing, and, subsequently, a spatial realignment to the first image in the series as a reference was performed. Slices with a detected movement that exceeded 2 mm

(translational) or 1° (rotational) in relation to the reference were removed. For studying the group effects, the data were normalized to the ICBM space template – European brains using seven-degree B-spline interpolation followed by smoothing with a Gaussian kernel of 8 mm full-width-at-half-maximum (FWHM) (Evans et al. 1992). While smoothing is necessary to produce reliable estimates of statistical significance using the theory of Gaussian random fields, it should be noted that the size of the smoothing kernel can influence the estimation of the true spatial extent of brain activity (Stelzer et al. 2014).

Statistical Modelling and Analysis

Brain Activity Analysis

Single subject and group analyses were performed with SPM12 (release 6685). A general linear model (GLM) was applied to partition the observed neural responses into components of interest, confounders and errors (Friston 1995). An event-related analysis estimated the BOLD responses evoked by the potentially noxious stimuli by modeling them as a delta function convolved with the canonical hemodynamic function as implemented in SPM12. The stimulus duration was 1 ms with a randomized interstimulus interval between 8 and 12 s. In the 1st level (single subject) analysis, all 30 noxious stimuli of phase 1 were modeled as a single regressor (“pain phase 1 regressor”) in both groups. In phase 2, all 30 noxious stimuli of Group P were identically modeled (“pain phase 2 regressor”). In Group A, the first painful stimuli and the pressing of the alarm bell were individually implemented as regressors of no interest, whereas the following 30 non-painful stimuli (“non-painful phase 2 regressor”) were modeled as regressors of interest. Additional confounders were incorporated in each analysis within the design matrix, including the six rotational and translational parameters from the rigid body transformation, obtained during the functional image realignment. Low-frequency fluctuations were removed with a high-pass

filter (128 s). The serial autocorrelation of the BOLD time series was modeled using a first-order autoregressive model (AR[1]). The computed contrast maps derived from each subject were then entered into a random effects (RFX) analysis.

To properly limit the amount of false positives, whole-brain topological inference using a cluster-based false discovery rate method (FDR) based on Gaussian Random Field Theory was applied (Chumbley and Friston 2009). The cluster defining threshold was set to $p < 0.001$. An initial threshold of $p < 0.001$ is recommended to avoid the pitfalls associated with cluster-based thresholding (Woo et al. 2014; Eklund et al. 2016). Only clusters that survived the FDR correction were used for the interpretation of the results. For within-group analyses, one-sample t-tests were performed, whereas for between-group analyses, independent two-sample t-tests were used as implemented in SPM12. The variance between groups was assumed to be unequal. The error covariance components were estimated using restricted maximum likelihood (REML). The activations and deactivations associated with each regressor were tested by means of simple positive and negative t-contrasts. To uncover any possible pre-injection differences in brain activity, phase 1 was compared between groups. Furthermore, the post-injection brain activity between groups was investigated by comparing phase 2. The potential effects of post- injection temporal discrepancies due to the additional painful stimuli in Group A can be neglected because adaptive changes in the sensory experience of the electrical stimulus within the experimental time window are not present (Brugger et al. 2012; Meier et al. 2014; Meier et al. 2015). Finally, the thresholded voxel SPM t-maps were color-coded and superimposed onto the avg152T1-MNI brain using xjview (http://www.alivelearn.net/xjview8/). To determine the exact OP area of the S2 region, the SPM anatomy toolbox (version 2.2c) was used (Eickhoff et al. 2005; Eickhoff et al. 2006b).

Functional Connectivity Analysis

The main advantage of the PPI analysis is that it assesses the co-variance between regions across time during a certain task, and therefore provides a test of task effects on connectivity. The generalized form of the context-dependent PPI approach (gPPI) increases the flexibility of the statistical modeling and improves single-subject model-fit, thereby increasing the sensitivity to true positive findings and a reduction in false positives (McLaren et al. 2012). Importantly, the co-variance is assessed on the neural level, which results in a change in the BOLD signal, rather than at the level of the BOLD signal, which is an indirect measure of neural activity (McLaren et al. 2012; Kim and Horwitz 2008). Therefore, a deconvolution step is mandatory to capture the neural signal on which the interaction analyses are performed. As such, the gPPI model might better capture the BOLD response and the associated underlying neural activity than a conventional task regressor. However, these analyses are not able to reveal directed links between regions (i.e., activity in region A causes activity in region B). Instead, these analyses allow inferences about the co-activation of regions across subjects and time, whereas the strength of co-activation is modulated by the task state (pain/analgesia).

For each subject, we extracted the deconvolved time course of 6 mm-spheres with peak coordinates of pain-related activity in the pINS and OP1 areas identified in the between-group brain activity analysis of phase 2 (see 3.3.2, MNI coordinates OP1: 54 -20 16, pINS: -42 -8 -4). Subsequently, separate psychological (pain/relief) and physiological regressors (time course of seed regions) and their PPI interaction, as well as the movement parameters, were included in the gPPI model. Furthermore, to avoid circularity, the main effect of the task was also modeled to detect functional connectivity effects over and above (orthogonal to) the main effect of the task (O'Reilly et al. 2012). The resulting whole-brain gPPI connectivity estimates were then evaluated using a

two sample t-test implemented in SPM12. The identified clusters were considered to be significant when falling below a cluster-corrected q (FDR) < 0.05.

5.3.4 Results

Stimulus Perception and Pain Relief

The electrical stimulus strength of the NI in phase 1 (5/11 NRS) did not differ between groups (Mann- Whitney U-test, p = 0.7). None of the subjects indicated any sensitization/habituation effects of the repetitive pain stimulus. Furthermore, all subjects reported a pricking pain perception, indicating predominantly A-delta fiber-mediated pain. Following the injection, the pain stopped at 2.8 min (SD = 3.73 min) in Group A. Although no longer painful, the stimulus was always perceived by the subjects, indicating incomplete anesthesia. In Group P, no subjects reported pain relief.

Brain Activity Results

Overall Brain Activity Phase 1 (Pain Phase)

The pooled group analysis of brain activation induced by the noxious stimulation yielded activity in several brain regions commonly reported in pain studies: insular, cingulate and somatosensory cortices, cerebellum, thalamus and frontal brain regions (q(FDR) < 0.05, Figure 1a, Table 1a).

For the brain activity results of phase 2 within each group (Figures 1b and 1c) please see Tables 1b and 1c.

Group Differences

Importantly, the between-group analysis of phase 1 revealed no significant activation differences (Table 1d). In contrast, the between-group comparison of

Table 1. Brain activity results of Phase 1 and Phase 2

Phase 1 > baseline, pooled groups (one-sample t-test, N = 28)

a.	cluster size	q(FDR)	t	MNI Peak coordinates (mm)			Brain Region
	971	<0.001	6.7	-2	-24	34	PCC
	1543	<0.001	6.64	-38	9	-10	Left insula
	2103	<0.001	6.58	50	44	10	Right DLPFC
	487	<0.001	6.32	40	-2	-4	Right Insula
	2951	<0.001	6.17	-2	-82	-16	Left cerebellum
	721	<0.001	5.94	-54	-46	32	Left IPC
	1176	<0.001	5.88	62	-40	38	Right IPC
	224	<0.002	5.64	-42	50	12	Left DLPFC
	259	<0.001	5.38	38	18	44	Right MFC
	385	<0.001	4.88	0	28	32	aMCC
	453	<0.001	4.51	18	-6	8	Right Thalamus
	141	<0.014	4.45	32	-82	-28	Right cerebellum (declive)

Phase 2 > baseline, Group A (one-sample t-test, N = 14)

b.	cluster size	q(FDR)	t	MNI Peak coordinates (mm)			Brain Region
	1242	<0.001	6.68	48	34	18	Right DLPFC
	680	<0.001	5.53	48	-44	48	Right SPC
	369	<0.001	5.2	-34	26	30	Left DLPFC
	301	<0.001	5.14	4	36	34	aMCC
	266	<0.001	5.12	-10	-16	16	Left Thalamus
	197	<0.004	4.98	24	54	-12	Right VLPFC
	131	<0.02	4.77	-10	-86	-30	Left Cerebellum (declive)
	169	<0.009	4.69	-28	-74	-28	Left Cerebellum (declive)
	137	<0.02	4.55	36	-60	-28	Right Cerebellum (declive)
	135	<0.02	4.29	14	-20	16	Right Thalamus
	113	<0.04	4.25	8	-76	40	Right IPC

Phase 2 > baseline, Group P (one-sample t-test, N = 14)

c.	cluster size	q(FDR)	t	MNI Peak coordinates (mm)			Brain Region
	13987	<0.001	8.24	34	38	26	Right DLPFC
	9887	<0.001	8.23	10	24	42	Right aMCC
	6189	<0.001	7.64	-44	-6	-4	Right insula
	473	<0.001	6.06	12	-12	8	Right Thalamus
	601	<0.001	5.94	6	-18	32	Right PCC

120	<0.001	5.57	-38	-24	16	Left insula
207	<0.002	5.35	-56	-64	6	Left IPC
401	<0.001	5.23	-12	-8	12	Left Thalamus
567	<0.001	5.17	0	-82	6	OC
106	<0.05	5.01	-14	14	62	Left SMA
202	<0.04	4.79	-6	-66	-32	Left Cerebellum (pyramis)

Group differences, Phase 1 (two-sample t-test, N = 28)

Group A > Group P, Group P > Group A

d.

cluster size	q(FDR)	t	MNI Peak coordinates (mm)			Brain Region
No significant clusters						

Group differences, Phase 2 (two-sample t-test, N = 28)

Group A > Group P

e.

cluster size	q(FDR)	t	MNI Peak coordinates (mm)			Brain Region
98	<0.05	5.54	-42	-8	-4	Left insula
61	<0.05	4.69	54	-20	16	Right S2 (OP1)

MNI = Montreal Neurological Institute, FDR = False discovery rate, PCC = posterior cingulate cortex, aMCC = anterior midcingulate cortex, DLPFC = dorsolateral prefrontal cortex, VLPFC = ventrolateral prefrontal cortex, IPC = inferior parietal cortex, SPC = superior parietal cortex, MFC = middle frontal gyrus, S2 = secondary somatosensory cortex, OC = occipital cortex

phase 2 revealed a distinct activation difference, reflected by persistent activation clusters in the ipsilateral pINS (q(FDR) < 0.05, peak MNI coordinate: -42 -8 -4, Figure 2a, Table 1e) and the contralateral S2 region, extending into the inferior parietal lobule (q(FDR) < 0.05, peak MNI 54 -20 16, Figure 2b, Table 1e) in Group P. Feeding the SPM anatomy toolbox with the peak coordinate [54 -20 16] yielded a probability of 56% (range 42-67%) for belonging to area OP1 and a 12% (range 9-13%) probability for OP4.

Functional Connectivity Results

Overall Functional Connectivity Phase 1

Using the pINS as a seed (Figure 3c), the pooled group analysis yielded an enhanced positive functional connectivity during noxious stimulation to the ipsilateral insula, bilateral ventrolateral prefrontal cortex (VLPFC), S1 and S2, superior parietal cortex (SPC) and inferior frontal gyrus (IFG) (q(FDR) < 0.05, Table 2a).

In contrast, the OP1 region (Figure 3a) revealed a positive functional coupling to the bilateral S2, right supplementary motor area (SMA), bilateral inferior parietal cortex (IPC), bilateral thalamus, left posterior midcingulate cortex (pMCC), caudate, cerebellum, and right occipital cortex (OC) (q(FDR) < 0.05, Table 3a).

For the functional connectivity results of phase 2 within each group please see Tables 2b, 2c (for pINS) and 3b, 3c (for OP1).

Group Differences

Using the pINS as a seed, phase 1 revealed no significant group differences (Table 2d). The between- group analysis of phase 2 demonstrated a positive functional coupling of the pINS exclusively to the culmen of the left cerebellum during pain relief (q(FDR) < 0.001, Figure 3d, Table 2e). The reverse contrast, Group P (phase 2) > Group A (phase 2), revealed no significant results.

In contrast, the OP1 between-group analysis yielded a significant enhanced functional coupling to bilateral clusters of the pMCC region during noxious stimulation (q(FDR) < 0.03, Figure 3d, Table 3e). The reverse contrast, Group A (phase 2) > Group P (phase 2), revealed no significant results.

5.3.5 Discussion

Our study results contribute to the ongoing validation of distinct pain-related brain mechanisms (Mano and Seymour 2015; Kucyi and Davis 2015; Davis et al.

Table 2. Functional connectivity results of Phase 1 and Phase 2 with pINS seed region

Phase 1 > baseline, pooled groups (one-sample t-test, N = 28)

a.

cluster size	q(FDR)	t	MNI Peak coordinates (mm)			Brain Region
119	<0.005	7.28	-40	-6	-6	Left insula
142	<0.002	6.06	48	38	-6	Right VLPFC
243	<0.001	5.81	56	-30	32	Right S2
180	<0.001	5.64	-16	-62	48	Left SPC
428	<0.001	5.5	56	22	22	Right IFG
210	<0.001	5.5	-48	10	12	Left IFG
127	<0.004	5.23	-40	34	2	Left VLPFC
146	<0.002	5.15	40	-38	60	Right PCG

Phase 2 > baseline, Group A (one-sample t-test, N = 14)

b.

cluster size	q(FDR)	t	MNI Peak coordinates (mm)			Brain Region
584	<0.001	6.21	-14	-60	-26	Left Cerebellum
278	<0.001	6.2	-42	6	-10	Left insula
177	<0.004	5.86	-16	-30	-28	Pons
87	<0.05	5.12	10	-64	-28	Right Cerebellum (declive)
255	<0.001	5.04	40	12	-8	Right insula
173	<0.004	5.01	22	-62	-4	Right fusiform gyrus
114	<0.02	4.87	2	-8	8	Right Thalamus
236	<0.001	4.74	34	-62	-22	Right Cerebellum (declive)
110	<0.02	4.39	-6	22	30	aMCC

Phase 2 > baseline, Group P (one-sample t-test, N = 14)

cluster size	q(FDR)	t	MNI Peak coordinates (mm)			Brain Region

c. No significant clusters

Group differences, Phase 1 (two-sample t-test, N = 28)

Group A > Group P, Group P > Group A

d. cluster size	q(FDR)	t	MNI Peak coordinates (mm)			Brain Region

no significant clusters

Group differences, Phase 2 (two-sample t-test, N = 28)

Group A > Group P

e. cluster size	q(FDR)	t	MNI Peak coordinates (mm)			Brain Region

289	<0.001	5.49	-14	-54	-28	Left cerebellum (culmen)
Group P > Group A						
No significant clusters						

MNI = Montreal Neurological Institute, FDR = False discovery rate, VLPFC = ventrolateral prefrontal cortex, SPC = superior parietal cortex, S2 = secondary somatosensory cortex, IFG = inferior frontal gyrus, PCG = postcentral gyrus

2015; Garcia-Larrea 2012b). The main finding confirms the prominent role of the operculo-insular cortex as an important node in pain processing. Furthermore, we identified novel and distinct neural interactions between the pINS/pMCC and OP1/cerebellum, indicating two functionally separate mechanisms during pain perception and relief.

Stimulus

The idea behind selecting a tooth as a target site for a purely nociceptive stimulus is not new (Chatrian et al. 1975) and relies on the observation that repetitive electrical stimuli reliably evoke painful short and sharp sensations (A-delta fiber-mediated pain) and no superimposed mechano- or thermosensations (Narhi et al. 1992; Brugger et al. 2011; Brugger et al. 2012; Meier et al. 2015; Meier et al. 2014). Nociceptive fibers are generally more susceptible to local analgesics than thickly myelinated fibers, as clinically demonstrated by a pressure sensation during dental extractions despite complete analgesia (Becker

Table 3. Functional connectivity results of Phase 1 and Phase 2 with OP1 seed region

Phase 1 > baseline, pooled groups (one-sample t-test, N = 28)

a.

			MNI Peak coordinates			
cluster size	q(FDR)	t		(mm)		Brain Region
3451	<0.001	7.88	-52	-26	16	Left S2
1085	<0.001	7.55	54	-20	16	Right S2
2666	<0.001	7.07	4	-4	60	Right SMA
610	<0.001	5.76	-18	-82	28	Left IPC
1638	<0.001	5.72	20	-82	-4	Right OC
496	<0.001	5.62	14	-82	20	Right IPC
553	<0.001	5.41	6	6	40	Left pMCC
309	<0.001	4.94	-46	-46	-28	Left cerebellum
97	<0.003	4.7	2	-14	16	Right Thalamus
182	<0.001	4.59	-2	10	6	Left caudate
86	<0.04	4.39	-18	-20	14	Left Thalamus

Phase 2 > baseline, Group A (one-sample t-test, N = 14)

b.

			MNI Peak coordinates			
cluster size	q(FDR)	t		(mm)		Brain Region
875	<0.001	7.31	8	10	36	aMCC
1611	<0.001	6.31	62	-20	14	Right S2
641	<0.001	5.76	-50	-24	10	Left S2
143	<0.004	5.72	20	-6	-24	Right Amygdala
114	<0.02	5.56	26	-14	0	Right putamen
168	<0.002	4.57	8	-60	-26	Right Cerebellum (fastigium)

Phase 2 > baseline, Group P (one-sample t-test, N = 14)

			MNI Peak coordinates			
cluster size	q(FDR)	t		(mm)		Brain Region
5851	<0.001	8.81	-6	6	36	aMCC
169	<0.002	6.59	54	-22	12	Right S2
137	<0.004	6.49	-38	-2	44	Left MFG
105	<0.02	5.72	-18	-84	30	Left IPC
252	<0.001	5.38	-28	-38	62	Left PCG
247	<0.001	5.25	50	-24	32	Right PCG
157	<0.003	5.22	22	-78	30	Right IPC

Group differences, Phase 1 (two-sample t-test, N = 28)

d. Group A > Group P

			MNI Peak coordinates			
cluster size	q(FDR)	t		(mm)		Brain Region

No significant clusters

Group P > Group A

No significant clusters

Group differences, Phase 2 (two-sample t-test, N = 28)

Group A > Group P

e.

cluster size	q(FDR)	t	MNI Peak coordinates (mm)			Brain Region
No significant clusters						
Group P > Group A						
149	<0.003	5.56	16	10	44	Right pMCC
71	<0.03	5.2	-12	4	36	Left pMCC

MNI = Montreal Neurological Institute, FDR = False discovery rate, aMCC = anterior midcingulate cortex, pMCC = posterior midcingulate cortex, DLPFC = dorsolateral prefrontal cortex, IPC = inferior parietal cortex, S2 = secondary somatosensory cortex, SMA = supplementary motor area, OC = occipital cortex, MFG = middle frontal gyrus, PCG = postcentral gyrus

and Reed 2012). Correspondingly, the subjects in our experiment reported that electrical stimuli evoked a distinct non-painful sensation at the target tooth after the onset of analgesia, which permitted a task-based activity and connectivity analysis. Furthermore, adaptive changes in the perception of the painful repetitive electrical stimulus (sensitization/habituation) within the time frame of the experiment were minimal as demonstrated in our previous experiments (Meier et al. 2015; Meier et al. 2014; Brugger et al. 2012). This allowed the exclusion of a continuous pain rating task that prevented the possible blurring effects associated with cognitive and/or motor aspects of pain intensity rating (Baliki et al. 2009; Oertel et al. 2012).

Posterior Insula and Parietal Operculum

The current results confirm accumulating evidence from human reports demonstrating that the operculo- insular region is the most consistently

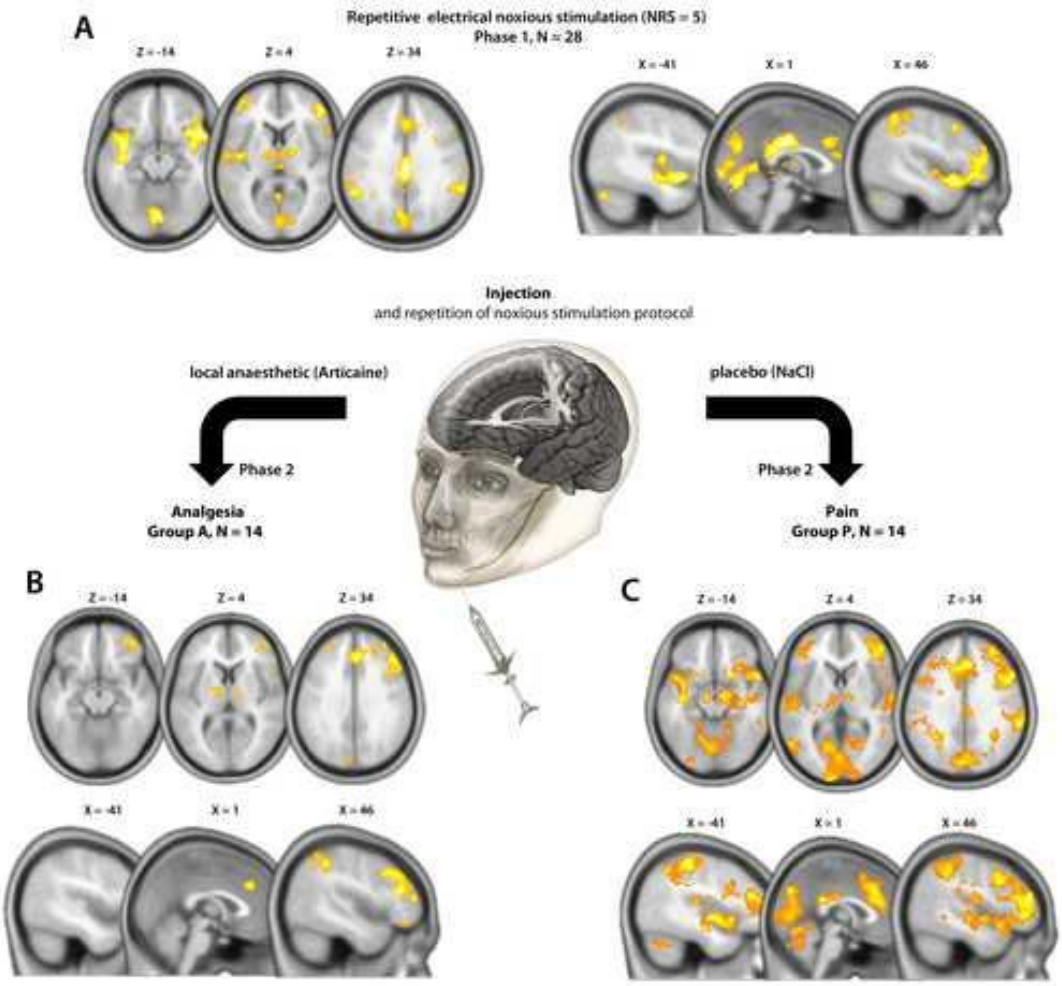

Figure 1: A. Overall brain activity results during the repetitive noxious stimulation in phase 1 (N = 28, one sample t-test). B. Post-Injection (articaine, Group A, N = 14) brain activity during pain relief. C. Post-injection brain activity (NaCl, Group P, N = 14). All results are thresholded with q(FDR)<0.05, cluster-based corrected.

activated area in acute pain (Garcia-Larrea 2012a; Oertel et al. 2012; Duerden and Albanese 2013; Favilla et al. 2014; Segerdahl et al. 2015). In support of this observation, the pINS and the medial parietal operculum are the only areas where electrical stimulation triggered somatic pain in pre-surgical patients (Mazzola et al. 2012b). Furthermore, electrophysiological recordings revealed that the earliest brain responses to noxious stimuli originate in the operculo-

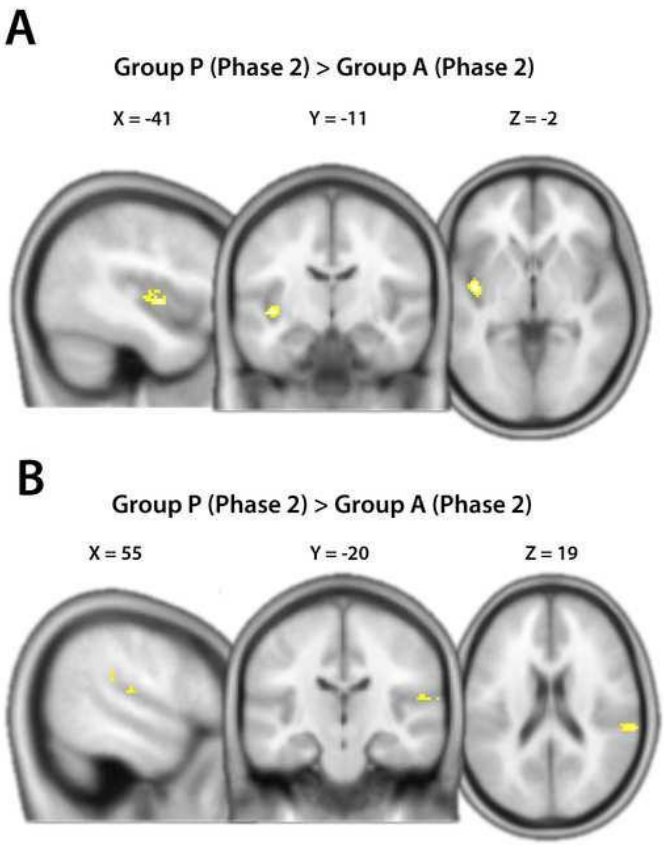

Figure 2: Between-group brain activity analyses (two sample t-test, N = 28). The contrast Group P (Phase 2) > Group A (Phase 2) showing brain activity strongly related to nociception revealed exclusive brain activity differences in the pINS (A) and S2 region (OP1). q(FDR)<0.05, cluster-based corrected.

insular cortex (Garcia-Larrea et al. 2003). On the other hand, by using intracerebral recordings, it has been recently shown that the pINS also responds to stimuli unrelated to nociception, which confutes the widespread assumption that the pINS serves as a pain-specific center (Liberati et al. 2016). Nevertheless, one should be cautious to not overintepret these results as a specific involvement of the pINS in pain perception cannot be excluded. In particular, as the local field potentials used in that study reflect the firing of cell populations, pain-specific neurons in the pINS cannot be excluded and further research in this area is needed. Surprisingly, the current investigation revealed an ipsilateral (left-sided) activation of the pINS. Yet, in contrast to the mainly contralateral spinothalamic input from spinal nerves, the trigeminal cortical representation is known to respond to ipsi- and bilateral receptive fields (Cusick et al. 1986; Lin et al. 1993; Jantsch et al. 2005). This is in keeping with observations from

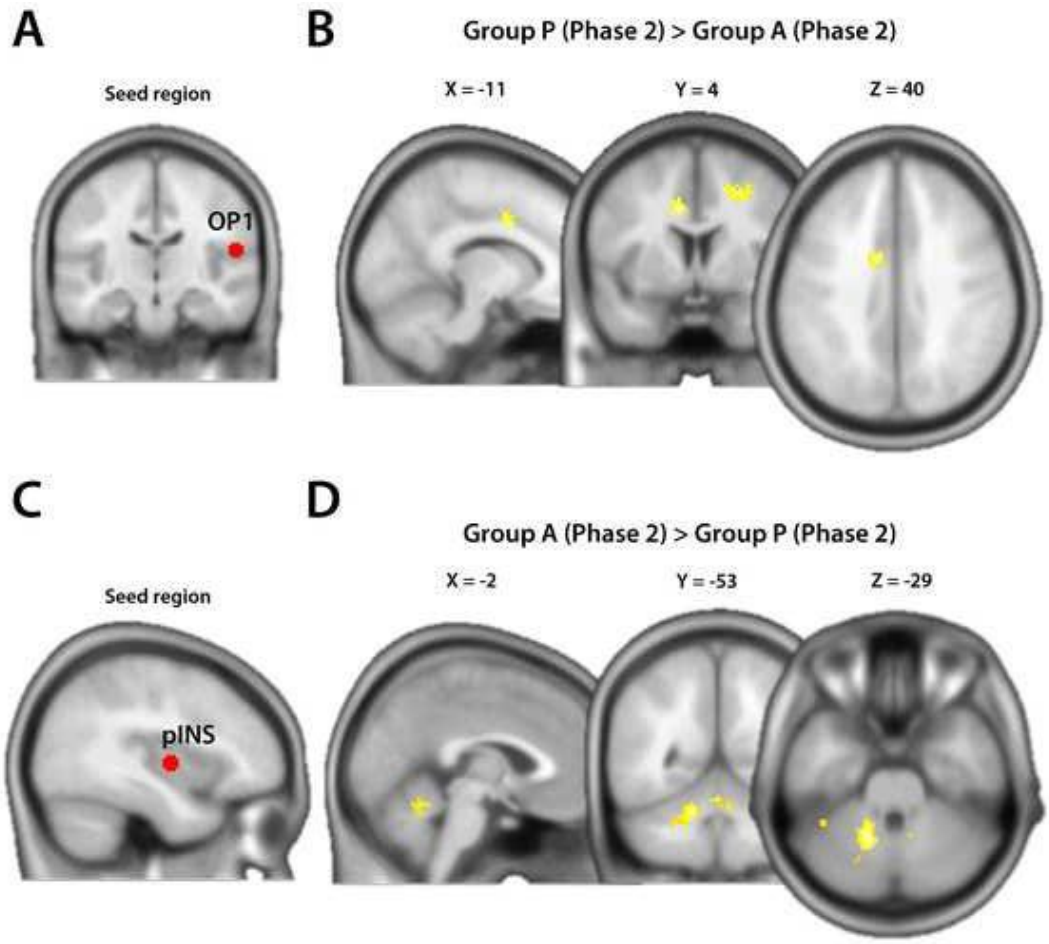

Figure 3: Whole-brain functional connectivity results using generalized psychophysical interactions (gPPI). The OP1 seed region (A) demonstrated an enhanced functional coupling to the aMCC during pain (B). The pINS seed region (C) showed an enhanced interaction with the cerebellar culmen during pain relief (D). q(FDR)<0.05, cluster-based corrected.

Rasmussen and Penfield who elicited ipsi- and bilateral sensations from cortical stimulation of the face and oral cavity areas in awake humans (PENFIELD 1947; RASMUSSEN and PENFIELD 1947). Supporting this observation, a minority of mandibular branch proprioceptive afferents cross the midline, and thus ascend homolaterally to the thalamus (Chen et al. 1997), and the insular region is known to receive bilateral input from the trigeminus (Dong et al. 1989). Furthermore, our results are in agreement with an experimental tooth pain study which demonstrated bilateral S2 activation and a clear dominance of tooth over hand

representation in the ipsilateral insula, although the two different stimulation modalities might have contributed to this difference (tooth: electrical vs. hand: mechanical) (Jantsch et al. 2005). Nevertheless, as we only stimulated and anesthetized a single tooth, a final conclusion about lateralization effects cannot be drawn, which is an important study limitation.

Furthermore, our results indicate a pain-related pINS activation that is located more anterior to the dorsal pINS activation reported in several pain studies (Henderson et al. 2011; Garcia-Larrea 2012a; Wager et al. 2013; Segerdahl et al. 2015). However, electrical stimulations in pre-surgical patients elicited somatic pain not only in the dorsal pINS regions but also in the widely distributed anterior portions of the pINS (Mazzola et al. 2012a). Moreover, a somatotopic organization of pain within the insular cortex was suggested, with the face being represented anterior to the upper and lower limbs (Mazzola et al. 2009). In keeping with this observation, another study applying painful trigeminal CO2 stimuli to the nasal mucosa revealed a pain-related activation in a more anterior region of the pINS that is comparable to the pINS activation of our study (Oertel et al. 2012).

Regarding the human parietal operculum, it is classified into four distinct cytoarchitectonic areas (OP1-4) which can be interpreted as anatomical correlates of the functionally defined human S2 region (Eickhoff et al. 2006a; Eickhoff et al. 2006b). Our results indicate a contralateral (right-sided) neural response of the OP1 area. This is in line with a previous report that demonstrated a right-sided dominance of activation in the S2/subcentral area during bilateral painful electrical tooth stimulation (Brugger et al. 2011). A meta-analysis indicated that painful stimuli are exclusively processed in the OP1 region, whereas non-painful stimuli are represented in the OP 2-4 region (Eickhoff et al. 2006a). Further support for this observation comes from lesion studies (Greenspan et al. 1999; Greenspan and Winfield 1992). In contrast,

another investigation detected pain-related effects exclusively in the OP 4 region, which raises doubts about a definitive answer regarding pain processing within the parietal operculum (Mazzola et al. 2012b).

Cingulate Cortex

Interestingly, the OP1 region demonstrated an enhanced functional coupling with the pMCC during noxious stimulation (Figure 3D). An anatomical classification of the cingulate cortex subregions has been proposed by Vogt and colleagues (Vogt et al. 2003; Vogt 2016). Of these, the MCC plays a key role in pain processing and is almost as consistently activated as the operculo-insular cortex (Vogt 2005; Frot et al. 2008). The observed neural interaction of the OP1 region with the pMCC closely corresponds with a study using intracerebral recordings of laser-evoked potentials showing the simultaneous processing of nociceptive information in both brain regions (Frot et al. 2008). Although our results indicate a highly pain-related relationship between the OP1 and pMCC, no pain-only area has been identified in the cingulate cortex to date (Vogt 2016). Alternatively, a multidimensional view including behavioral goals such as avoiding noxious stimuli has been proposed (Vogt 2005). It is assumed that the pMCC is involved in the withdrawal reactions from the painful stimulus in maintaining connections to the motor cortex and SMA for the preparation of voluntary movements (Buchel et al. 2002; Niddam et al. 2005; Vogt 2016). Withdrawal from the pain stimulus has to be operational at very short latencies and is, therefore, not dependent on prior sequential processing through other cortical areas (Frot et al. 2008).

Cerebellum

Very few studies to date have attempted to unveil the cerebellum's function in pain. A review by Moulton and colleagues summarizing animal and human

reports indicated that the cerebellum receives primary nociceptive afferents and that the electrical and pharmacological stimulation of the cerebellum can modulate pain processing (Moulton et al. 2010). Further, cerebellar lesions can lead to altered pain perception (Ruscheweyh et al. 2014). Although cerebellar activity occurs consistently in the presence of acute pain (Apkarian et al. 2005; Peyron et al. 2000), little is known about the specific role of the cerebellum regarding pain perception. Recently, the posterior cerebellum has been shown to process the overlapping and multimodal inputs from motor control and pain (Coombes and Misra 2016). Animal electrophysiological studies demonstrate direct evidence of the afferent input from nociceptors to the cerebellum (VanGilder 1975; Garwicz et al. 1998; Moulton et al. 2010), e.g., A-delta fiber stimulation leads to activation in Purkinje cells in the anterior lobe of the cerebellum in cats (Ekerot et al. 1987). Furthermore, accumulating evidence from human reports demonstrates that the cerebellar processing may be more directly related to pain and nociceptive modulation (Bingel et al. 2002; Helmchen et al. 2003; Moulton et al. 2011). In support of this, noxious heat produced cerebellar activation even under general anesthesia using propofol (Hofbauer et al. 2004). By considering the current results, the noxious stimulation in phase 1 led to cerebellar activation that was widely distributed in the posterior and anterior lobes. In contrast, the pINS seed region demonstrated an exclusive functional coupling with the cerebellar culmen in the anterior lobe during pain relief, suggesting a distinct nociceptive modulatory relationship between these two brain regions. Evidence supporting this observation comes from a rat study where microinjections of morphine into the cerebellar culmen resulted in acute analgesia (Dey and Ray 1982). Moreover, a recent study identified three functional cerebellar clusters during noxious stimulation, among which one significant cluster mainly involved the culmen that was functionally connected to the bilateral posterior portions of the insula (Diano et al. 2016). These results

indicate a potential role of the pINS and cerebellar culmen in basic nociceptive processing and modulation.

Conclusion

The neural block of trigeminal nociceptive primary afferents leads to a significant activity reduction in the pINS and OP1 regions, but not in other pain-associated brain areas. The current findings thus strengthen the evidence for the unique relevance of the operculo-insular cortex in pain perception. The pINS and OP1 seed regions seem to maintain separate neural cross-talks that might be related to pain relief (cerebellar culmen) and immediate withdrawal behavior (pMCC). However, it must be noted that these conclusions are based on reverse inference. Thus, the likelihood of the reverse inference being true is a function of the degree to which the brain mechanism (e.g. pINS – cerebellum connectivity) is exclusively triggered by the proposed psychological state (pain relief). Nonetheless, the current results support the conceptual framework that during the pain experience, localized nociceptive nodes interact with distributed brain targets.

Acknowledgements

This work was supported by a grant from the Swiss Dental Association and partly by Glaxo Smith Kline, Consumer Healthcare, Weybridge, UK. In addition, we would like to thank all volunteers who participated in the current study.

Conflicts of Interest

The authors declare that they have no conflict of interest.

5.3.6 References

Apkarian AV (2013) A brain signature for acute pain. Trends Cogn Sci 17(7):309–310. doi: 10.1016/j.tics.2013.05.001

Apkarian AV, Bushnell MC, Treede R-D, Zubieta J-K (2005) Human brain mechanisms of pain perception and regulation in health and disease. Eur J Pain 9(4):463–484. doi: 10.1016/j.ejpain.2004.11.001

Baliki MN, Geha PY, Apkarian AV (2009) Parsing pain perception between nociceptive representation and magnitude estimation. J Neurophysiol 101(2):875–887. doi: 10.1152/jn.91100.2008

Becker DE, Reed KL (2012) Local anesthetics: review of pharmacological considerations. Anesth Prog 59(2):90-101; quiz 102-3. doi: 10.2344/0003-3006-59.2.90

Beissner F, Brandau A, Henke C, Felden L, Baumgartner U, Treede R-D, Oertel BG, Lotsch J (2010) Quick discrimination of A(delta) and C fiber mediated pain based on three verbal descriptors. PLoS One 5(9):e12944. doi: 10.1371/journal.pone.0012944

Bingel U, Quante M, Knab R, Bromm B, Weiller C, Buchel C (2002) Subcortical structures involved in pain processing: evidence from single-trial fMRI. Pain 99(1-2):313–321

Brugger M, Ettlin DA, Meier M, Keller T, Luechinger R, Barlow A, Palla S, Jancke L, Lutz K (2011) Taking Sides with Pain - Lateralization aspects Related to Cerebral Processing of Dental Pain. Front Hum Neurosci 5:12. doi: 10.3389/fnhum.2011.00012

Brugger M, Lutz K, Bronnimann B, Meier ML, Luechinger R, Barlow A, Jancke L, Ettlin DA (2012) Tracing toothache intensity in the brain. J Dent Res 91(2):156–160. doi: 10.1177/0022034511431253

Buchel C, Bornhovd K, Quante M, Glauche V, Bromm B, Weiller C (2002) Dissociable neural responses related to pain intensity, stimulus intensity, and

stimulus awareness within the anterior cingulate cortex: a parametric single-trial laser functional magnetic resonance imaging study. J Neurosci 22(3):970–976

Chatrian GE, Canfield RC, Knauss TA, Eegt EL (1975) Cerebral responses to electrical tooth pulp stimulation in man. An objective correlate of acute experimental pain. Neurology 25(8):745–757

Chen WH, Lan MY, Chang YY, Liu JS, Chou MS, Chen SS (1997) Bilateral cheiro-oral syndrome. Clin Neurol Neurosurg 99(4):239–243

Chumbley JR, Friston KJ (2009) False discovery rate revisited: FDR and topological inference using Gaussian random fields. Neuroimage 44(1):62–70. doi: 10.1016/j.neuroimage.2008.05.021

Coghill RC, Sang CN, Maisog JM, Iadarola MJ (1999) Pain intensity processing within the human brain: a bilateral, distributed mechanism. J Neurophysiol 82(4):1934–1943

Coombes SA, Misra G (2016) Pain and motor processing in the human cerebellum. Pain 157(1):117– 127. doi: 10.1097/j.pain.0000000000000337

Corah NL (1969) Development of a dental anxiety scale. J Dent Res 48(4):596

Cowan A (1977) Clinical assessment of a new local anesthetic agent-carticaine. Oral Surg Oral Med Oral Pathol 43(2):174–180

Craig ADB (2014) Topographically organized projection to posterior insular cortex from the posterior portion of the ventral medial nucleus in the long-tailed macaque monkey. J Comp Neurol 522(1):36–63. doi: 10.1002/cne.23425

Cusick CG, Wall JT, Kaas JH (1986) Representations of the face, teeth and oral cavity in areas 3b and 1 of somatosensory cortex in squirrel monkeys. Brain Res 370(2):359–364

Davis KD, Bushnell MC, Iannetti GD, St Lawrence K, Coghill R (2015) Evidence against pain specificity in the dorsal posterior insula. F1000Res 4:362. doi: 10.12688/f1000research.6833.1

Dey PK, Ray AK (1982) Anterior cerebellum as a site for morphine analgesia and post-stimulation analgesia. Indian J Physiol Pharmacol 26(1):3–12

Diano M, D'Agata F, Cauda F, Costa T, Geda E, Sacco K, Duca S, Torta DM, Geminiani GC (2016) Cerebellar Clustering and Functional Connectivity During Pain Processing. Cerebellum 15(3):343– 356. doi: 10.1007/s12311-015-0706-4

Dong WK, Salonen LD, Kawakami Y, Shiwaku T, Kaukoranta EM, Martin RF (1989) Nociceptive responses of trigeminal neurons in SII-7b cortex of awake monkeys. Brain Res 484(1-2):314–324

Duerden EG, Albanese M-C (2013) Localization of pain-related brain activation: a meta-analysis of neuroimaging data. Hum Brain Mapp 34(1):109–149. doi: 10.1002/hbm.21416

Eickhoff SB, Amunts K, Mohlberg H, Zilles K (2006a) The human parietal operculum. II. Stereotaxic maps and correlation with functional imaging results. Cereb Cortex 16(2):268–279. doi: 10.1093/cercor/bhi106

Eickhoff SB, Schleicher A, Zilles K, Amunts K (2006b) The human parietal operculum. I. Cytoarchitectonic mapping of subdivisions. Cereb Cortex 16(2):254–267. doi: 10.1093/cercor/bhi105

Eickhoff SB, Stephan KE, Mohlberg H, Grefkes C, Fink GR, Amunts K, Zilles K (2005) A new SPM toolbox for combining probabilistic cytoarchitectonic maps and functional imaging data. Neuroimage 25(4):1325–1335. doi: 10.1016/j.neuroimage.2004.12.034

Ekerot CF, Gustavsson P, Oscarsson O, Schouenborg J (1987) Climbing fibres projecting to cat cerebellar anterior lobe activated by cutaneous A and C fibres. J Physiol 386:529–538

Eklund A, Nichols TE, Knutsson H (2016) Cluster failure: Why fMRI inferences for spatial extent have inflated false-positive rates. Proc Natl Acad Sci U S A 113(28):7900–7905. doi: 10.1073/pnas.1602413113

Evans AC, Marrett S, Neelin P, Collins L, Worsley K, Dai W, Milot S, Meyer E, Bub D (1992) Anatomical mapping of functional activation in stereotactic coordinate space. Neuroimage 1(1):43–53

Favilla S, Huber A, Pagnoni G, Lui F, Facchin P, Cocchi M, Baraldi P, Porro CA (2014) Ranking brain areas encoding the perceived level of pain from fMRI data. Neuroimage 90:153–162. doi: 10.1016/j.neuroimage.2014.01.001

Friston KJ (1995) Commentary and opinion: II. Statistical parametric mapping: ontology and current issues. J Cereb Blood Flow Metab 15(3):361–370. doi: 10.1038/jcbfm.1995.45

Frot M, Mauguiere F, Magnin M, Garcia-Larrea L (2008) Parallel processing of nociceptive A-delta inputs in SII and midcingulate cortex in humans. J Neurosci 28(4):944–952. doi: 10.1523/JNEUROSCI.2934-07.2008

Garcia-Larrea L (2012a) Insights gained into pain processing from patients with focal brain lesions.

Neurosci Lett 520(2):188–191. doi: 10.1016/j.neulet.2012.05.007

Garcia-Larrea L (2012b) The posterior insular-opercular region and the search of a primary cortex for pain. Neurophysiol Clin 42(5):299–313. doi: 10.1016/j.neucli.2012.06.001

Garcia-Larrea L, Frot M, Valeriani M (2003) Brain generators of laser-evoked potentials: from dipoles to functional significance. Neurophysiol Clin 33(6):279–292

Garwicz M, Jorntell H, Ekerot CF (1998) Cutaneous receptive fields and topography of mossy fibres and climbing fibres projecting to cat cerebellar C3 zone. J Physiol 512 (Pt 1):277–293

Greenspan JD, Lee RR, Lenz FA (1999) Pain sensitivity alterations as a function of lesion location in the parasylvian cortex. Pain 81(3):273–282

Greenspan JD, Winfield JA (1992) Reversible pain and tactile deficits associated with a cerebral tumor compressing the posterior insula and parietal operculum. Pain 50(1):29–39

Helmchen C, Mohr C, Erdmann C, Petersen D, Nitschke MF (2003) Differential cerebellar activation related to perceived pain intensity during noxious thermal stimulation in humans: a functional magnetic resonance imaging study. Neurosci Lett 335(3):202–206

Henderson LA, Rubin TK, Macefield VG (2011) Within-limb somatotopic representation of acute muscle pain in the human contralateral dorsal posterior insula. Hum Brain Mapp 32(10):1592– 1601. doi: 10.1002/hbm.21131

Hofbauer RK, Fiset P, Plourde G, Backman SB, Bushnell MC (2004) Dose-dependent effects of propofol on the central processing of thermal pain. Anesthesiology 100(2):386–394

Jantsch HHF, Kemppainen P, Ringler R, Handwerker HO, Forster C (2005) Cortical representation of experimental tooth pain in humans. Pain 118(3):390–399. doi: 10.1016/j.pain.2005.09.017

Kambalimath DH, Dolas RS, Kambalimath HV, Agrawal SM (2013) Efficacy of 4 % Articaine and 2 % Lidocaine: A clinical study. J Maxillofac Oral Surg 12(1):3–10. doi: 10.1007/s12663-012-0368-4 Keller T, Popovic MR, Pappas IPI, Muller P-Y (2002) Transcutaneous functional electrical stimulator

"Compex Motion". Artif Organs 26(3):219–223

Kenshalo DR, Iwata K, Sholas M, Thomas DA (2000) Response properties and organization of nociceptive neurons in area 1 of monkey primary somatosensory cortex. J Neurophysiol 84(2):719–729

Kim J, Horwitz B (2008) Investigating the neural basis for fMRI-based functional connectivity in a blocked design: application to interregional correlations and psycho-physiological interactions. Magn Reson Imaging 26(5):583–593. doi: 10.1016/j.mri.2007.10.011

Kucyi A, Davis KD (2015) The dynamic pain connectome. Trends Neurosci 38(2):86–95. doi: 10.1016/j.tins.2014.11.006

Liberati G, Klocker A, Safronova MM, Ferrao Santos S, Ribeiro Vaz J-G, Raftopoulos C, Mouraux A (2016) Nociceptive Local Field Potentials Recorded from the Human Insula Are Not Specific for Nociception. PLoS Biol 14(1):e1002345. doi: 10.1371/journal.pbio.1002345

Lin LD, Murray GM, Sessle BJ (1993) The effect of bilateral cold block of the primate face primary somatosensory cortex on the performance of trained tongue-protrusion task and biting tasks. J Neurophysiol 70(3):985–996

Mano H, Seymour B (2015) Pain: a distributed brain information network? PLoS Biol 13(1):e1002037. doi: 10.1371/journal.pbio.1002037

Matthews PM, Hampshire A (2016) Clinical Concepts Emerging from fMRI Functional Connectomics.

Neuron 91(3):511–528. doi: 10.1016/j.neuron.2016.07.031

Mazzola L, Faillenot I, Barral F-G, Mauguiere F, Peyron R (2012a) Spatial segregation of somato- sensory and pain activations in the human operculo-insular cortex. Neuroimage 60(1):409–418. doi: 10.1016/j.neuroimage.2011.12.072

Mazzola L, Isnard J, Peyron R, Guenot M, Mauguiere F (2009) Somatotopic organization of pain responses to direct electrical stimulation of the human insular cortex. Pain 146(1-2):99–104. doi: 10.1016/j.pain.2009.07.014

Mazzola L, Isnard J, Peyron R, Mauguiere F (2012b) Stimulation of the human cortex and the experience of pain: Wilder Penfield's observations revisited. Brain 135(Pt 2):631–640. doi: 10.1093/brain/awr265

McLaren DG, Ries ML, Xu G, Johnson SC (2012) A generalized form of context-dependent psychophysiological interactions (gPPI): a comparison to standard approaches. Neuroimage 61(4):1277–1286. doi: 10.1016/j.neuroimage.2012.03.068

Meier ML, Brugger M, Ettlin DA, Luechinger R, Barlow A, Jancke L, Lutz K (2012) Brain activation induced by dentine hypersensitivity pain--an fMRI study. J Clin Periodontol 39(5):441–447. doi: 10.1111/j.1600-051X.2012.01863.x

Meier ML, de Matos, Nuno M P, Brugger M, Ettlin DA, Lukic N, Cheetham M, Jancke L, Lutz K (2014) Equal pain-Unequal fear response: enhanced susceptibility of tooth pain to fear conditioning. Front Hum Neurosci 8:526. doi: 10.3389/fnhum.2014.00526

Meier ML, Widmayer S, Abazi J, Brugger M, Lukic N, Luchinger R, Ettlin DA (2015) The human brain response to dental pain relief. J Dent Res 94(5):690–696. doi: 10.1177/0022034515572022 Melzack R (1990) Phantom limbs and the concept of a neuromatrix. Trends Neurosci 13(3):88–92

Moulton EA, Elman I, Pendse G, Schmahmann J, Becerra L, Borsook D (2011) Aversion-related circuitry in the cerebellum: responses to noxious heat and unpleasant images. J Neurosci 31(10):3795–3804. doi: 10.1523/JNEUROSCI.6709-10.2011

Moulton EA, Schmahmann JD, Becerra L, Borsook D (2010) The cerebellum and pain: passive integrator or active participator? Brain Res Rev 65(1):14–27. doi: 10.1016/j.brainresrev.2010.05.005

Mouraux A, Diukova A, Lee MC, Wise RG, Iannetti GD (2011) A multisensory investigation of the functional significance of the "pain matrix". Neuroimage 54(3):2237–2249. doi: 10.1016/j.neuroimage.2010.09.084

Narhi M, Jyvasjarvi E, Virtanen A, Huopaniemi T, Ngassapa D, Hirvonen T (1992) Role of intradental A- and C-type nerve fibres in dental pain mechanisms. Proc Finn Dent Soc 88 Suppl 1:507–516

Niddam DM, Chen L-F, Wu Y-T, Hsieh J-C (2005) Spatiotemporal brain dynamics in response to muscle stimulation. Neuroimage 25(3):942–951. doi: 10.1016/j.neuroimage.2004.12.004

Oertel BG, Preibisch C, Martin T, Walter C, Gamer M, Deichmann R, Lotsch J (2012) Separating brain processing of pain from that of stimulus intensity. Hum Brain Mapp 33(4):883–894. doi: 10.1002/hbm.21256

O'Reilly JX, Woolrich MW, Behrens TEJ, Smith SM, Johansen-Berg H (2012) Tools of the trade: psychophysiological interactions and functional connectivity. Soc Cogn Affect Neurosci 7(5):604– 609. doi: 10.1093/scan/nss055

PENFIELD W (1947) Some observations on the cerebral cortex of man. Proc R Soc Lond B Biol Sci 134(876):329–347

Peyron R, Laurent B, Garcia-Larrea L (2000) Functional imaging of brain responses to pain. A review and meta-analysis (2000). Neurophysiol Clin 30(5):263–288

RASMUSSEN T, PENFIELD W (1947) Further studies of the sensory and motor cerebral cortex of man.

Fed Proc 6(2):452–460

Ruscheweyh R, Kuhnel M, Filippopulos F, Blum B, Eggert T, Straube A (2014) Altered experimental pain perception after cerebellar infarction. Pain 155(7):1303–1312. doi: 10.1016/j.pain.2014.04.006

Schwenzer N, Ehrenfeld M (eds) (2009) Zahn-Mund-Kiefer-Heilkunde: Zahnärztliche Chirurgie: Lokale Schmerzausschaltung (Lokalanästhesie). Thieme, Stuttgart

Segerdahl AR, Mezue M, Okell TW, Farrar JT, Tracey I (2015) The dorsal posterior insula subserves a fundamental role in human pain. Nat Neurosci 18(4):499–500. doi: 10.1038/nn.3969

Shyu B-C, Sikes RW, Vogt LJ, Vogt BA (2010) Nociceptive processing by anterior cingulate pyramidal neurons. J Neurophysiol 103(6):3287–3301. doi: 10.1152/jn.00024.2010

Stelzer J, Lohmann G, Mueller K, Buschmann T, Turner R (2014) Deficient approaches to human neuroimaging. Front Hum Neurosci 8:462. doi: 10.3389/fnhum.2014.00462

VanGilder JC (1975) Cerebellar evoked potentials from 'C' fibers. Brain Res 90(2):302–306

Vierck CJ, Whitsel BL, Favorov OV, Brown AW, Tommerdahl M (2013) Role of primary somatosensory cortex in the coding of pain. Pain 154(3):334–344. doi: 10.1016/j.pain.2012.10.021

Vogt BA (2005) Pain and emotion interactions in subregions of the cingulate gyrus. Nat Rev Neurosci 6(7):533–544. doi: 10.1038/nrn1704

Vogt BA (2016) Midcingulate cortex: Structure, connections, homologies, functions and diseases. J Chem Neuroanat 74:28–46. doi: 10.1016/j.jchemneu.2016.01.010

Vogt BA, Berger GR, Derbyshire SWG (2003) Structural and functional dichotomy of human midcingulate cortex. Eur J Neurosci 18(11):3134–3144

Wager TD, Atlas LY, Lindquist MA, Roy M, Woo C-W, Kross E (2013) An fMRI-based neurologic signature of physical pain. N Engl J Med 368(15):1388–1397. doi: 10.1056/NEJMoa1204471

Woo C-W, Krishnan A, Wager TD (2014) Cluster-extent based thresholding in fMRI analyses: pitfalls and recommendations. Neuroimage 91:412–419. doi: 10.1016/j.neuro

6 General Discussion and Conclusion

Each study conducted within the frame of this doctoral thesis has its own specific discussion section, where the results are discussed, put into an appropriate scientific context and where the study limitations are thematized. The scope of this chapter is thus broader with an emphasis on the contributions of the presented studies for the answering of the main goal of this thesis.

The overall aim of this work was to tackle methodical issues in ^{1}H-MRS pain research in order to foster the establishment of this highly valuable method for answering some of the most urging topics in the field of human pain research.

The **first study** conducted in this thesis (reproducibility study) addressed the common issue regarding anatomical and functional specificity. In this work, the typical approach usually applied in ^{1}H-MRS studies was reversed: Instead of simply defining the measurement voxel dimensions necessary to achieve a certain SNR with the cost of high levels of interpretive ambiguity, our approach prioritized adequate regional and functional specificity and investigated possible resulting data quality limitations caused by this strategy. In my opinion, this may be the only accurate way to obtain meaningful information regarding certain processes-of-interest in small brain structures related to pain processing as such processes could otherwise be obscured by partial volume effects. Based on the evidence from pain research focusing on the specific roles of cytoarchitectonically and functionally distinct sub-compartments of the cingulate (pgACC and aMCC) and insular cortices, the rationale was to optimize voxel specificity optimally accounting for the boundaries of such highly specified substructures and to investigate the associated reproducibility of neurochemical quantification. The report showed that quantification in these pain-relevant subregions is feasible and reproducible using standard sequences and equipment in a modest amount of time. Although this work did not directly contribute to the field of pain neuroscience, it is nevertheless of importance due to various

reasons. First of all, this work showed that neurochemical measurements with optimized anatomical and functional specificity is possible, hence potentially encouraging other groups to apply ^{1}H-MRS to these substructures of the cingulate and insular cortices in various pain investigations. As an example, pain-associated neurochemical patterns obtained from distinct small subregions of the cingulate and insular cortex might be compared to further corroborate their specific roles in pain processing. In addition, the combination of ^{1}H-MRS and fMRI might foster a more thorough understanding of brain activity changes in these subregions, and in connectivity patterns between these subregions to other brain areas by providing complementary information about neurotransmitter systems. Secondly, this reproducibility work represents a solid foundation for the planning of future ^{1}H-MRS pain studies in such areas by providing information about potential variance sources and expected variation levels, enabling the calculation of needed sample sizes for within- and between-subjects designs. Thirdly, this work also pointed out the limitations of the applied standard ^{1}H-MRS methods in dealing with signal disturbances. As an example, spectral resolution from the pgACC was 25% broader compared to the other regions probably due to pulsatile effects of the arteria cerebri anterior, resulting in reduced spectral linewidth due to B_0-shifts. Thus, the application of a MC-PRESS sequence to the pgACC might be highly beneficial due to the post-hoc correction of B_0-shifts by frequency alignment of the water peaks.

Nevertheless, it also shall be mentioned that new methods are emerging to further improve anatomical and functional specificity. New sequence types such as the “spatially selective excitation in two dimensions” (2D-SSE) enables the acquisition of highly specific ^{1}H-MRS data by means of voxels with arbitrary shapes. This technique allows the free definition of measurement volume shapes for an optimal tracing of the contours of a region-of-interest (Waxmann et al.,

2016). However, reproducibility examinations using this 2D-SSE technique to pain-relevant structures and their sub-compartments are still pending.

The **second study** successfully addressed the issue regarding functional ^{1}H-MRS investigations in the human brainstem. This is crucial as pointed out in the section 4.1 considering the multitude of animal studies linking neurochemical aberrations in brainstem structures to the etiology and maintenance of ongoing pain conditions (Sessle, 2000; Terayama et al., 2000; Porreca et al., 2002; Tracey and Mantyh, 2007; Graeff and Del-Ben, 2008; Ren and Dubner, 2011; Takeda et al., 2011; Denk et al., 2014; Samineni et al., 2017). As a first step in the closure of this scientific gap, this study investigated the feasibility of neurochemical quantification in the human TBSNC and the method's sensitivity to detect induced neurochemical alterations in this brainstem structure. This study is important from various points of view. On the one hand, the applied MC-PRESS sequences successfully coped with brainstem-inherent signal disturbances, allowing the obtainment of highly reproducible data from a voxel with 2.4 cm^3 volume. Furthermore, this study suggests that neurochemical alterations are identifiable by detecting concentration decreases in tNAA and GABA in association with experimental orofacial pain stimulation. However, the pain-specificity of the observed neurochemical dynamics in the TBSNC cannot be clearly answered with this study as only painful stimuli were applied for the induction of neurochemical changes. For this purpose, a replication of this experiment is planned with the addition of a non-painful condition in order to potentially differentiate nociceptive and somatosensory signal processing at brainstem level.

As mentioned in the sections 3.1.4 and 4.1, this method could be very well suited for investigations in structures of the DPMS, including the PAG and RVM. This is of crucial importance regarding the eminent role of this brainstem allocated network in the regulation and modulation of nociceptive stimuli. Neurochemical

information obtained from the PAG and RVM may provide important cues about the differentiation of pro- and anti-nociceptive processes. In upcoming studies, we are going to apply the same procedure from the TBSNC-study to the human PAG and RVM. First tests are highly promising, showing high quality data from the PAG with a voxel size of only 1 cm^3.

The **third study** deviated from the focus on ^{1}H-MRS by investigating pain-related processes in the brain using fMRI. Nevertheless, this study adds a valuable dimension to this doctoral thesis. This study applied a novel approach to identify and characterize regions showing discriminatory properties between non-painful from painful sensations. Instead of applying different stimuli intensities, the stimulus strength was kept constant, but the perceived intensity was modulated via the application of a nerve block using a lidocaine injection. Compared to the placebo condition, the lidocaine injection resulted in significant BOLD reductions in the posterior insula and parietal operculum, but not in other pain-related brain structures. These findings could hint to a unique relevance of the operculo-insular cortex in coding of the transition from non-painful to painful experiences and vice versa.

The replication of this study using ^{1}H-MRS might provide additional valuable insights into the neural processes underlying the transition from painful to non-painful sensations. In the first study (reproducibility study), the measurement characteristics in the posterior insula were already thoroughly investigated, providing a solid foundation for a replication of this study using ^{1}H-MRS.

7 References

Apkarian, A.V., Bushnell, M.C., Treede, R.-D., and Zubieta, J.-K. (2005). Human brain mechanisms of pain perception and regulation in health and disease. European journal of pain (London, England) *9*, 463–484.

Baliki, M.N., Baria, A.T., and Apkarian, A.V. (2011). The cortical rhythms of chronic back pain. The Journal of neuroscience : the official journal of the Society for Neuroscience *31*, 13981–13990.

Baliki, M.N., Mansour, A.R., Baria, A.T., and Apkarian, A.V. (2014). Functional reorganization of the default mode network across chronic pain conditions. PloS one *9*, e106133.

Baliki, M.N., Petre, B., Torbey, S., Herrmann, K.M., Huang, L., Schnitzer, T.J., Fields, H.L., and Apkarian, A.V. (2012). Corticostriatal functional connectivity predicts transition to chronic back pain. Nature neuroscience *15*, 1117–1119.

Bartha, R. (2007). Effect of signal-to-noise ratio and spectral linewidth on metabolite quantification at 4 T. NMR in biomedicine *20*, 512–521.

Bolwerk, A., Seifert, F., and Maihöfner, C. (2013). Altered resting-state functional connectivity in complex regional pain syndrome. The journal of pain : official journal of the American Pain Society *14*, 1107-1115.e8.

Bráz, J.M., Sharif-Naeini, R., Vogt, D., Kriegstein, A., Alvarez-Buylla, A., Rubenstein, J.L., and Basbaum, A.I. (2012). Forebrain GABAergic neuron precursors integrate into adult spinal cord and reduce injury-induced neuropathic pain. Neuron *74*, 663–675.

DaSilva, A.F., and DosSantos, M.F. (2012). The role of sensory fiber demography in trigeminal and postherpetic neuralgias. Journal of dental research *91*, 17–24.

DaSilva, A.F.M., Becerra, L., Makris, N., Strassman, A.M., Gonzalez, R.G., Geatrakis, N., and Borsook, D. (2002). Somatotopic activation in the human trigeminal pain pathway. The Journal of neuroscience : the official journal of the Society for Neuroscience *22*, 8183–8192.

Davis, K.D., and Moayedi, M. (2013). Central mechanisms of pain revealed through functional and structural MRI. Journal of neuroimmune pharmacology : the official journal of the Society on NeuroImmune Pharmacology *8*, 518–534.

Denk, F., McMahon, S.B., and Tracey, I. (2014). Pain vulnerability. A neurobiological perspective. Nature neuroscience *17*, 192–200.

D'Esposito, M., Deouell, L.Y., and Gazzaley, A. (2003). Alterations in the BOLD fMRI signal with ageing and disease. A challenge for neuroimaging. Nature reviews. Neuroscience *4*, 863–872.

Dreher, W., and Leibfritz, D. (2005). New method for the simultaneous detection of metabolites and water in localized in vivo 1H nuclear magnetic resonance spectroscopy. Magnetic resonance in medicine *54*, 190–195.

Farrell, M.J., Laird, A.R., and Egan, G.F. (2005). Brain activity associated with painfully hot stimuli applied to the upper limb. A meta-analysis. Human brain mapping *25*, 129–139.

Graaf, R.A. de (2007). In Vivo NMR Spectroscopy (John Wiley & Sons, Ltd: Chichester, UK).

Graeff, F.G., and Del-Ben, C.M. (2008). Neurobiology of panic disorder. From animal models to brain neuroimaging. Neuroscience and biobehavioral reviews *32*, 1326–1335.

Gutzeit, A., Meier, D., Froehlich, J.M., Hergan, K., Kos, S., V Weymarn, C., Lutz, K., Ettlin, D., Binkert, C.A., Mutschler, J., Sartoretti-Schefer, S., and Brügger, M. (2013). Differential NMR spectroscopy reactions of anterior/posterior and right/left insular subdivisions due to acute dental pain. European radiology *23*, 450–460.

Gutzeit, A., Meier, D., Meier, M.L., Weymarn, C. von, Ettlin, D.A., Graf, N., Froehlich, J.M., Binkert, C.A., and Brügger, M. (2011). Insula-specific responses induced by dental pain. A proton magnetic resonance spectroscopy study. European radiology *21*, 807–815.

Henderson, L.A., Peck, C.C., Petersen, E.T., Rae, C.D., Youssef, A.M., Reeves, J.M., Wilcox, S.L., Akhter, R., Murray, G.M., and Gustin, S.M. (2013). Chronic pain. Lost inhibition? The Journal of neuroscience : the official journal of the Society for Neuroscience *33*, 7574–7582.

Henry, M.E., Lauriat, T.L., Shanahan, M., Renshaw, P.F., and Jensen, J.E. (2011). Accuracy and stability of measuring GABA, glutamate, and glutamine by proton magnetic resonance spectroscopy. A phantom study at 4 Tesla. Journal of magnetic resonance (San Diego, Calif. : 1997) *208*, 210–218.

Hock, A., Wilm, B., Zandomeneghi, G., Ampanozi, G., Franckenberg, S., Zoelch, N., Wyss, P.O., Zanche, N. de, Nordmeyer-Maßner, J., Kraemer, T., Thali, M., Ernst, M., Kollias, S., and Henning, A. (2016). Neurochemical profile of the human cervical spinal cord determined by MRS. NMR in biomedicine *29*, 1464–1476.

Hong, S.-T., and Pohmann, R. (2013). Quantification issues of in vivo (1) H NMR spectroscopy of the rat brain investigated at 16.4 T. NMR in biomedicine *26*, 74–82.

Kanowski, M., Kaufmann, J., Braun, J., Bernarding, J., and Tempelmann, C. (2004). Quantitation of simulated short echo time 1H human brain spectra by LCModel and AMARES. Magnetic resonance in medicine *51*, 904–912.

Koush, Y., Elliott, M.A., Scharnowski, F., and Mathiak, K. (2013). Real-time automated spectral assessment of the BOLD response for neurofeedback at 3 and 7T. Journal of neuroscience methods *218*, 148–160.

Kreis, R. (2004). Issues of spectral quality in clinical 1H-magnetic resonance spectroscopy and a gallery of artifacts. NMR in biomedicine *17*, 361–381.

Kucyi, A., and Davis, K.D. (2015). The dynamic pain connectome. Trends in neurosciences *38*, 86–95.

Lauritzen, M., Mathiesen, C., Schaefer, K., and Thomsen, K.J. (2012). Neuronal inhibition and excitation, and the dichotomic control of brain hemodynamic and oxygen responses. NeuroImage *62*, 1040–1050.

Linnman, C., Moulton, E.A., Barmettler, G., Becerra, L., and Borsook, D. (2012). Neuroimaging of the periaqueductal gray. State of the field. NeuroImage *60*, 505–522.

Loeser, J.D., and Melzack, R. (1999). Pain. An overview. The Lancet *353*, 1607–1609.

Loggia, M.L., Kim, J., Gollub, R.L., Vangel, M.G., Kirsch, I., Kong, J., Wasan, A.D., and Napadow, V. (2013). Default mode network connectivity encodes clinical pain. An arterial spin labeling study. Pain *154*, 24–33.

Logothetis, N.K. (2008). What we can do and what we cannot do with fMRI. Nature *453*, 869–878.

Logothetis, N.K., Pauls, J., Augath, M., Trinath, T., and Oeltermann, A. (2001). Neurophysiological investigation of the basis of the fMRI signal. Nature *412*, 150–157.

Mainero, C., Boshyan, J., and Hadjikhani, N. (2011). Altered functional magnetic resonance imaging resting-state connectivity in periaqueductal gray networks in migraine. Annals of neurology *70*, 838–845.

Mangia, S., Tkác, I., Logothetis, N.K., Gruetter, R., van de Moortele, P.-F., and Uğurbil, K. (2007). Dynamics of lactate concentration and blood oxygen level-dependent effect in the human visual cortex during repeated identical stimuli. Journal of neuroscience research *85*, 3340–3346.

Matos, N.M.P. de, Hock, A., Wyss, M., Ettlin, D.A., and Brügger, M. (2017). Neurochemical dynamics of acute orofacial pain in the human trigeminal brainstem nuclear complex. NeuroImage *162*, 162–172.

May, A. (2011). Structural brain imaging. A window into chronic pain. The Neuroscientist : a review journal bringing neurobiology, neurology and psychiatry *17*, 209–220.

Mazzola, L., Faillenot, I., Barral, F.-G., Mauguière, F., and Peyron, R. (2012a). Spatial segregation of somato-sensory and pain activations in the human operculo-insular cortex. NeuroImage *60*, 409–418.

Mazzola, L., Isnard, J., Peyron, R., and Mauguière, F. (2012b). Stimulation of the human cortex and the experience of pain. Wilder Penfield's observations revisited. Brain : a journal of neurology *135*, 631–640.

Mills, E.P., Di Pietro, F., Alshelh, Z., Peck, C.C., Murray, G.M., Vickers, E.R., and Henderson, L.A. (2018). Brainstem Pain-Control Circuitry Connectivity in Chronic Neuropathic Pain. The Journal of neuroscience : the official journal of the Society for Neuroscience *38*, 465–473.

Mouraux, A., Diukova, A., Lee, M.C., Wise, R.G., and Iannetti, G.D. (2011). A multisensory investigation of the functional significance of the "pain matrix". NeuroImage *54*, 2237–2249.

Mumuni, A.N., and McLean, J. (2017). Dynamic MR Spectroscopy of brain metabolism using a non-conventional spectral averaging scheme. Journal of neuroscience methods *277*, 113–121.

Mutso, A.A., Petre, B., Huang, L., Baliki, M.N., Torbey, S., Herrmann, K.M., Schnitzer, T.J., and Apkarian, A.V. (2014). Reorganization of hippocampal functional connectivity with transition to chronic back pain. Journal of neurophysiology *111*, 1065–1076.

Napadow, V., LaCount, L., Park, K., As-Sanie, S., Clauw, D.J., and Harris, R.E. (2010). Intrinsic brain connectivity in fibromyalgia is associated with chronic pain intensity. Arthritis and rheumatism *62*, 2545–2555.

Ogawa, S., Lee, T.-M., Nayak, A.S., and Glynn, P. (1990). Oxygenation-sensitive contrast in magnetic resonance image of rodent brain at high magnetic fields. Magnetic resonance in medicine *14*, 68–78.

Peyron, R., Laurent, B., and García-Larrea, L. (2000). Functional imaging of brain responses to pain. A review and meta-analysis (2000). Neurophysiologie clinique = Clinical neurophysiology *30*, 263–288.

Porreca, F., Ossipov, M.H., and Gebhart, G.F. (2002). Chronic pain and medullary descending facilitation. Trends in neurosciences *25*, 319–325.

Provencher, S.W. (1993). Estimation of metabolite concentrations from localizedin vivo proton NMR spectra. Magnetic resonance in medicine *30*, 672–679.

Provencher, S.W. (2001). Automatic quantitation of localized in vivo 1H spectra with LCModel. NMR in biomedicine *14*, 260–264.

Ren, K., and Dubner, R. (2011). The role of trigeminal interpolaris-caudalis transition zone in persistent orofacial pain. International review of neurobiology *97*, 207–225.

Samineni, V.K., Grajales-Reyes, J.G., Copits, B.A., O'Brien, D.E., Trigg, S.L., Gomez, A.M., Bruchas, M.R., and Gereau, R.W. (2017). Divergent Modulation of Nociception by Glutamatergic and GABAergic Neuronal Subpopulations in the Periaqueductal Gray. eNeuro *4*.

Scholz, J., and Woolf, C.J. (2002). Can we conquer pain? Nature neuroscience *5 Suppl*, 1062–1067.

Sessle, B.J. (2000). Acute and chronic craniofacial pain. Brainstem mechanisms of nociceptive transmission and neuroplasticity, and their clinical correlates. Critical Reviews in Oral Biology & Medicine *11*, 57–91.

Sessle, B.J. (2016). Acute and Chronic Craniofacial Pain. Brainstem Mechanisms of Nociceptive Transmission and Neuroplasticity, and Their Clinical Correlates. Critical Reviews in Oral Biology & Medicine *11*, 57–91.

Stagg, C.J. (2013). Magnetic resonance spectroscopy. Tools for neuroscience research and emerging clinical applications (Academic Press: Amsterdam).

Takeda, M., Matsumoto, S., Sessle, B.J., Shinoda, M., and Iwata, K. (2011). Peripheral and Central Mechanisms of Trigeminal Neuropathic and Inflammatory Pain. Journal of Oral Biosciences *53*, 318–329.

Terayama, R., Guan, Y., Dubner, R., and Ren, K. (2000). Activity-induced plasticity in brain stem pain modulatory circuitry after inflammation. Neuroreport *11*, 1915–1919.

Tracey, I., and Mantyh, P.W. (2007). The cerebral signature for pain perception and its modulation. Neuron *55*, 377–391.

Upadhyay, J., Knudsen, J., Anderson, J., Becerra, L., and Borsook, D. (2008). Noninvasive mapping of human trigeminal brainstem pathways. Magnetic resonance in medicine *60*, 1037–1046.

Waxmann, P., Mekle, R., Schubert, F., Brühl, R., Kuehne, A., Lindel, T.D., Seifert, F., Speck, O., and Ittermann, B. (2016). A new sequence for shaped voxel spectroscopy in the human brain using 2D spatially selective excitation and parallel transmission. NMR in biomedicine *29*, 1028–1037.

Weissman-Fogel, I., Granovsky, Y., Crispel, Y., Ben-Nun, A., Best, L.A., Yarnitsky, D., and Granot, M. (2009). Enhanced presurgical pain temporal summation response predicts post-thoracotomy pain intensity during the acute postoperative phase. The journal of pain : official journal of the American Pain Society *10*, 628–636.

Wyss, P.O., Hock, A., and Kollias, S. (2017). The Application of Human Spinal Cord Magnetic Resonance Spectroscopy to Clinical Studies. A Review. Seminars in ultrasound, CT, and MR *38*, 153–162.

Yarnitsky, D., Crispel, Y., Eisenberg, E., Granovsky, Y., Ben-Nun, A., Sprecher, E., Best, L.-A., and Granot, M. (2008). Prediction of chronic post-operative pain. Pre-operative DNIC testing identifies patients at risk. Pain *138*, 22–28.

Yu, R., Gollub, R.L., Spaeth, R., Napadow, V., Wasan, A., and Kong, J. (2014). Disrupted functional connectivity of the periaqueductal gray in chronic low back pain. NeuroImage. Clinical *6*, 100–108.

Zhu, X.H., and Chen, W. (2001). Observed BOLD effects on cerebral metabolite resonances in human visual cortex during visual stimulation. A functional (1)H MRS study at 4 T. Magnetic resonance in medicine *46*, 841–847.

8 Acknowledgements

I did not undertake this journey alone. As I walked this path, I was always accompanied by people.

First, I would thank the doctoral committee (Prof. Dr. Martin Meyer and PD Dominik A. Ettlin) for giving me the opportunity to take this journey by providing the frame of this doctoral thesis.

Second, my thanks and appreciations go to people of Institute for Biomedical Engineering of the Swiss Federal Institute of Technology which provided me invaluable support: Dr. Dieter Meier for introducing me to MR Spectroscopy and Dr. Roger Lüchinger for his support in all kinds of MR-related issues. In particular, I would like to thank Dr. Andreas Hock for his passion for the project and exceptional expertise regarding MR Spectroscopy, which enabled me to take the new routes in direction of feasible brainstem ^{1}H-MRS experiments.

My utmost gratitude goes to Dr. Mike Brügger for his outstanding dedication and endurance as supervisor and mentor. He always made sure I stayed on track, supported me in overcoming obstacles encountered along the way, provided me the valuable freedom to choose new directions and backed me up when the projects were taking longer than expected.

Finally, I would like to thank especially my wife Helen for her comfort, support, patience and understanding during my ups and downs along this sometimes very difficult endeavor.

9 Curriculum Vitae

Name	Prates de Matos
Prename	Nuno Miguel
Address	Rosenbergstrasse 3
	9230 Flawil
Date of birth	July 8, 1985
Marital status	married
Citizenship	Portugal

Career

Feb 2018-present	**University of Zurich, Center for Dental Medicine,** Clinic for Oral Surgery & Clinic for Masticatory Disorders (Prof. Dr. Martin Rücker) • Research Associate
Aug. 2014- Jan 2018	**University Hospital Zurich**, Institute for Complementary and Integrative Medicine (Prof. Dr. Claudia Witt) • Research Associate
Sept. 2010- Dec. 2012	**University of Zurich,** Department of Neuropsychology • Research Assistant
Jan. 2011-Sept. 2011	**Cantonal Hospital Winterthur,** Department of Radiology • Research Assistant
June 2011-Sept. 2011	**University Hospital Zurich**, Department of Neuropsychology (Supervisor Prof. Dr. Peter Brugger) • Research internship
March 2010-Juli 2010	**University of Zurich,** Department of Neuropsychology (Supervisor Dr. Kai Lutz)

- Research internship

Education

2012-2017 **University of Zurich: PhD study**
PhD program in Psychology, Division Neuropsychology

- Title of PhD thesis: Investigation of the human brain neurochemistry in pain-related cortical areas and brainstem

2010-2012 **University of Zurich: Master of Science (Msc.) in Psychology**

- Specification in Cognitive Neuroscience
- Minor in Biology
- Title of master thesis: Differences in Pawlowian Conditioning in Dependence of Stimulation Site (Original Title: Unterschiede in der pawlowschen Furchtkonditionierung in Abhängigkeit des Stimulationsortes) (Supervisors: Dr. Michael Meier and Prof. Dr. Lutz Jäncke)

2006-2010 **University of Zurich**

- Bachelor of Science (Bsc.) in Psychology
- Minor in Biology
- Title of bachelor thesis: Improvement of Athletic Performance by Means of TMS, tDCS and Neurofeedback (Original title: Sportliche Leistungssteigerung mittels TMS, tDCS und Neurofeedback) (Supervisor: Dr. Lea Hilty)